

Reviewed Preprint

Published from the original preprint after peer review and assessment by eLife.

[About eLife's process](#)

Reviewed Preprint posted

16 March 2023

Posted to bioRxiv

12 January 2023

Sent for peer review

11 January 2023

Analysis of CDPK1 targets identifies a trafficking adaptor complex that regulates microneme exocytosis in *Toxoplasma*

Alex W Chan , Malgorzata Broncel , Nicole Haseley , Sundeep Chakladar , Elena Andree , Alice L Herneisen , Emily Shortt , Moritz Treeck , Sebastian Lourido

Whitehead Institute for Biomedical Research, Cambridge, MA , USA • Biology Department, Massachusetts Institute of Technology, Cambridge, MA , USA • Signaling in Apicomplexan Parasites Laboratory, The Francis Crick Institute, London , UK

Abstract

Apicomplexan parasites use Ca^{2+} -regulated exocytosis to secrete essential virulence factors from specialized organelles called micronemes. Ca^{2+} -dependent protein kinases (CDPKs) are required for microneme exocytosis; however, the molecular events that regulate trafficking and fusion of micronemes with the plasma membrane remain unresolved. Here, we combine sub-minute resolution phosphoproteomics and bio-orthogonal labeling of kinase substrates in *Toxoplasma gondii* to identify 163 proteins phosphorylated in a CDPK1-dependent manner. In addition to known regulators of secretion, we identify uncharacterized targets with predicted functions across signaling, gene expression, trafficking, metabolism, and ion homeostasis. One of the CDPK1 targets is a putative HOOK activating adaptor. In other eukaryotes, HOOK homologs form the FHF complex with FTS and FHIP to activate dynein-mediated trafficking of endosomes along microtubules. We show the FHF complex is partially conserved in *T. gondii*, consisting of HOOK, an FTS homolog, and two parasite-specific proteins (TGGT1_306920 and TGGT1_316650). CDPK1 kinase activity and HOOK are required for the rapid apical trafficking of micronemes as parasites initiate motility. Moreover, parasites lacking HOOK or FTS display impaired microneme protein secretion, leading to a block in the invasion of host cells. Taken together, our work provides a comprehensive catalog of CDPK1 targets and reveals how vesicular trafficking has been tuned to support a parasitic lifestyle.

eLife assessment

This **important** study significantly advances our understanding of the calcium signaling pathway mediated by the kinase CDPK1, in the protozoan parasite *Toxoplasma gondii*. The evidence supporting the authors' conclusions is in many parts **convincing**, with rigorous biochemical and microscopy analysis. The work will be of broad interest to researchers in the field of signal transduction and protozoan biology.

Introduction

Ca^{2+} -regulated exocytosis is ubiquitous among eukaryotes. This signaling paradigm regulates an array of processes such as neurotransmitter release in neurons, hormone secretion in endocrine cells, and histamine secretion in mast cells (Pang and Südhof, 2010). Ca^{2+} -regulated exocytosis is also critical for apicomplexan parasites that are the causative agents of rampant, lifethreatening diseases including malaria, toxoplasmosis, and cryptosporidiosis (Havelaar et al., 2015). Central to their pathogenesis is their ability to transition from intracellular replicative stages to extracellular motile stages, which involves a unique form of cellular movement called gliding, egress from the primary host cell, and invasion into a new host. These processes are driven by the Ca^{2+} -regulated exocytosis of apicomplexan-specific membrane-bound organelles called micronemes and rhoptries.

The sequential exocytosis of micronemes and rhoptries is required to promote extracellular motile stages of the parasite (Blader et al., 2016; Carruthers and Sibley, 1997). Micronemes are localized to the parasite apex and their positioning is dependent on cortical microtubules, ultrastable filaments that polymerize down the length of the parasite (Chen et al., 2015; Leung et al., 2017; Wang et al., 2021). Exocytosis of microneme cargo enables host cell rupture by releasing perforin-like proteins during egress and translocation of exposed adhesins required for gliding and attachment to new host cells (Carruthers and Sibley, 1997; Carruthers and Tomley, 2008; Kafack et al., 2009). Multiple microneme proteins, including the associated cysteine repeat modular proteins (CRMP) complex, are also required to trigger the exocytosis of rhoptries upon host cell contact (Kessler et al., 2008; Singer et al., 2022; Sparvoli et al., 2022). Rhoptry proteins include effectors that modulate host responses and transmembrane proteins that are embedded into the host plasma membrane to enable active invasion (Bradley and Sibley, 2007; Lamarque et al., 2011; 2014; Ong et al., 2010; Tyler and Boothroyd, 2011). Intracellular Ca^{2+} release is necessary and sufficient to trigger the rapid trafficking and exocytosis of micronemes (Carruthers et al., 1999a; b; Endo et al., 1982; Sidik et al., 2016). While Ca^{2+} is also necessary for rhoptry discharge, exocytosis relies on additional cellular processes such as microneme exocytosis (Coleman et al., 2018; Segev-Zarko et al., 2022). While the exocytosis of micronemes and rhoptries is known to be critical for parasite motility, the mechanisms linking Ca^{2+} signaling to their trafficking and fusion to the plasma membrane are still unclear. Ca^{2+} signals in apicomplexans are primarily transduced by Ca^{2+} -dependent protein kinases (CDPKs) (Billker et al., 2009; Farrell et al., 2012; Garrison et al., 2012; Kumar et al., 2017; Lourido et al., 2012; Lourido and Moreno, 2015; Luo et al., 2005; Márquez-Nogueras et al., 2021; McCoy et al., 2012; Sebastian et al., 2012). CDPKs are serine/threonine protein kinases that are unique to apicomplexans and plants. CDPKs are activated by directly binding to Ca^{2+} , in contrast to Ca^{2+} /calmodulin-dependent protein kinases (CaMKs) found in animals, which are indirectly regulated by Ca^{2+} -bound calmodulin (CaM) (Ojo et al., 2010; Wernimont et al., 2010). CDPKs are crucial for apicomplexan infection—yet are absent from mammals—making them attractive drug targets; however, their mechanisms of action are still not well understood at a cellular and molecular level. In *T. gondii*, Ca^{2+} -dependent protein kinase 1 (CDPK1) is required for the Ca^{2+} -regulated exocytosis of micronemes, impacting all steps of parasite motility including egress, gliding, and invasion (Lourido et al., 2010). Small-molecule competitive inhibitors against CDPK1 have been identified and have shown some activity against *T. gondii* (Doggett et al., 2014; Johnson et al., 2012; Lourido et al., 2013; Winzer et al., 2015). Identifying the signaling pathways regulated by CDPK1 could reveal the pathways controlling microneme and rhoptry exocytosis.

The Ca^{2+} that activates CDPK1 and other cellular processes is released from intracellular stores following cyclic nucleotide-mediated activation of protein kinase G (PKG) (Bisio and

zaprinas or BIPPO that indirectly activate PKG (Figure 1A) (Lourido et al., 2012; Nofal et al., 2022; Sidik et al., 2016; Yuasa et al., 2005). PDE inhibition activates PKG within seconds and triggers the Ca^{2+} and lipid signaling nodes controlling parasite motility, including the exocytosis of micronemes (Figure 1A) (Lourido et al., 2012; Yuasa et al., 2005). The identity of the CDPK1 substrates that contribute to the regulation of microneme exocytosis remains unknown. Determining CDPK1-dependent phosphorylation is challenging because the signaling pathways controlling parasite motility are rapid and integrate signals from multiple kinases.

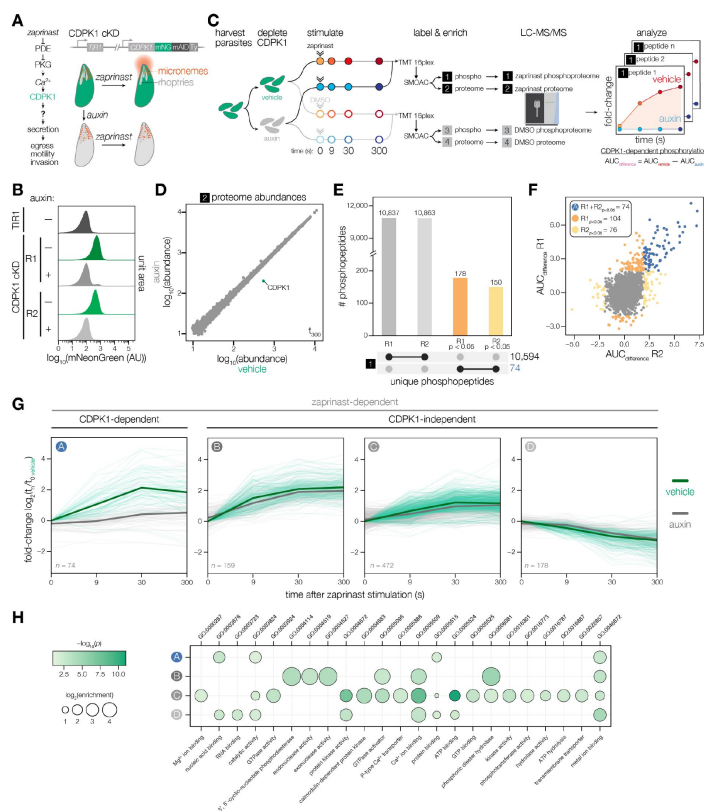


Figure 1.

Identifying CDPK1-dependent phosphorylation with sub-minute resolution.

(A) Stimulating parasites with zaprinast triggers Ca^{2+} -mediated activation of CDPK1, resulting in the secretion of microneme proteins (red) required for motile stages of the parasite. Conditional knockdown (cKD) of CDPK1 endogenously tagged with mNeonGreen-mAID-Ty (green) after auxin treatment. (B) Flow cytometry of mNeon-Green (mNG) fluorescence in extracellular CDPK1 cKD or parental TIR1 parasites treated with vehicle or auxin for 3.5 hrs. (C) Schematic of phosphoproteomic time course. Parasites were harvested prior to CDPK1 depletion with auxin for 3.5 hrs, followed by stimulation with zaprinast or vehicle (DMSO). Samples were collected at 0, 9, 30, and 300 sec. The experiment was performed in biological replicates. Samples were labeled with TMTpro, pooled for analysis, and phosphopeptides were enriched using SMOAC prior to LC-MS/MS. Four sets of samples were generated: enriched phosphoproteomes for

zaprinas [1] and DMSO [3], and proteomes for zaprinast [2] and DMSO [4]. Mock reporter ion intensities enabling relative quantification for a given peptide are shown to illustrate fold-change of unique phosphopeptide abundances during zaprinast stimulation. CDPK1-dependent phosphorylation is determined by calculating the area under the curve (AUC) difference between vehicle and auxin treatment conditions. (D) Protein abundances in the zaprinast proteome set [2] at 300 sec comparing vehicle- and auxin-treated CDPK1 cKD parasites. (E) UpSet plot for the number of phosphopeptides identified in the enriched zaprinast phosphoproteome [1] across individual replicates. Phosphopeptides exhibiting CDPK1-dependent phosphorylation with $p < 0.05$ are indicated. (F) Scatter plot of $AUC_{\text{difference}}$ values of enriched zaprinast phosphopeptides [1] across biological replicates. Significance was determined by comparing the distribution of $AUC_{\text{difference}}$ values from zaprinast phosphopeptides [1] to a null distribution of DMSO phosphopeptides [3] for individual replicates. (G) CDPK1-dependent and zaprinast-dependent phosphopeptide abundances over time. Ratios of zaprinast-treated samples relative to the vehicle-treated (no auxin) $t = 0$ samples. Median ratios of a group (solid lines). Individual phosphopeptides (opaque lines). CDPK1-dependent phosphopeptides (Group A) determined as described in F. Zaprinast-dependent phosphopeptides (Groups B, C, and D) were determined by comparing the distribution of AUC_{vehicle} values from zaprinast phosphopeptides [1] to a null distribution of DMSO phosphopeptides [3]. Groups were determined by projection-based clustering. (H) GO terms enriched among phosphopeptides undergoing a significant change after zaprinast stimulation. Significance was determined using a hypergeometric test.

Global phosphoproteomic studies found that Ca^{2+} -dependent phosphorylation included proteins involved in signal transduction, motility, exocytosis, cytoskeleton, in addition to many proteins with unknown functions; however, the functional relevance and organization of these proteins—especially CDPK1—in regulating exocytosis remain unclear ((Herneisen et al., 2022); (Invergo et al., 2017); (McCoy et al., 2012); (Nofal et al., 2022); (Treeck et al., 2014), 2011). Here, we utilized time-resolved phosphoproteomics and chemical genetics to identify 163 proteins phosphorylated by CDPK1. Our comprehensive analysis of CDPK1 not only identified phosphoregulation of known factors involved in parasite motility, but also revealed new regulators of exocytosis. We identified a conserved HOOK complex that is phosphorylated by CDPK1 and is required for microneme exocytosis by mediating the rapid trafficking of micronemes during parasite motility.

Results

Identifying CDPK1-dependent phosphorylation with sub-minute resolution

We examined the effect of CDPK1 on the phosphoproteome. To control the expression of CDPK1, we endogenously tagged the kinase with a C-terminal auxin-inducible degron (AID) for rapid conditional knockdown upon treating parasites with auxin (**Figure 1A**) (Brown et al., 2018; Shortt et al., 2022; Smith et al., 2022). CDPK1 was robustly depleted from extracellular parasites following auxin treatment for 3.5 hrs (**Figure 1B**). We compared vehicle- and auxin-treated parasites at four timepoints in the 5 min following zaprinast stimulation (0, 9, 30, and 300 sec) to capture the earliest changes following Ca^{2+} flux (**Figure 1C**). We used TMTpro labeling to multiplex 16 samples enabling analysis of a complete time course comparing vehicle- and auxin-treated parasites in biological duplicate in a single LC-MS/MS experiment (Li et al., 2020). Samples treated with DMSO instead of zaprinast served as a control. We enriched for phosphopeptides using sequential metal-oxide affinity chromatography (SMOAC) (Tsai et al., 2014). In total, we generated four datasets: an enriched zaprinast phosphoproteome [1], a zaprinast proteome (unenriched) [2], an enriched DMSO phosphoproteome [3], and a DMSO proteome (unenriched) [4]. Of the 4,255 parasite proteins quantified in the zaprinast proteome by LC-MS/MS, CDPK1 was the only protein with a greater than two-fold depletion in parasites treated with auxin (**Figure 1D**). The remainder of the proteome was largely stable (median log₂-fold change = -0.002 ± 0.089 M.A.D).

We first quantified peptide abundances across time relative to the 0 sec vehicle-treated time point to identify CDPK1-dependent phosphorylation, which yielded kinetic profiles of individual phosphopeptides in vehicle and auxin conditions (**Figure 1C**). The zaprinast phosphoproteome included 2,570 phosphorylated proteins, represented by 10,594 unique phosphopeptides quantified across both biological replicates (**Figure 1E**). We calculated the area under the curve (AUC) of individual phosphopeptide profiles for vehicle ($\text{AUC}_{\text{vehicle}}$) and auxin ($\text{AUC}_{\text{auxin}}$) conditions. To identify the subset of phosphopeptides exhibiting CDPK1-dependent phosphorylation, we calculated the difference between AUC values ($\text{AUC}_{\text{difference}}$) by comparing the distribution of $\text{AUC}_{\text{difference}}$ values in the zaprinast phosphoproteome to a null distribution derived from the DMSO phosphoproteome (**Figure 1—figure supplement S1**). This approach allowed us to account for the variability among AUCs under conditions that did not exhibit dynamic changes. We identified 74 unique CDPK1-dependent phosphopeptides across both biological replicates (Group A), belonging to 69 proteins (**Figure 1E–F**). Additionally, we identified peptides that were zaprinast responsive—despite being CDPK1-independent—by comparing the distribution of $\text{AUC}_{\text{vehicle}}$ values in the zaprinast phosphoproteome to a null distribution derived from the DMSO

phosphoproteome, resulting in 809 unique phosphopeptides representing 501 proteins. We utilized projection-based clustering to sort kinetic profiles of CDPK1-independent peptides into three groups, in which Group B and Group C contained phosphopeptides that increased in abundance and Group D contained phosphopeptides that decreased in abundance ([Figure 1G](#), [Figure 1—figure supplement S1](#)) ([Thrun and Ultsch, 2021](#)). Significant changes at the peptide level are attributed to altering levels of phosphorylation as opposed to protein levels. Of the 543 proteins exhibiting zaprinast-dependent phosphorylation, 484 were quantified at the proteome level. When comparing the 300 to 0 sec time points, zaprinast-dependent proteins displayed no significant changes (median \log_2 -fold change = 0 ± 0.074 M.A.D). This was consistent with the rapid time scale of these experiments and the overall stability of the 4,255 proteins quantified in the proteome (median \log_2 -fold change = 0.01 ± 0.089 M.A.D).

Gene ontology analysis identified several classes of genes that may be relevant to the regulation of za-prinast responses within the different groups ([Figure 1H](#)). CDPK1-independent phosphorylation and dephosphorylation was prevalent amongst proteins regulating cyclic nucleotide signaling (AC β , GC, UGO, PDE1, PDE2, PDE7, PDE9, PDE10, and PKG), lipid signaling (PI4K, PI4P5K, PI-PLC, DGK1, and PAP1), and Ca²⁺ signaling (CDPK2A and CDPK3). CDPK1-independent phosphorylation was also observed on downstream proteins regulating microneme exocytosis (APH and DOC2.1), rhoptry exocytosis (ARO, AIP, PL3, and NdP2), gliding motility (AKMT and MyoA), and homeostasis/biogenesis (NHE3, VHA1, NST2, and ERK7). MyoA phosphorylation was observed at S20 and S21, which was previously shown to be phosphorylated by CDPK3 and required for gliding motility ([Gaji et al., 2015](#)). SCE1 phosphorylation was observed at S225, which was previously shown to be phosphorylated by CDPK3 and required to relieve inhibition during Ca²⁺-stimulated egress ([McCoy et al., 2017](#)). Our analysis highlights temporally-resolved changes in the phosphoproteome in response to zaprinast stimulation. We identify a subset of proteins phosphorylated by CDPK1 that likely represent factors involved in motility-related exocytosis, which we discuss in further detail below.

Myristoylation modulates CDPK1 activity and alters its interacting partners

CDPK1 was found to be myristoylated on Gly2 ([Broncel et al., 2020](#)). Myristoylation results in lipid modifications on proteins that can impact membrane targeting and protein-protein interactions ([Martin et al., 2011](#); [Wright et al., 2014](#)). The myristoylated proteome of *T. gondii* was recently characterized using metabolic tagging and enrichment ([Broncel et al., 2020](#)). In this approach, parasites were grown in the presence of a myristic acid analogue containing a terminal alkyne group (YnMyr) that allowed enrichment of labeled proteins through click chemistry ([Heal et al., 2011](#)). We assessed whether myristoylation of CDPK1 affects the kinase's function. We validated myristoylation of CDPK1 using myristoylation-dependent pull downs followed by immunoblot detection and MS analysis ([Figure 2—figure supplement S2](#)). To investigate the role of myristoylation on CDPK1 function, an inducible knock-down strain (iKD) was generated by introducing a mAID-Myc tag at its C terminus ([Figure 2—figure supplement S2](#)). Auxin-dependent depletion was confirmed using immunoblot ([Figure 2—figure supplement S2](#)). Depletion of CDPK1 abolished ionophore-induced egress, as expected from previous results ([Figure 2—figure supplement S2](#)) ([Lourido et al., 2010](#)). Next, we complemented the iKD parasites by introducing HA-tagged WT (cWT) or myristoylation defective (cMut, G2A) copies of *CDPK1* into the *UPRT* locus ([Figure 2A](#)). We verified correct integration of both complementation constructs ([Figure 2—figure supplement S2](#)), and confirmed their equivalent and constitutive expression, as well as the auxin sensitivity of the endogenous mAID-tagged CDPK1 ([Figure 2B](#)). As predicted, the cMut allele was not myristoylated, based on acylation-dependent pull downs and immunoblotting ([Figure 2C](#)).

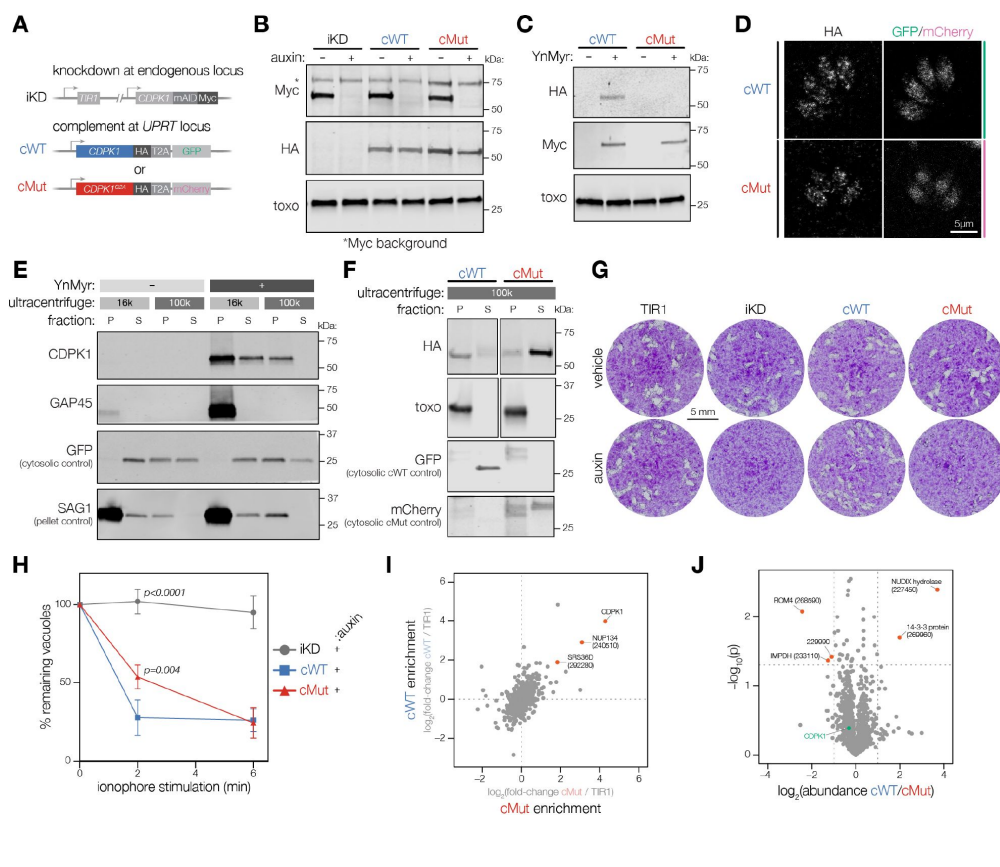


Figure 2.

Myristoylation modulates CDPK1 activity and alters its interacting partners.

(A) Complementation strategy used to evaluate the functional importance of CDPK1 myristoylation. See [Figure 2—figure supplement S2](#) for the construction of the iKD line. (B) Immunoblot demonstrating the auxin-dependent depletion of endogenous CDPK1 in the iKD, cWT, and cMut parasites (Myc) as well as equivalent expression of the complements (HA). *T. gondii* (tox) antibody was used as a loading control. (C) Biochemical validation of

complemented lines by YnMyr-dependent pull down. Enrichment of WT and Mut complements (HA). The inducible endogenous CDPK1 (Myc) and *T. gondii* (tox) antibody was used as enrichment and loading controls, respectively. (D) Localization of the complemented versions of CDPK1 and corresponding cytosolic reporters within cWT (GFP) and cMut (mCherry) by immunofluorescence. (E) Myristoylation-dependent subcellular partitioning of CDPK1. Localization of YnMyr-enriched CDPK1 was evaluated using differential centrifugation. The partitioning into pellet [P] and supernatant [S] fractions was detected by immunoblot (CDPK1) and compared to doubly acylated GAP45. GFP and SAG1 were used as S and P controls, respectively. As only half of the supernatant fraction was removed from the high-speed pellet (100,000 × g), the GFP signal is present in the latter. (F) Partitioning of complemented WT and mutant CDPK1 after high speed centrifugation (HA). *T. gondii* (tox) antibody was used as a P control whereas GFP and mCherry were used as S controls for cWT and cMut, respectively. (G) Plaque assays demonstrating that myristoylation of CDPK1 is important for the lytic cycle of *T. gondii*. (H) Lack of CDPK1 myristoylation delays ionophore-induced egress from host cells. Each data point is an average of *n* = 3 biological replicates, error bars represent standard deviation. Significance calculated using 1-way ANOVA with Tukey's multiple comparison test. See [Figure 2—figure supplement S2](#) for vehicle controls. (I) Immunoprecipitation-MS (IP-MS) of CDPK1-HA in cWT, cMut, and untagged TIR1 parasites across *n* = 2 biological replicates. Significantly enriched proteins (red) for proteins with more than three unique peptides, *p*_{cWT} < 0.05, and *p*_{cMut} < 0.05, and log₂ fold-change > 1 across both pull-downs; *t*-tests and Benjamini-Hochberg corrected. (J) IP-MS fold-enrichment comparing cWT and cMut pull-downs. Significantly enriched proteins (red) for proteins with more than 3 unique peptides, *p* < 0.05, and log₂ fold-change > 1 or < -1; *t*-test and Benjamini-Hochberg corrected.

Given that myristoylation is frequently reported to facilitate membrane association, we examined the localization of cWT and cMut CDPK1 by immunofluorescence ([Figure 2D](#)). No clear differences were detected between the punctate cytosolic patterns of cWT and cMut. We explored possible effects of myristoylation on the subcellular fractionation of CDPK1 resolved using differential centrifugation ([Figure 2E](#)). First, we evaluated the fractionation pattern of the endogenous, myristoylated CDPK1. YFP-expressing parasites were metabolically labeled with Myr or YnMyr and lysed in a hypotonic buffer to preserve intact membrane structures. Next, lysates were fractionated to generate a low-speed pellet and

supernatant at 16,000 x *g*. The low-speed supernatant was fractionated further into a high-speed pellet and supernatant at 100,000 x *g*. Click reaction based pull down and immunoblotting were used to resolve myristoylation-dependent partitioning. In contrast to the doubly acylated GAP45, which was present exclusively in the low-speed pellet, myristoylated CDPK1 was observed in the low-speed pellet and supernatant, and the high-speed pellet (**Figure 2E**), suggesting a potential association with membranous structures or higher molecular weight complexes. We next used both the cWT and cMut lines to elucidate any myristoylation-dependent changes to CDPK1 localization. While cWT could be found predominantly in the high-speed pellet, loss of myristoylation released cMut into the high-speed supernatant confirming an association with membranous structures or large protein complexes (**Figure 2F**).

To evaluate the role of CDPK1 myristoylation in parasite fitness, we performed plaque assays comparing the various strains (**Figure 2G**). In the presence of the endogenous copy of CDPK1, both complemented lines developed normally. However, upon auxin-mediated depletion of endogenous CDPK1, cMut plaque size substantially decreased. This finding demonstrates that one or more steps of the *T. gondii* lytic cycle are negatively affected by the loss of CDPK1 myristoylation. In light of CDPK1's known function, we next explored whether CDPK1 myristoylation might impact the parasite's ability to egress from host cells. In the absence of auxin, cWT, cMut, and the parental line (iKD) egressed within two min of ionophore stimulation (**Figure 2—figure supplement S2**). While cWT parasites maintained similar egress kinetics following auxin treatment, cMut parasites showed a significant delay after two min of treatment (**Figure 2H**). This egress delay was overcome by six min, suggesting that CDPK1 myristoylation is important for ionophore-induced egress, but not essential.

Finally, we wanted to examine whether myristoylation of CDPK1 affects its interactions with other proteins, which may occur by direct binding to the kinase or by indirect association with a shared membrane structure. We performed immunoprecipitation mass spectrometry (IP-MS) on HA-tagged CDPK1 from cWT, cMut, and untagged TIR1 parasites after hypotonic lysis. CDPK1 was the most significantly enriched protein across both cWT and cMut pulldowns when compared to untagged controls (**Figure 2I**). Two additional proteins were significantly enriched along with CDPK1: NUP134 (TGGT1_240510) and SRS36D (TGGT1_292280). Comparing the cWT and cMut pulldowns, we found two proteins preferentially associated with cWT: NUDIX hydroxylase (TGGT1_227450) and a 14-3-3 protein (TGGT1_269960) (**Figure 2J**). Loss of myristoylation appears to enhance interactions with three different proteins: ROM4 (TGGT1_268590), a putative T complex protein 1 alpha subunit (TGGT1_229990), and IMP dehydrogenase (TGGT1_233110). Genome-wide knockout screen data suggest that NUP134 and the putative T complex protein 1 are the only putative interacting partners required for parasite fitness (Sidik et al., 2016). NUP134 binds and co-localizes with the nuclear pore complex, whereas the putative T complex protein 1 may function as an ATP-dependent chaperone (Courjol et al., 2017). CDPK1 is localized primarily to the cytoplasm of the parasite and partially in the nucleus, which could explain its interactions with NUP134 (Ojo et al., 2010; Lourido et al., 2010). ROM4 is an integral membrane protease required to shed secreted microneme proteins through proteolysis, and its knockdown impaired gliding motility and invasion of host cells (Buguliskis et al., 2010). ROM4 localizes to the plasma membrane of parasites but was enriched with cytosolic CDPK1 and was not observed in our sub-minute resolution phosphoproteomics. Our pulldowns did not reveal a membrane compartment association for myristoylated CDPK1 but did identify interacting proteins enriched in cytosolic and myristoylated CDPK1. Given the annotated functions of these interacting proteins, the factors are unlikely to participate in the motility-related functions of CDPK1. Additional studies will be required to understand how myristoylation influences CDPK1 activity.

Identification of direct CDPK1 targets through thiophosphorylation

Our phosphoproteomic time course experiment identified proteins exhibiting CDPK1-dependent phosphorylation in live parasites, which includes direct and indirect substrates of the kinase. CDPK1 is unusual among apicomplexan and metazoan kinases in that it contains a glycine at its gatekeeper residue, resulting in an expanded ATP-binding pocket that can accommodate bulky ATP analogues. CDPK1 can use bulky analogues like N6-furfuryladenosine (kinetin)-5-O-[3-thiotriphosphate] (KTPyS) to thiophosphorylate its substrates in parasite lysates (Lourido et al., 2013). Thiophosphorylated substrates can subsequently be enriched with an iodoacetyl resin (Blethrow et al., 2008). Specificity can be assessed by comparison to mutant parasites harboring a G128M gatekeeper mutation in CDPK1 (CDPK1^M) that retains kinase activity but prevents it from using KTPyS. Previous studies using lysates identified a small set of six putative CDPK1-dependent substrates; however, these studies lost the target specificity conferred by the subcellular context and lacked the accuracy and sensitivity of quantitative proteomic approaches (Lourido et al., 2013).

We implemented several modifications to the thiophosphorylation procedure that improved identification of CDPK1 targets (Figure 3A) (Rothenberg et al., 2016). First, we used stable isotope labeling of amino acids in cell culture (SILAC) to directly compare thiophosphorylation in WT (CDPK1^G) and mutant (CDPK1^M) parasites. Second, we used parasites semi-permeabilized with the bacterial toxin aerolysin—as opposed to the preparations of detergent-lysed parasites used in prior methods. Aerolysin forms 3-nm pores in the plasma membrane which permit the diffusion of small molecules but not proteins, enabling us to perform labeling reactions without drastically disrupting the concentration or localization of proteins (Iacovache et al., 2006). Lastly, we prevented non-specific extracellular substrate labeling due to premature lysis by treating semi-permeabilized parasites with 1B7, a nanobody that allosterically inhibits CDPK1 but does not enter the cytosol of semi-permeabilized parasites (Figure 3B) (Ingram et al., 2015).

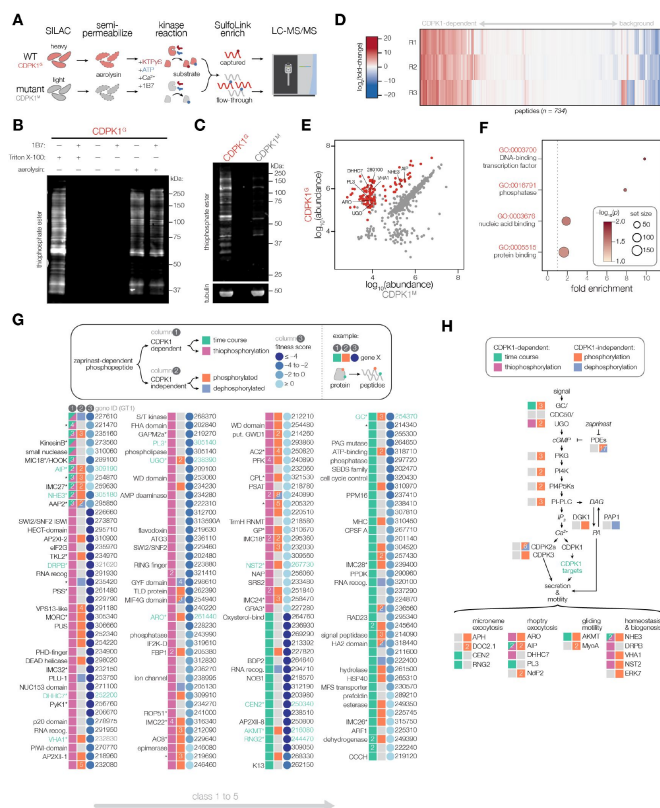


Figure 3.

Identifying the direct substrates of CDPK1.

(A) Schematic describing a strategy to identify direct substrates of CDPK1. WT (CDPK1^G) and mutant (G128M; CDPK1^M) parasites were grown in SILAC media for multiplexed quantitation. Extracellular parasites were semi-permeabilized with aerolysin, enabling diffusion of small molecules but not proteins. CDPK1 substrate labeling was initiated by treating semi-permeabilized parasites with Ca²⁺, KTPyS, ATP, and 1B7. While CDPK1 in both WT and mutant parasites can utilize ATP to phosphorylate substrates, only WT parasites can use KTPyS to thiophosphorylate substrates.

Thiophosphorylated peptides were specifically enriched and the remaining flow-through was saved for whole proteome analysis. Enriched and whole proteome samples were analyzed by LC-MS/MS. **(B)** 1B7 nanobody treatment inhibits non-specific extracellular kinase activity of CDPK1. Thiophosphorylated substrates were detected in lysates using an anti-thiophosphate ester antibody immunoblot. Extracellular CDPK1 activity (lane 1) was blocked by 1B7 (lane 2). Aerolysin treatment resulted in intracellular labeling (lane 5) that was

unaffected by 1B7 (lane 6). **(C)** Thiophosphorylation performed in aerolysin-treated parasites comparing WT (CDPK1^G) and mutant (CDPK1^M) strains. Detection was performed as in B. Tubulin was used as a loading control. **(D)** Heatmap quantification of peptides using LC-MS/MS. Fold-change of peptide abundance shown as a ratio of WT (CDPK1^G) to mutant (CDPK1^M) abundances. Experiment was performed in n = 3 biological replicates. **(E)** Abundances of unique peptides after thiophosphorylation in CDPK1^G and CDPK1^M parasites across n = 3 biological replicates. Significantly enriched phosphorylated peptides are colored in red (-log₁₀(p)*fold-change > 4), one-tailed t-test. **(F)** GO terms enriched among significant phosphopeptides from E. Significance was determined using a hypergeometric test. **(G)** Putative targets of CDPK1 determined by sub-minute phosphoproteomics and thiophosphorylation of direct substrates. For a given CDPK1 target gene, the presence of a unique peptide phosphorylated in a CDPK1-dependent manner (column 1) is indicated if identified in the time course (green) and/or thiophosphorylation (magenta). The presence of additional unique phosphorylated peptides exhibiting zaprinast-dependent effects (column 2) is indicated if the peptide was phosphorylated (orange) or dephosphorylated (blue). Numbered boxes indicate multiple unique peptides. Fitness scores (column 3) obtained from genome-wide KO screen data (blues). Lower scores indicate gene is required for lytic stages of the parasite. Gene names (left), TGGT1 gene IDs (right). Gene names with asterisks (*) are associated with published data. **(H)** Signaling diagram describing parasite motility. Proteins exhibiting CDPK1-dependent phosphorylation by either sub-minute phosphoproteomics or thiophosphorylation are indicated (green). Proteins exhibiting CDPK1-independent phosphorylation (red) or dephosphorylation (blue) are indicated.

Thiophosphorylation experiments were performed in biological triplicate comparing CDPK1^G and CDPK1^M parasites. We assessed thiophosphorylation labeling by immunoblot, identifying an array of proteins specifically labeled in CDPK1^G, but not CDPK1^M parasites (**Figure 3C**). MS analyses quantified the abundance of peptides in CDPK1^G relative to CDPK1^M parasites, identifying 734 unique peptides across three biological replicates (**Figure 3D**). Samples from CDPK1^G parasites were significantly enriched in phosphorylated peptides, consistent with CDPK1-mediated thiophosphorylation of targets (**Figure 3E**). 123 peptides across 104 proteins were likely direct substrates of CDPK1. GO enrichment analysis

treatment disrupts native ion concentrations and detaches the plasma membrane from the inner membrane complex (IMC) (Wichroski et al., 2002). We therefore proceeded to consider the thiophosphorylated substrates in the context of the time-resolved phosphoproteomics.

CDPK1 targets participate in pathways controlling parasite motility

Considering the thiophosphorylation and time-resolved phosphoproteomics, we arrived at a prioritization scheme to identify 163 proteins phosphorylated in a CDPK1-dependent manner (Figure 3G). Proteins were divided into five classes based on the overlap of phosphorylated sites between both approaches. Class 1 contains five proteins for which the same phosphorylated site was identified in both the time course and thiophosphorylation experiments. Class 2 contains four proteins for which phosphorylated sites identified across both approaches were within 50 amino acid residues of one another. Class 3 contains two proteins that were enriched by thiophosphorylation and were also CDPK1-dependent in the time course, but the identified sites were more than 50 residues apart. Class 4 contains 93 proteins that were exclusively enriched by thiophosphorylation. Lastly, Class 5 contains 59 proteins that were CDPK1-dependent exclusively in the time course and are likely indirect targets of the kinase. Proteins within each class were further stratified by fitness scores reported from genome-wide knockout screens, with lower scores representing genes more essential for parasite fitness in cell culture (Sidik et al., 2016). Of the 163 targets of CDPK1, 72 proteins across all classes also displayed changes in zaprinast-dependent phosphorylation at distinct sites that were independent of CDPK1. This overlap suggests that some proteins modified by CDPK1 are also regulated by additional kinases and phosphatases.

We hypothesized that regulators of exocytosis would be found among the targets of CDPK1. Of the 163 protein targets, 38 have been previously localized and/or functionally characterized (indicated with asterisks; Figure 3G). Of these 38 proteins, 13 have been implicated in regulating motile stages of the parasite (Figure 3H, Figure 3—figure supplement S3). Among the candidates associated with microneme exocytosis, centrin 2 (CEN2) and RNG2 have previously been localized to tubulin-based structures in the apical complex of the parasite, and their knockdown is sufficient to inhibit secretion of microneme proteins and block host cell invasion (Katris et al., 2014; Lentini et al., 2019; Leung et al., 2019). Candidates associated with rhoptry exocytosis include the armadillo repeats only protein (ARO), ARO-interacting protein (AIP), palmitoyl acyltransferase DHHC7, and patatin-like phospholipase (PL3) (Beck et al., 2013; Mueller et al., 2013; 2016; Wilson et al., 2020). ARO and DHHC7 both localize to the cytosolic face of rhoptries, where they influence the recruitment of AIP and AC. Knockdown of either DHHC7 or ARO disrupts the localization of mature rhoptries, inhibiting the secretion of rhoptry proteins required for invasion. Another potential CDPK1 target, the apical complex lysine methyltransferase (AKMT), rapidly relocates from the apical complex to the parasite body during Ca^{2+} -regulated motility, and its knockdown impairs the gliding motility of parasites required for invasion and egress (Heaslip et al., 2011). Other putative CDPK1 targets participate in homeostasis and biogenesis of secretory organelles, such as the vacuolar type Na^+/H^+ exchanger (NHE3), dynamin-related protein B (DrpB), V-ATPase a1 (VHA1), and GDP-fucose transporter (NST2). NHE3-knockout parasites exhibit sensitivity to osmotic shock and dysregulated cytosolic Ca^{2+} , resulting in reduced secretion of microneme proteins and an inhibition of invasion (Francia et al., 2011). DrpB was previously identified as a CDPK1 target, and its depletion results in severe defects in the biogenesis of micronemes and rhoptries (Breinich et al., 2009; Lourido et al., 2013). VHA1 and NST2 participate in the maturation of microneme and rhoptry proteins (Bandini et al., 2019; Stasic et al., 2019). Lastly, signaling proteins regulating intracellular cGMP levels, such as the guanylate cyclase (GC) and the unique GC organizer (UGO), were also phosphorylated in a CDPK1-dependent manner (Bisio et al., 2019; Brown and Sibley, 2018; Yang et al., 2019). CDPK1 acts downstream of GC-mediated production of cGMP,

which may suggest regulatory feedback on Ca^{2+} release, as has been suggested for CDPK3 (Nofal et al., 2022). These data demonstrate that identification of CDPK1 targets can uncover proteins involved in Ca^{2+} -regulated exocytosis.

To identify new factors involved in Ca^{2+} -regulated secretion, we prioritized Class 1 and Class 2 candidates. Seven candidates in this category lack functional annotation or have been associated with apical structures: TGGT1_227610, TGGT1_221470, TGGT1_-235160, TGGT1_254870, KinesinB (TGGT1_273560), a small nuclease (TGGT1_310060), and TGGT1_-289100 (MIC18). TGGT1_221470 was previously identified as a CDPK1 substrate after a pull down from parasite lysates but remained functionally uncharacterized (Lourido et al., 2013). KinesinB localizes to cortical microtubules, TGGT1_254870 localizes to the apical complex, and TGGT1_289100 co-localizes with micronemes, each of which are parasite structures relevant to exocytosis (Butler et al., 2014; Leung et al., 2017; Long et al., 2017). Of these candidates, only TGGT1_227610 and TGGT1_289100 appear to be required for parasite fitness (Long et al., 2017; Sidik et al., 2016). Despite prior annotation as a microneme protein, TGGT1_289100 lacks a signal peptide and is localized to the cytosol by spatial proteomics (Butler et al., 2014; Barylyuk et al., 2020). Instead, TGGT1_-289100 is predicted to have an N-terminal Hook domain and extensive coiled-coil domains (Simm et al., 2015; Söding et al., 2005) with homology to activating adaptors that bind to endosomes and activate super-processive dynein-mediated trafficking towards the minus end of microtubules (Figure 4A) (Bielska et al., 2014; Guo et al., 2016; Zhang et al., 2014). The predicted polarity of cortical microtubules and their association with micronemes support a model where the vesicles are trafficked by dyneins towards the apical end of the parasite (Chen et al., 2015; Leung et al., 2017; Wang et al., 2021). We observed extensive CDPK1-dependent phosphorylation between the Hook and coiled-coil domains of TGGT1_289100 (S167, S177, and S189–191), consistent with potential regulation of the putative adaptor. These data motivated functional characterization of this factor—henceforth referred to as HOOK.

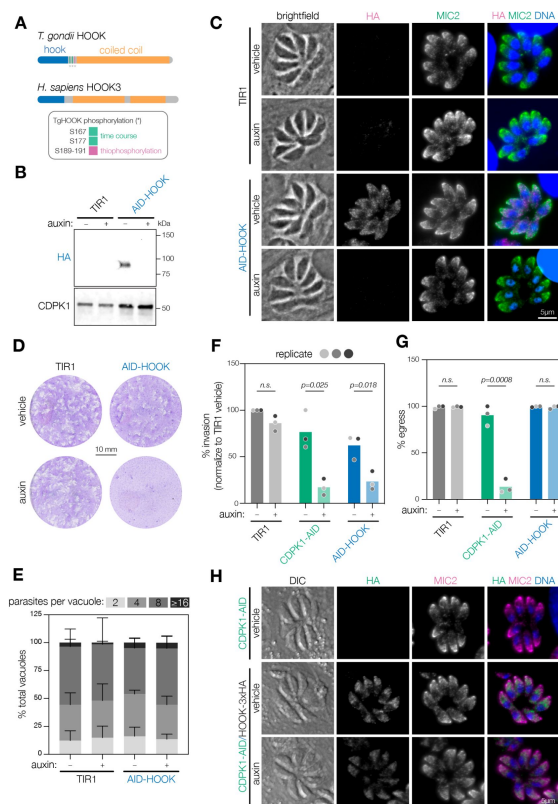


Figure 4.

HOOK is required for host cell invasion, but dispensable for egress.

(A) Schematic of *T. gondii* and *H. sapiens* HOOK protein domains. HOOK domain (blue), coiled-coil domain (yellow), sites phosphorylated by CDPK1 (red). **(B)** Immunoblot of HOOK conditional knockdown parasites (AID-HOOK) after auxin treatment for 40 hrs compared to untagged TIR1 parasites. CDPK1 was used as a loading control. **(C)** AID-HOOK is visualized in fixed intracellular parasites by immunofluorescence after auxin treatment for 24 hrs. Hoechst and MIC2 are used as counterstains. **(D)** Plaque assays of host cells infected with TIR1 or AID-HOOK parasites for 8 days in auxin. Host cells are stained with crystal violet. **(E)** Replication assays of host cells infected with TIR1 or AID-HOOK parasites in auxin for 24 hrs. Parasites per vacuole were quantified from immunofluorescence on fixed intracellular parasites. $p > 0.9$. Two-way ANOVA. **(F)** Invasion assays of untagged TIR1, CDPK1-AID, and AID-HOOK parasites treated auxin for 40 hrs. Medians are plotted for $n = 3$ biological replicates (different shades of gray); n.s., $p > 0.05$, Welch's t-test. **(G)** Parasite egress stimulated with zaprinast following treatment with auxin for 24 hrs. Egress was monitored by live microscopy. Percent egress plotted for $n = 3$ biological replicates, n.s., $p > 0.05$, Welch's t-test. **(H)** HOOK tagged with a C-terminal 3xHA in CDPK1 cKD parasites (CDPK1-AID) visualized in fixed intracellular parasites by immunofluorescence as in D.

A Hook domain protein phosphorylated by CDPK1 regulates parasite invasion

To study the role of HOOK during the acute stages of the parasite, we generated a conditional knockdown by fusing an HA-mAID tag to its N terminus (AID-HOOK; [Figure 4—Figure supplement S4](#)). HOOK was depleted from parasites following 24–40 hrs of auxin treatment, as determined by immunoblotting or immunofluorescence microscopy ([Figure 4B–C](#)). In contrast to previous observations that localized HOOK to micronemes, we observed only partial co-localization with micronemes with a majority of HOOK localized to the cytosol ([Figure 4C](#)). Plaque formation was impaired when AID-HOOK parasites were grown in the presence of auxin, consistent with the strong effect on parasite fitness reported from genome-wide knockout screens ([Figure 4D](#)) (Sidik et al., 2016). These results indicate that HOOK is required during the acute stages of *T. gondii*. Parasite replication was not affected following 24 hrs of auxin treatment ([Figure 4E](#)). Microneme and rhoptry biogenesis were also unaffected following 24 hrs of auxin treatment immunofluorescence analysis ([Figure 4C](#), [Figure 4—figure supplement S4](#)). These data suggest HOOK functions during stages associated with parasite motility, such as parasite invasion and egress. Parasites depleted of HOOK displayed reduced invasion efficiency, consistent with that of CDPK1-depleted parasites ([Figure 4F](#)). We noted that even in the absence of auxin treatment AID-HOOK parasites required longer incubations to reach comparable levels of invasion to wildtype, suggesting that manipulation of the N terminus partially affects HOOK function.

HOOK depletion only partially recapitulates the effects of CDPK1 loss. Parasites depleted of CDPK1 were unable to egress—as documented previously (Lourido et al., 2010; 2012)—whereas depletion of HOOK had no effect on parasite egress ([Figure 4G](#)). Finally, we also examined whether the stability of CDPK1 affected HOOK expression by tagging the C terminus of HOOK with a 3xHA tag in CDPK1 cKD parasites (HOOK-3xHA). HOOK localization and abundance was unaffected by depleting parasites of CDPK1 for 24 hrs as determined by immunofluorescence ([Figure 4H](#)). Taken together, our results indicate that HOOK is required for invasion of host cells, but dispensable for egress.

HOOK forms a complex that regulates parasite invasion

Opisthokont HOOK proteins function in complexes to activate dynein-mediated trafficking of vesicular cargo along microtubules (Bielska et al., 2014; Christensen et al., 2021; Gillingham et al., 2014; Guo et al., 2016; Xu et al., 2008; Yao et al., 2014). In *D. melanogaster* and mammals, HOOK proteins have been shown to form dimers and bind FTS and FHIP via a C-terminal region that interacts with vesicular cargo (Krämer and Phistry, 1996; Xu et al., 2008; Lee et al., 2018; Christensen et al., 2021). To identify analogous binding partners of HOOK in *T. gondii*, we performed IP-MS on lysates from HOOK-3xHA parasites and an untagged control ([Figure 5A](#)). Three proteins showed comparable enrichment to HOOK-3xHA: TGGT1_264050, TGGT1_316650, and TGGT1_306920. Like FTS, TGGT1_264050 bears homology to E2 ubiquitin-conjugating enzymes, but lacks the catalytic cysteine required for enzymatic activity at position 162. Because of these shared features and their homology, we designated TGGT1_264050 as FTS. To confirm that FTS forms a complex with HOOK, we investigated its localization and performed reciprocal IPs. We fused a 3xHA tag to the C terminus of FTS and observed a similar localization to HOOK by immunofluorescence: primarily cytosolic with partial overlap with micronemes ([Figure 5B](#)). To identify binding partners of FTS, we performed IP-MS on FTS-3xHA parasite lysates and compared protein enrichment to the HOOK-3xHA IP ([Figure 5C](#)). Four proteins were significantly enriched in the reciprocal IP experiments—HOOK, FTS, TGGT1_316650, and TGGT1_306920—confirming the four-member complex.

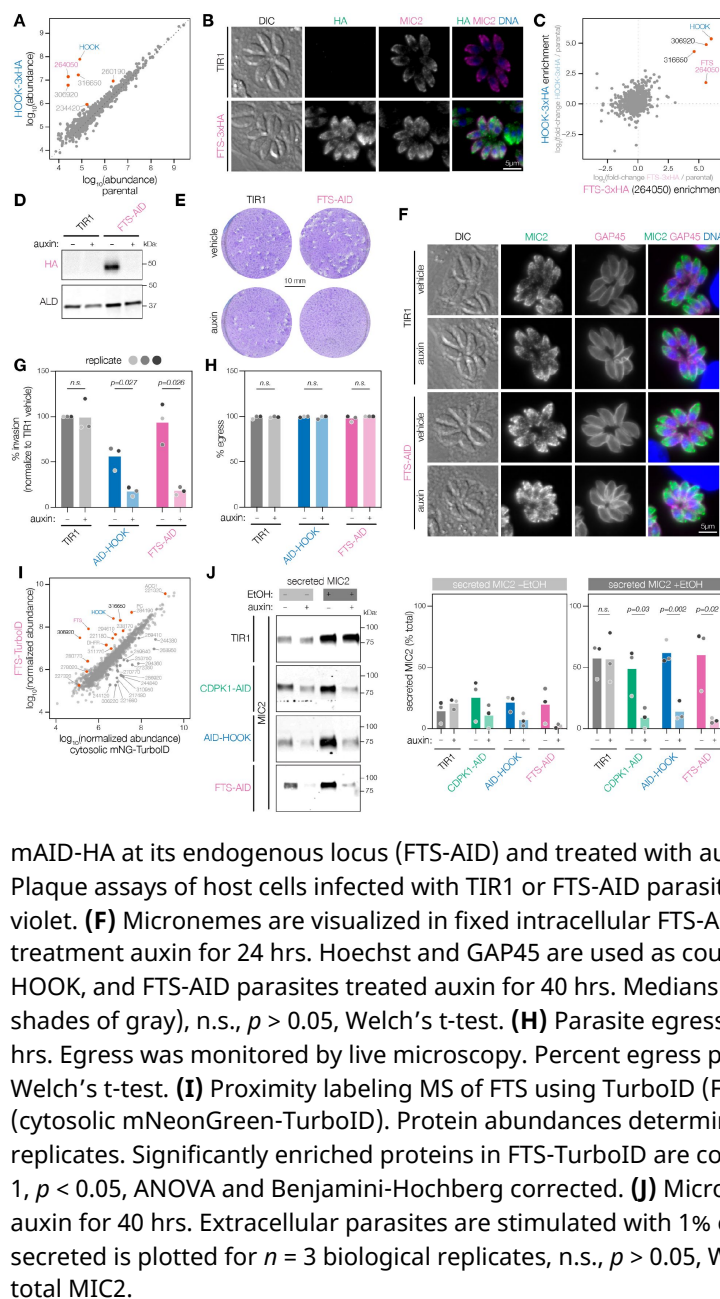


Figure 5.

The HOOK complex is required for microneme exocytosis.

(A) IP-MS of HOOK-3xHA or untagged parasites. Protein abundances determined by LC-MS/MS are shown for $n = 3$ biological replicates. Significantly enriched proteins (red) based on more than 3 unique peptides and $p < 0.05$; ANOVA and Benjamini-Hochberg corrected. **(B)** FTS-3xHA visualized in fixed intracellular parasites by immunofluorescence after treatment with auxin for 24 hrs. Hoechst and MIC2 are used as counterstains. **(C)** Reciprocal IP-MS of HOOK-3xHA and FTS-3xHA. FTS is tagged with a C-terminal 3xHA epitope at the endogenous locus (FTS-3xHA). IP enrichment is shown as the fold-change of protein abundances in tagged versus untagged strains determined by LC-MS/MS across $n = 3$ biological replicates. Significantly enriched proteins (red), for proteins with more than 3 unique peptides, $p_{HOOK} < 0.05$, and $p_{FTS} < 0.05$; ANOVA and Benjamini-Hochberg corrected. **(D)** Immunoblot of FTS cKD parasites. FTS is tagged with an C-terminal

mAID-HA at its endogenous locus (FTS-AID) and treated with auxin for 40 hrs. ALD is used as a loading control. **(E)** Plaque assays of host cells infected with TIR1 or FTS-AID parasites for 8 days in auxin. Host cells are stained with crystal violet. **(F)** Micronemes are visualized in fixed intracellular FTS-AID and TIR1 parasites by immunofluorescence after treatment auxin for 24 hrs. Hoechst and GAP45 are used as counterstains. **(G)** Invasion assays of untagged TIR1, AID-HOOK, and FTS-AID parasites treated auxin for 40 hrs. Medians are plotted for $n = 3$ biological replicates (different shades of gray), n.s., $p > 0.05$, Welch's t-test. **(H)** Parasite egress stimulated zaprinast following auxin treatment for 24 hrs. Egress was monitored by live microscopy. Percent egress plotted for $n = 3$ biological replicates, n.s., $p > 0.05$, Welch's t-test. **(I)** Proximity labeling MS of FTS using TurboID (FTS-TurboID) compared to a cytosolic TurboID control (cytosolic mNeonGreen-TurboID). Protein abundances determined by LC-MS/MS are shown for $n = 3$ biological replicates. Significantly enriched proteins in FTS-TurboID are colored in red (red and blue), unique peptides > 3, ratio > 1, $p < 0.05$, ANOVA and Benjamini-Hochberg corrected. **(J)** Microneme protein secretion assays of parasites treated with auxin for 40 hrs. Extracellular parasites are stimulated with 1% ethanol (EtOH) and 3% IFS for 1.5 hrs. Percent MIC2 secreted is plotted for $n = 3$ biological replicates, n.s., $p > 0.05$, Welch's t-test. See [Figure 5—figure supplement S5](#) for total MIC2.

To determine whether FTS functions in the same pathway as HOOK, we generated a conditional knockdown by fusing an AID-HA tag to the C terminus of FTS (FTS-AID; [Figure 5—Figure supplement S5](#)). FTS was readily depleted from parasites following 40 hrs of auxin treatment ([Figure 5D](#)). FTS depletion completely blocked plaque formation ([Figure 5E](#)). Similar to HOOK, depletion of FTS had no observable effect on parasite replication or microneme biogenesis ([Figure 5—figure supplement S5](#), [Figure 5F](#)). During the motile stages of the parasite, FTS depletion resulted in a block in invasion efficiency but had no effect on egress, phenocopying the effects of HOOK depletion ([Figure 5G](#), [Figure 5H](#)). FTS appeared to tolerate tagging better than HOOK, since the FTS-AID parasites behaved normally in the absence of auxin. These data suggest that HOOK and FTS form a functional complex required for parasite invasion.

We pursued enzyme-catalyzed proximity labeling to complement IP-MS studies and capture transient protein interactions (Branon et al., 2018). In this approach, cells express a protein

of interest tagged with the promiscuous biotin ligase TurboID. Addition of a biotin substrate to live cells results in biotinylation within a few nanometers of the TurboID-tagged protein, in a matter of minutes. Biotinylated proteins can be enriched from cellular lysates using streptavidin-affinity purification and identified using MS. Proximity labeling was recently used to characterize the cargo diversity of distinct human FHF complexes in human cells (Christensen et al., 2021). To identify additional proteins that interact with the *T. gondii* HOOK complex, we performed proximity labeling after fusing TurboID to the C terminus of FTS, which was more amenable to tagging compared to HOOK (Figure 5I, Figure 5—figure supplement S5). As a control, we used parasites expressing a cytosolic mNeonGreen-TurboID that would broadly label cytosolic proteins and identify non-specific interactions (Figure 5—figure supplement S5).

Of the 14 proteins significantly enriched in FTS-TurboID parasites, members of the HOOK complex (HOOK, FTS, TGGT1_306920, and TGGT1_316650) were the top four most enriched proteins. In humans, proximity labeling studies suggest FTS and FHIP bind at the C terminus of the HOOK dimer to mediate FHIP binding to RAB5 endosomes (Christensen et al., 2021). Our FTS proximity labeling results suggest that TGGT1_306920 and TGGT1_316650 may also bind in this manner. Among the other significantly-enriched proteins, PC and ACC1 encode carboxylases known to be covalently modified by biotin and likely represent nonspecific enrichment. DHFR enrichment is likely due to its use as a selectable marker when generating the FTS-TurboID strain. TGGT1_294610 and TGGT1_280770 are a putative histone lysine methyltransferase and regulator of chromosome condensation (RCC1)-repeat containing protein, respectively, and have no characterized functions. Of the remaining enriched proteins that lack annotations, TGGT1_221180 was previously localized to micronemes by spatial proteomics and contains a transmembrane domain, suggesting a molecular link between the HOOK complex and micronemes (Barylyuk et al., 2020).

The HOOK complex promotes invasion by regulating microneme exocytosis

To determine whether the HOOK complex is required for microneme exocytosis, we directly measured secretion of the microneme protein MIC2. Microneme exocytosis exposes integral membrane proteins like MIC2 that function as adhesins during gliding motility. These adhesins subsequently undergo proteolytic cleavage and are released into the supernatant, which can be analyzed by immunoblot (Carruthers et al., 2000). Quantification of the proportion of secreted MIC2 was performed by generating a standard curve from unstimulated lysates. Strikingly, parasites depleted of either member of the HOOK complex were severely impaired in their ability to secrete microneme proteins (Figure 5J, Figure 5—figure supplement S5). Inhibition of the complex led to a similar degree of secretion impairment as CDPK1 depletion. Together, these data suggest that HOOK and FTS form a functional complex that is required for microneme exocytosis.

Microneme trafficking depends on CDPK1 activity and HOOK

We hypothesized that if the HOOK complex is required for sustained microneme exocytosis, then depletion of HOOK would inhibit trafficking of micronemes during parasite motility. Dynamic relocation of micronemes can be visualized using live microscopy of parasites expressing the integral microneme protein CLAMP fused to mNeonGreen (CLAMP-mNG) (Figure 6A) (Sidik et al., 2016). To trigger microneme exocytosis, parasites are treated with zaprinast to stimulate a rise in intracellular Ca^{2+} and activate CDPK1. Dynamic relocation of micronemes is defined as the CLAMP-mNG signal that concentrates at the apical end of the parasite over time. To quantify microneme relocation, mNG signal is measured, over

comparing the instant of zaprinast addition to the time point just prior to parasite egress of the uninhibited zaprinast-stimulated controls (Figure 6A).

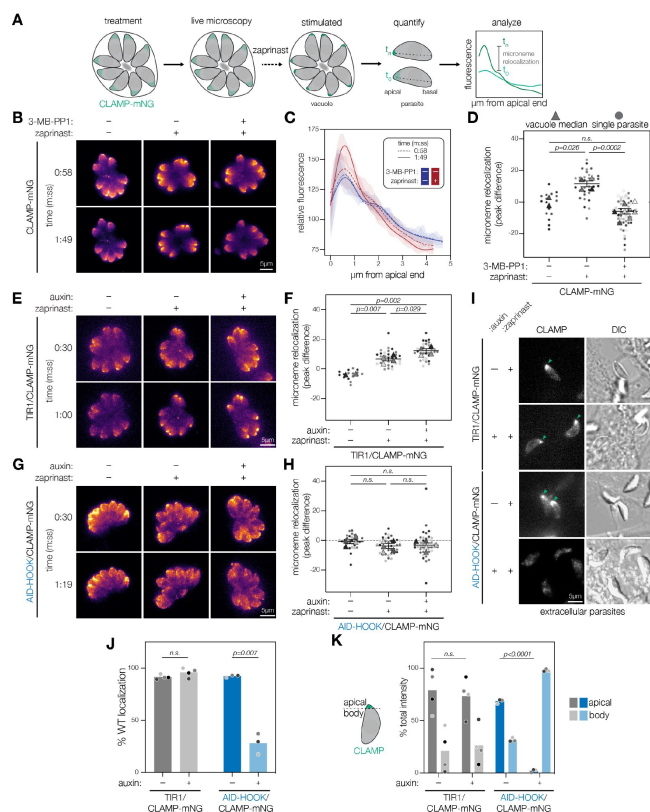


Figure 6.

CDPK1 activity and HOOK are required for microneme trafficking during parasite motility stages.

(A) Schematic to analyze microneme trafficking during parasite motile stages. Intracellular parasites expressing microneme protein CLAMP endogenously tagged with mNeonGreen (CLAMP-mNG). Parasites are treated either with 3-MB-PP1 (inhibit CDPK1) or auxin (for conditional knockdown). Live microscopy was performed to detect CLAMP-mNG signal over time. Zaprinast was added at 1 min or 30 sec to stimulate microneme relocalization to the apical end of the parasite. Fluorescence intensities across the apical-basal axis of each individual parasite within a vacuole was measured across time. Microneme relocalization was quantified by calculating the difference of maximum CLAMP intensity between time points preceding drug addition and egress. **(B)** Maximum intensity projections at single time points of CLAMP-mNG parasites treated with 3 μ M 3-MB-PP1 or vehicle and zaprinast. **(C)** Relative fluorescence intensity of CLAMP-mNG signal across the apical-basal axis of parasites in B. Zaprinast (red) or vehicle (blue). Splines mean intensity

for all parasites in each vacuole are shown with SD shaded. **(D)** Microneme relocalization. SuperPlots showing vacuole median peak differences are displayed as triangles. Individual parasites are displayed as circles. Replicates are differentially shaded, n.s., $p > 0.05$, unpaired t -test. **(E)** Maximum intensity projections at single time points of TIR1/CLAMP-mNG parasites treated with auxin and stimulated with zaprinast. **(F)** Microneme relocalization was quantified for TIR1/CLAMP-mNG parasites as in D. **(G)** Maximum intensity projections at single time points of AID-HOOK/CLAMP-mNG parasites treated auxin and stimulated with zaprinast. **(H)** Microneme relocalization was quantified for AID-HOOK/CLAMP-mNG parasites as in D. **(I)** Maximum intensity projections of extracellular TIR1/CLAMP-mNG and AID-HOOK/CLAMP-mNG parasites. **(J)** Percent of extracellular parasites in I with WT CLAMP-mNG localization, n.s., $p > 0.05$, Welch's t -test. **(K)** Percent total CLAMP-mNG signal intensity in the apical versus body of extracellular parasites, n.s., $p > 0.05$, Welch's t -test.

We first assessed whether CDPK1 kinase activity is required for microneme relocalization using the specific inhibitor 3-MB-PP1 (Lourido et al., 2010). We incubated parasites with 3-MB-PP1 for 30 min, imaged for 1 min to establish a baseline, and then stimulated with zaprinast. Parasites pre-treated with DMSO relocalized micronemes as expected; however, microneme relocalization was blocked when CDPK1 was inhibited by 3-MB-PP1 (Figure 6B–D). These results indicate microneme relocalization depends on CDPK1 kinase activity.

We next assessed whether HOOK is also required for microneme relocalization. We fused an mNG reporter to the C terminus of CLAMP in AID-HOOK parasites and TIR1 parasites as a control (Figure 6—Figure supplement S6). We treated parasites with auxin for 24 hrs prior to stimulation with zaprinast. Microneme relocalization was unaffected in TIR1/CLAMP-mNG parasites treated with auxin (Figure 6E–F). By contrast, microneme relocalization did not occur in intracellular AID-HOOK parasites regardless of auxin treatment (Figure 6G–H). We attributed the lack of relocalization in vehicle-treated parasites to the hypomorphism resulting from N-terminal tagging, which is consistent with the delayed invasion and

reduced plaque size documented for this strain. To determine whether vehicle-treated AID-HOOK parasites relocated micronemes over longer periods, we examined CLAMP-mNG localization in extracellular parasites after egress. While vehicle-treated AID-HOOK parasites were able to relocate micronemes, parasites depleted of HOOK exhibited a striking microneme localization dispersed throughout the cytosol (Figure 6I–J). As expected, TIR1/CLAMP-mNG parasites maintained the apical relocalization of micronemes regardless of auxin treatment in extracellular parasites. We used an alternative metric for microneme relocalization to account for the disorganized localization of micronemes in parasites depleted of HOOK. We quantified the percent of the total CLAMP-mNG signal localized to the apical end versus the remaining body of the parasite (Figure 6K). The apical region cutoffs were experimentally derived from vehicle-treated TIR1/CLAMP-mNG parasites and defined as the apical 12.5% of the parasite. While a majority of CLAMP-mNG signal was localized to the apical region of TIR1/CLAMP-mNG parasites, most of the CLAMP-mNG signal observed in parasites depleted of HOOK was found in the parasite body. Micronemes rapidly adopt an aberrant localization in the absence of HOOK during parasite motility. These results indicate that CDPK1 kinase activity and HOOK are required for microneme trafficking during parasite motility.

Discussion

In this study, we sought to identify new regulators of Ca^{2+} -mediated exocytosis in *T. gondii* by studying the targets of a key regulator, the kinase CDPK1. We identified 163 proteins phosphorylated in a CDPK1-dependent manner using sub-minute resolution phosphoproteomics and thiophosphorylation for direct substrate capture. We determined that myristoylation of CDPK1 contributes to the kinase's function during the lytic cycle. 13 of the identified CDPK1 targets have previously described functions in parasite motility, revealing possible points of regulation within relevant signaling pathways. Furthermore, we characterized a new regulator of microneme exocytosis called HOOK, which forms a stable complex with FTS and two other proteins. Homologs of HOOK and FTS participate in dynein-mediated vesicular trafficking in other organisms. In *T. gondii*, knockdown of HOOK or FTS blocked invasion of host cells and altered rapid microneme trafficking during Ca^{2+} -regulated motility. Overall, we show how studying parasite signaling pathways can illuminate the cellular adaptations that support parasitism.

Over the past decade, several efforts have sought to characterize phosphorylation within apicomplexans. Improvements in phosphopeptide enrichment and mass spectrometry have enabled global characterization of the phosphoproteomes from *T. gondii* tachyzoites and *P. falciparum* schizonts, trophozoites, and ring-stages (Treeck et al., 2011; Solyakov et al., 2011; Pease et al., 2013). Coupling such approaches with genetic and pharmacological tools has enabled the deconvolution of kinase-specific effects from the vast global phosphorylation program (Blomqvist et al., 2020; Fang et al., 2017; Invergo et al., 2017; Nofal et al., 2022; Pease et al., 2018; Treeck et al., 2014), revealing the activation of MyoA-mediated gliding by TgCDPK3, the roles of PbCDPK4 and PbSRPK1 during male gametogenesis, and the erythrocytic-stage effects of PfCDPK1, PfPK7, and PfCDPK5 (Blomqvist et al., 2020; Fang et al., 2017; Gaji et al., 2015; Invergo et al., 2017; Pease et al., 2018; Tang et al., 2014). Attributing individual phosphorylation events to specific kinases can be complicated by cumulative changes or adaptation of the signaling networks in knockouts. Chemical genetic approaches can more precisely inhibit the activity of a given kinase at the time of the assay, while controlling for off-target effects, and have been used to characterize PfPKG-dependent phosphorylation (Alam et al., 2015; Brochet et al., 2014). Kinetically-resolved phosphoproteomics has enabled a more nuanced understanding of signaling cascades during parasite motility (Invergo et al., 2017; Herneisen et al., 2022; Nofal et al., 2022). While such technical advances have led to more in-depth phosphoproteome mapping, identifying

the direct targets of a given kinase remains a key challenge to structuring the observed changes into signaling pathways.

To resolve direct and indirect effects on the phospho-proteome for *T. gondii* CDPK1, we combined two complementary approaches: temporally-resolved phosphoproteomics and bio-orthogonal labeling of direct substrates. We implemented several methodological advances. Rapid conditional knockdown using the auxin-inducible degron system resulted in rapid and specific depletion of the kinase of interest for the phosphoproteomic studies (Brown et al., 2018). Additionally, quantification and coverage by mass spectrometry were improved through TMTpro multiplexing and ion mobility spectrometry (FAIMS) (Van Vranken et al.; Bekker-Jensen et al., 2020). We also improved on the low coverage observed in previous thiophosphorylation experiments with parasite lysates (Lourido et al., 2013; Fang et al., 2017) by maintaining a more native signaling environment using aerolysin semi-permeabilization, SILAC-based peptide quantification, and shortened labeling times (Rothenberg et al., 2016). These approaches characterize proteome-wide phosphorylation kinetics in live parasites and reveal direct kinase-substrate relationships for CDPK1.

Myristoylation of CDPK1 contributes to its function. Contrary to previous reports describing the kinase as cytosolic or nuclear (Ojo et al., 2010; Pomel et al., 2008), we demonstrate that myristoylated CDPK1 is at least partially associated with structures that can be fractionated from the cytoplasm by differential centrifugation. Loss of myristoylation led to CDPK1 release from the insoluble fraction. The ortholog of CDPK1 in *P. berghei*, PbCDPK4, also displays myristoylation-specific functions during male gametogenesis: myristoylated PbCDPK4 is critical for the first genome replication, whereas the non-myristoylated PbCDPK4 is important for the completion of gametogenesis (Fang et al., 2017). Myristoylation could impact CDPK1's ability to access certain targets efficiently. However, such interactions appear to be too weak or transient to be captured by immunoprecipitation. Mutating the myristoylation site of CDPK1 only modestly affected ionophore-induced egress. However, minor effects in these key transitions may be magnified over repeated lytic cycles, which may explain the more substantial impact of losing CDPK1 myristoylation on plaque formation. Alternatively, other kinases may compensate for decreased CDPK1 activity, particularly under hyperactivated conditions like stimulated egress. A plausible candidate for compensation is CDPK2A, which also appears to be myristoylated, despite lacking an N-terminal MG motif, and was recently shown to display epistatic interactions with CDPK1 (Broncel et al., 2020; Shortt et al., 2022).

CDPK1 plays a critical role in the transition from the replicative intracellular stages to motile extracellular stages (Lourido et al., 2010; Shortt et al., 2022). During this transition parasites must execute rapid cellular changes that involve the exocytosis of micronemes and rhoptries, reorganization of the cytoskeleton, gliding motility, and maintenance of ion homeostasis (Blader et al., 2015). CDPK1 has also been suggested to control the actomyosin system and extrusion of the conoid (Tosetti et al., 2019). Our detailed target analysis suggests CDPK1 regulates—and possibly helps coordinate—multiple pathways. We revealed over a hundred CDPK1 targets with diverse predicted functions, including many relevant to phenotypes dependent on CDPK1. In addition to the effects on microneme trafficking examined in this study, our results point to a direct link between CDPK1 and rhoptry exocytosis. Ca^{2+} has been implicated in rhoptry discharge, as the rhoptry-localized Ca^{2+} -binding FER2 is required for rhoptry exocytosis (Coleman et al., 2018). We observed a preponderance of CDPK1-dependent phosphorylation on proteins regulating rhoptry exocytosis, including DHHC7, ARO, and AIP. Phosphorylation on ARO was observed near the N-terminal acylation sites required for rhoptry targeting and may regulate the bundling and positioning of mature rhoptries during motile stages (Mueller et al., 2016). However, formally demonstrating the relationship between Ca^{2+} /CDPK1 and rhoptry discharge is complicated

only two are docked for exocytosis at a given time (Aquilini et al., 2021; Mageswaran et al., 2021; Segev-Zarko et al., 2022). Regulating the activity of ARO during motile stages may influence the ability to mobilize and re-dock rhoptries in preparation for invasion. Considering how different CDPK1 substrates function, we expect the various phenotypes associated with CDPK1 will depend on distinct sets of substrates.

Although CDPK1 is known to mediate microneme exocytosis (Lourido et al., 2010), the precise molecular events controlling this process have remained elusive. In this study, we determined that CDPK1 activity is required for the Ca^{2+} -stimulated trafficking of micronemes to the apical end. This phenotype depends on HOOK, one of the CDPK1 targets uncovered by both global phosphoproteomics and thiophosphorylation studies. Despite prior annotation as a microneme protein (Butler et al., 2014), HOOK likely functions as an activating adaptor in *T. gondii* based on homology to other Hook proteins and the functional characterization we have performed. In particular, immunoprecipitation of HOOK identified three interacting proteins: FTS, TGGT1_316650, and TGGT1_306920. In *H. sapiens*, *A. nidulans*, and *D. melanogaster*, Hook proteins complex with FTS and FHIP (the FHF complex), to link cargo to the dynein machinery for trafficking along microtubules (Bielska et al., 2014; Gillingham et al., 2014; Guo et al., 2016; Xu et al., 2008; Yao et al., 2014). FHF complexes have been shown to recognize early endosomes via FHIP binding to RAB5 (Bielska et al., 2014; Guo et al., 2016; Zhang et al., 2014). Homology to FHIP was lacking in TGGT1_316650 and TGGT1_306920. However, genome-wide knockout screens indicate TGGT1_306920 is critical for parasite fitness, leading us to speculate that it may mediate cargo binding in a manner structurally distinct from known adaptors. Additional work will be needed to elucidate the function of the HOOK complex and to understand how it mediates trafficking of apicomplexan-specific organelles.

Our results place the HOOK complex downstream of CDPK1, regulating the stimulated relocation of micronemes to the apical end of parasites. However, the HOOK complex only partially explains CDPK1's role during egress. Whereas CDPK1 depletion blocks egress entirely, parasites depleted of HOOK or FTS exit host cells, despite subsequent defects in microneme secretion and invasion. Microneme discharge is required for egress, supplying adhesins for gliding motility and the perforin PLP1 to rupture the parasitophorous vacuole membrane (Kafsack et al., 2009). It therefore appears that the initial round of microneme discharge during egress depends on CDPK1, and only subsequent rounds require the HOOK complex. Indeed, a fraction of micronemes are already found docked at the apical complex prior to the transition from the replicative to the motile stages, and may constitute the first round of microneme exocytosis (Mageswaran et al., 2021; Sun et al., 2022). Dynein-mediated trafficking might become important immediately following egress when continuous microneme discharge is necessary, as is the case during gliding motility and invasion. Consistent with this hypothesis, depletion of the dynein light chain 8a (DLC8a) yielded similar phenotypes to HOOK and FTS knockdown: intact egress but dysfunctional microneme protein secretion, gliding motility, and invasion (Lentini et al., 2019). Loss of DLC8a also led to defects in rhoptry positioning, which were not observed in HOOK knockdowns (Lentini et al., 2019), so other activating adaptors may be involved in rhoptry trafficking. Our results suggest that the HOOK complex has been specifically adapted for microneme trafficking in *T. gondii*.

Several aspects of microneme trafficking remain to be determined. The precise nature of the dynein complex is poorly understood. Eukaryotes typically express a single cytoplasmic dynein heavy chain. In *T. gondii*, TGGT1_294550 is the top candidate for the cytoplasmic dynein heavy chain (DHC) as it contains the necessary domains, is conserved among apicomplexans, and is required for parasite fitness (Lentini et al., 2019; Sidik et al., 2016). Other putative DHCs in the *T. gondii* genome are likely axonemal dyneins required for flagellar function in sexual-stage parasites. It also remains unknown how the HOOK complex binds to micronemes. In *H. sapiens* and *D. melanogaster*, RAB5 on vesicles interacts with FHIP in the HOOK complex (Bielska et al., 2014; Gillingham et al., 2014; Guo et al., 2016; Xu et

al., 2008; Yao et al., 2014). We speculate that TGGT1_306920 may serve the role of FHIP within the HOOK complex but its binding partner on micronemes remains unknown. RAB5A and RAB5C have been implicated in the biogenesis of micronemes, but their roles during exocytosis have not been explored (Kremer et al., 2013). Understanding how micronemes are recognized may elucidate how cargo specificity is achieved and regulated.

Ca^{2+} signaling has been tuned to support apicomplexan-specific cellular processes but identifying and integrating effectors within the pathway has remained a major bottleneck. Signaling effectors conserved amongst eukaryotes are often integrated into apicomplexan cellular pathways in novel or unusual ways. Here, we identified candidate downstream effectors of the Ca^{2+} -regulated kinase CDPK1 by monitoring proteome-wide protein phosphorylation. In addition to creating a catalog of candidates for future characterization, we identified, characterized, and integrated the HOOK complex downstream of CDPK1 within the Ca^{2+} signaling network controlling microneme exocytosis. Lastly, our results are the first to implicate activating adaptors as critical factors for the pathogenesis of an apicomplexan organism by promoting exocytic trafficking.

Materials & Methods

Cell culture

T. gondii parasites were grown in human foreskin fibroblasts (HFFs, ATCC SRC-1041) maintained in DMEM (GIBCO 11965118) supplemented with 3% inactivated fetal calf serum and 10 $\mu\text{g}/\text{mL}$ gentamicin (Thermo Fisher Scientific), referred to as media. When noted, DMEM was supplemented with 10% inactivated fetal bovine serum (IFS) and 10 $\mu\text{g}/\text{mL}$ gentamicin, referred to as 10% IFS media. Parasites and HFFs were grown at 37°C/5% CO_2 unless indicated otherwise.

Parasite transfection and strain construction

Genetic background of parasite strains

T. gondii RH strains were used as genetic backgrounds for this study. All strains contain the $\Delta ku80\Delta hxprrt$ mutations to facilitate homologous recombination (Huynh and Carruthers, 2009). TIR1 expresses the TIR1-FLAG ubiquitin ligase and the CAT enzyme conferring chloramphenicol resistance (Brown et al., 2017).

Transfection

Parasites were pelleted at 1000 x *g* for 5 to 10 min and resuspended with Cytomix (10 mM KPO_4 , 120 mM KCl, 0.15 mM CaCl_2 , 5 mM MgCl_2 , 25 mM HEPES, 2 mM EDTA, 2 mM ATP, and 5 mM glutathione) and combined with DNA to a final volume of 400 μL . Parasites were electroporated using an ECM 830 Square Wave electroporator (BTX) in 4 mm cuvettes with the following setting: 1.7 kV, 2 pulses, 176 μs pulse length, and 100 msec interval.

Endogenous tagging of CDPK1 (CDPK1-AID)

CDPK1-AID was generated in the study (Shortt et al., 2022). Briefly, V5-mNG-mAID-Ty was PCR amplified from pBM050 (V5-TEV-mNG-mAID-Ty; GenBank: OM640006) to attach homology arms to TGGT1_301440 (CDPK1). DNA was co-transfected with a Cas9 expression plasmid targeting CDPK1 in TIR1 parasites. mNG-expressing parasites were isolated using FACS and subcloned by limiting dilution. Tagging was confirmed by PCR, flow cytometry, and immunoblotting.

Endogenous tagging of CDPK1 (iKD) and complementation (cWT and cMut)

Generating the inducible CDPK1 knock-down strain (iKD CDPK1). The pTUB1_YFP_mAID_3HA vector was amplified by inverse PCR using primer pair P1/P2 to substitute the 3xHA tag sequence for a Myc tag encoding sequence (Brown et al., 2017). A Cas9 expression plasmid targeting the 3'UTR of *CDPK1* was generated by inverse PCR on pSag1_Cas9-U6_-sgUPRT using primers P3/P4 (Shen et al., 2014). The sequence encoding *mAID-Myc-HXGPRT* was PCR amplified using primer pair P5/P6 and co-transfected into TIR1 parasites with the Cas9 expression plasmid. Recombinant parasites were selected 24 hrs posttransfection by addition of mycophenolic acid (MPA; 25 µg/mL) and xanthine (XAN; 50 µg/mL) to culture medium. Lines were cloned, and successful 5' and 3' integration of the *mAID-Myc-HXGPRT* cassette was confirmed using primer pairs P30/P31 and P32/P33. Absence of WT was confirmed using primers P34/P35.

Generating the cWT and cMut CDPK1 complementation strain. To generate the complementation construct, pUPRT_CDPK1_HA_T2A_GFP (GenBank: Pending), the *CDPK1* 5'UTR was amplified from genomic DNA using primer pair P7/P8. Recodonomized *CDPK1* cDNA-HA sequence was synthesized (GeneArt strings, Life Technologies) and amplified with appropriate overhangs using primers P9/P10. Sequence encoding *T2A-GFP* was amplified from an in-house unpublished plasmid using primer pair P11/P12. The three resulting fragments were Gibson cloned into the PacI-linearized pUPRT_HA vector (Reese et al., 2011). To generate the complementation construct, pUPRT_CDPK1(G2A)-HA_T2A_mCherry (GenBank: Pending), the *CDPK1* 5'UTR was amplified from genomic DNA using primer pair P13/P8. Recodonomized CDPK1-HA was amplified from pUPRT_CDPK1_HA_T2A_GFP with appropriate overhangs using primers P14/P15. Primers P13/P15 were used to introduce a G2A point mutation within *CDPK1*. Sequence encoding *T2A-mCherry* was amplified from an in-house unpublished plasmid using primer pair P11/P16. The three resulting PCR amplicons were Gibson cloned into the PacI-linearized pUPRT_HA vector. Complementation plasmids were linearized with AclI and individually co-transfected with the Cas9 expression plasmid targeting the *UPRT* locus. Transgenic parasites were subjected to 5'-fluoro-2'-deoxyuridine (FUDR) selection (5 µM) 24 hrs post transfection. Resistant parasites were cloned, and successful 5' and 3' integration was confirmed using primer pairs P36/P37 and P38/P39, respectively. Disruption of the endogenous *UPRT* locus was confirmed using primer pair P40/P41.

Endogenous tagging of genes

Genes were endogenously tagged using the previously described high-throughput tagging (HiT) strategy (Smith et al., 2022). Cutting units specific to each gene were purchased as gene fragments (IDT gBlocks; P22 and P23) and integrated with the following empty HiT vector backbones via Gibson assembly: pALH086 (V5-mAID-HA; GenBank: ON312869), pALH047 (V5-3HA; GenBank: ON312868), and pALH173 (TurboID-Ty; GenBank: Pending).

Between 30 and 50 µg of each vector was linearized with BsaI and co-transfected with 50 µg of the pSS014 Cas9 expression plasmid (GenBank: OM640002). Vectors targeting *TGGT1_289100* (*HOOK*) were transfected into TIR1 or CDPK1-AID. Vectors targeting *TGGT1_264050* (*FTS*) were transfected into TIR1. Parasites underwent drug selection for approximately 1 week in 10% IFS media with 3 µM pyrimethamine or 25 µg/mL mycophenolic acid and 50 µg/mL xanthine, followed by subcloning into 96-well plates. Single clones were screened for tag expression by PCR, immunofluorescence, or immunoblot. PCR validation was performed using the primers P44/P45 (FTS-AID) and P46/P47 (FTS-TurboID).

Endogenous tagging of HOOK N terminus

AID-HOOK N-terminal tagging was generated by PCR amplifying the gene fragment encoding the *HA-mAID* with homology arms to *HOOK* (IDT gBlock; P17) using the primers P18/19. A

sgRNA targeting *HOOK* was assembled into the pSS013 Cas9 expression plasmid (GenBank: OM640003) using the primers P20/P21. 10 µg of the PCR product was transfected with 50 µg of the Cas9 expression plasmid. Parasites were subcloned into 96-well plates. Single clones were screened using PCR primers P42/P43 and validated by immunofluorescence and immunoblot.

TIR1/pMIC2-mNeonGreen-TurboID-Ty

pMIC2-mNG-TurboID-Ty was amplified with primers P24/P25 from pALH184 (pMIC2-mNG-TurboID-Ty-3'DHFR; GenBank: Pending) with homology arms to the 5 and 3 ends of a defined, neutral genomic locus (Markus et al., 2019). Amplified DNA was cotransfected with the Cas9 expression plasmid targeting the neutral locus (pBM041; GenBank: MN019116). mNeonGreen-expressing parasites were isolated by FACS and subcloned in 96-well plates. Expression was confirmed by fluorescence.

Endogenous tagging of CLAMP mNeonGreen

DNA was amplified using PCR from pGL015 (V5-mNG-mAID-Ty; GenBank: OM640005) with homology arms targeting the C terminus of *TGGT1_265790* (*CLAMP*) using the primers P26/P27. A sgRNA targeting *CLAMP* was assembled into the pSS013 Cas9 expression plasmid (GenBank: OM640003) using the primers P28/P29. Between 5 and 10 µg of *mNeonGreen* DNA was co-transfected with 50 µg of the Cas9 expression plasmid targeting *CLAMP* into TIR1 and AID-HOOK. Parasites were grown in 10% IFS media until lysing the HFF monolayer, followed by FACS-mediated isolation of mNeonGreen expressing parasites and subcloning into 96-well plates. Single clones were screened for mNeonGreen expression by PCR using primers P48/P49 and live microscopy.

Sub-minute phosphoproteomics

Parasite harvest and treatment

T. gondii tachyzoites from the RH strain CDPK1-AID were used to infect nine 15 cm dishes. 3.75×10^7 parasites were used to infect each dish in 20 mL of media. Approximately 24 hrs later, the media of eight dishes was replaced with 15 mL of media containing 1 µM of compound 1 to block egress and synchronize parasites by inhibiting PKG (Donald et al., 2006; Hopp et al., 2012; Taylor et al., 2010). The media of the ninth dish was replaced with media containing DMSO. On day 2, parasites were harvested when the monolayer of HFFs in the DMSO dish were approximately 80% lysed. The eight dishes treated with compound 1 were washed once with 10 mL of warm 1X PBS, once with 30 mL of warm 1X PBS, and incubated with 10 mL of warm FluoroBrite (Fluorobrite DMEM A1896701, 4 mM glutamine, 10 µg/mL gentamicin) for 10 min at 37°C. Infected HFFs were scraped and passed through a 27G needle to mechanically liberate parasites and passed through a 5 µm filter. Parasites were pelleted at 1000 x g at 4°C for 10 min, resuspended in 10 mL of FluoroBrite and a 1:250 dilution was used to count parasites (approximately 2.25×10^9 total parasites).

Parasites were pelleted at 1000 x g at 4°C for 7 min and resuspended in 2 mL of FluoroBrite. 1 mL of parasites were diluted into a total volume of 40 mL of FluoroBrite containing either 500 µM of auxin or vehicle of 1X PBS and incubated at 37°C for 3.5 hrs. 50 µL of auxin- or vehicle-treated parasites and untagged TIR1 parasites were analyzed by flow cytometry (Miltenyi MACSQuant VYB) to detect mNeonGreen fluorescence. After confirming depletion of CDPK1, parasites were pelleted at 1000 x g for 10 min at room temperature and resuspended in 210 µL of 500 µM auxin or vehicle of PBS diluted in FluoroBrite. To obtain a time course, the 0 sec time point was first collected by mixing 16 µL of parasites with 4 µL of 5X DMSO (0.5% DMSO in FluoroBrite) and immediately lysed with 20 µL of 2X Lysis Buffer (10% SDS, 100 mM TEAB pH 7.5, 2 mM MgCl₂, and 2X HALT protease and phosphatase

inhibitors). To obtain the 9, 30, and 300 sec time points, 80 μ L of parasites in 1.5 mL tubes were incubated in a ThermoMixer (Eppendorf) set to 37°C. The parasites were stimulated by adding 20 μ L of warmed 5X zaprinast (500 μ M zaprinast in FluoroBrite) or a vehicle of 5X DMSO. At each time point, 20 μ L of stimulated parasites were transferred directly into 20 μ L of 2X Lysis Buffer to quench the reaction. Complete time courses were collected sequentially in the following order: auxin-treated stimulated with zaprinast, vehicle-treated stimulated with zaprinast, auxin-treated stimulated with DMSO, and vehicle-treated stimulated with DMSO. Lysates were treated with benzonase at a final concentration of 5 units/ μ L to remove DNA and were immediately subjected to protein cleanup and digestion.

Protein cleanup and digestion

Proteins were prepared for mass spectrometry using a modified version of the S-trap protocol (Protifi). Proteins in lysates were reduced with 5 mM TCEP for 10 min at 55°C and alkylated with 15 mM MMTS for 10 min at room temperature. The lysates were acidified to a final concentration of 1.2% v/v phosphoric acid. A 6X volume of S-trap binding buffer (90% methanol, 100 mM TEAB, pH 7.55) was mixed to each sample to precipitate proteins. The solution was loaded onto S-trap micro columns (Protifi) and spun at 4,000 \times g for 1 min until all the solution had passed through the column. The columns were washed four times with 150 μ L of S-trap binding buffer and centrifuged at 4,000 \times g for 1 min between each wash. Proteins were digested on-column with 0.75 μ g of trypsin (Promega) in 50 mM TEAB pH 8.5 overnight at 37°C in a humidified incubator. Digested peptides were eluted in three steps at 4,000 \times g for 1 min: 40 μ L of 50 mM TEAB, 40 μ L of 0.2% formic acid, and 35 μ L of 50% acetonitrile/0.2% formic acid. The peptide concentrations of eluted peptides were quantified using the Pierce Fluorometric Peptide Assay (Thermo Fisher Scientific) according to manufacturer's instructions. The remaining samples were frozen in liquid nitrogen and lyophilized.

TMTpro labeling

Lyophilized peptides were resuspended in 100 mM TEAB pH 8.5 to peptide concentrations of 1.6 μ g/ μ L. TMTpro reagents (Thermo Fisher Scientific; A44522 LOT# VI306829) were resuspended in acetonitrile to 25 μ g/ μ L. 80 μ g of peptides in 50 μ L were combined with 250 μ g of TMTpro reagent in 10 μ L to achieve approximately a 3:1 label:peptide weight/weight ratio (Zecha et al., 2019). The TMTpro labels were assigned to minimize reporter ion interference and inter batch variability in the following scheme: Replicate 1 auxin: 0, 9, 30, 300 sec (126, 128C 130C, 132C); Replicate 1 vehicle: 0, 9, 30, 300 sec (127N, 129N, 131N, 133N); Replicate 2 auxin: 0, 9, 30, 300 sec (127C, 129C, 131C, 133C); Replicate 2 vehicle: 0, 9, 30, 300 sec (128N, 130N, 132N, 134) (Brenes et al., 2019). The zaprinast and DMSO samples were incubated for 1 hr at room temperature shaking at 400 rpm. Unreacted TMTpro reagent was quenched with hydroxylamine at a final concentration of 0.2%. The samples were pooled, acidified to 3% with formic acid, and were processed using the EasyPep Maxi Sample Prep column (Thermo Fisher Scientific) according to the manufacturer's instructions. 5% of the eluate volume was reserved as the unenriched proteome sample. The remaining eluted peptides were frozen in liquid nitrogen and lyophilized.

Phosphopeptide enrichment

Phosphopeptides were enriched using the Sequential enrichment from Metal Oxide Affinity Chromatography (SMOAC) protocol according to manufacturer instructions (Tsai et al., 2014). First, the High-Select TiO₂ Phosphopeptide Enrichment Kit (Thermo Fisher Scientific) was used to enrich phosphopeptides from lyophilized TMTpro-labeled samples. The flow-through and contents of the first wash were pooled, frozen in liquid nitrogen, and lyophilized, along with the eluate. Second, the High-Select Fe-NTA Phosphopeptide Enrichment Kit (Thermo Fisher Scientific) was used to enrich phosphopeptides from the pooled flow-through and

first wash from the previous enrichment. The eluted phosphopeptides were frozen in liquid nitrogen and lyophilized.

Fractionation

The enriched and unenriched samples were fractionated with the Pierce High pH Reversed-Phase Peptide Fractionation Kit (Thermo Fisher Scientific) according to manufacturer instructions for TMT-labeled peptides. The acetonitrile wash was omitted for enriched samples to prevent loss of phosphopeptides. The eluted peptides from the High-Select TiO₂ Phosphopeptide Enrichment and High-Select Fe-NTA Phosphopeptide Enrichment were pooled prior to fractionation. 100 µg of unenriched samples were fractionated. 8 fractions were collected for each TMTpro set: zaprinast phosphoproteome (enriched) [1], zaprinast proteome (unenriched) [2], DMSO phosphoproteome (enriched) [3], and DMSO proteome (unenriched) [4]. The fractions were frozen in liquid nitrogen and lyophilized.

MS data acquisition

Lyophilized peptides were resuspended in approximately 15 µL (enriched) or 50 µL (unenriched) of 0.1% formic acid and were analyzed on an Exploris 480 Orbitrap mass spectrometer equipped with a FAIMS Pro source (Bekker-Jensen et al., 2020) connected to an EASY-nLC 1200 chromatography system using 0.1% formic acid as Buffer A and 80% acetonitrile/0.1% formic acid as Buffer B. Peptides were loaded onto a heated analytical column (ES900, Thermo, PepMap RSLC C18 3 µm, 100 Å, 75 µm x 15 cm, 40°C) via trap column (164946, Thermo, Acclaim PepMap C18 3 µm, 100 Å, 75 µm x 20 mm nanoViper). Peptides were separated at 300 nL/min. Enriched samples were separated on a gradient of 5–20% B for 110 min, 20–28% B for 10 min, 28–95% B for 10 min, 95% B for 10 min, 95–2% B for 2 min, 2% B for 2 min, 2–98% B for 2 min, 98% B for 2 min, 98–2% B for 2 min, and 2% B for 2 min. Unenriched samples were separated on a gradient of 5–25% B for 110 min, 25–40% B for 10 min, 40–95% B for 10 min, 95% B for 10 min, 95–2% B for 2 min, 2% B for 2 min, 2–98% B for 2 min, 98% B for 2 min, 98–2% B for 2 min, and 2% B for 2 min. The orbitrap and FAIMS were operated in positive ion mode with a positive ion voltage of 1800V; with an ion transfer tube temperature of 270°C; using a standard FAIMS resolution and compensation voltage of –50 and –65V, an inner electrode temperature of 100°C and outer electrode temperature 80°C with 4.5 mL/min carrier gas. DDA analysis was performed with a cycle time of 1.5 sec. Full scan spectra were acquired in profile mode at a resolution of 60,000, with a scan range of 400–1400 m/z, 300% AGC target, maximum injection time of 50 msec, intensity threshold of 5 x 10⁴, 2–5 charge state, dynamic exclusion of 30 sec, mass tolerance of 10 ppm, purity threshold of 70%, and purity window of 0.7. MS2 spectra were generated with a HCD collision energy of 32 at a resolution of 45,000 using TurboTMT settings with a first mass at 110 m/z, an isolation window of 0.7 m/z, 200% AGC target, and maximum injection time of 120 msec.

Phosphoproteomic time course analysis

Raw files were analyzed in Proteome Discoverer 2.4 (Thermo Fisher Scientific) to generate peak lists and protein and peptide IDs using Sequest HT (Thermo Fisher Scientific) and the ToxoDB release 49 GT1 protein database. The maximum missed cleavage sites for trypsin was limited to 2. Precursor and fragment mass tolerances were 10 ppm and 0.02 Da, respectively. The following modifications were included in the search: dynamic oxidation (+15.995 Da; M), dynamic phosphorylation (+79.966 Da; S,T,Y), dynamic acetylation (+42.011 Da; N-terminus), static TMTpro (+304.207 Da; any N-terminus), static TMTpro (+304.207 Da; K), and static methylthio (+45.988 Da; C). TMTpro 16plex isotope correction values were accounted for (Thermo Fisher Scientific; A44522 LOT# VI306829). Peptides identified in each sample were filtered by Percolator to achieve a maximum FDR of 0.01 (Käll et al., 2007; 2008a; b). Site localization scores were generated using ptmRS, with phosphoRS and use of

diagnostic ions set to true (Taus et al., 2011). Reporter ion quantification used an integration tolerance of 20 ppm on the most confident centroid. For reporter ion quantification, unique peptides were quantified using a co-isolation threshold of 50, and average reporter signal-to-noise ratio of 10. Abundances were normalized on the total protein amount. Protein level and peptide level ratios were generated for each time point relative to 0 sec vehicle-treated parasites stimulated with DMSO.

Exported peptide and protein abundance files from Proteome Discoverer 2.4 were loaded into R (version 4.1.1). To determine CDPK1-dependent phosphorylation, log₂ ratios for peptide abundances in DMSO and zaprinast-treated samples derived from Proteome Discoverer were used. Only phosphorylated peptides quantified across all time points were used for analysis. Area under the curve (AUC) values were calculated for individual peptides undergoing vehicle (AUC_{vehicle}) and auxin (AUC_{auxin}) treatment using trapezoidal integration. AUC differences (AUC_{difference}) were calculated by taking the difference between AUC_{vehicle} and AUC_{auxin} values. The distribution of zaprinast AUC_{difference} values were tested against a null distribution derived from the DMSO AUC_{difference} values to calculate z-scores and p-values using a two-tailed t-test. Replicates 1 and 2 were analyzed independently and phosphopeptides with p-values < 0.05 across both replicates were determined to be CDPK1-dependent (Group A). Peptides exhibiting phosphorylation independent of CDPK1 (Group B, C, and D) were determined similarly, but compared the distribution of zaprinast AUC_{vehicle} values to a null distribution of DMSO AUC_{vehicle} values and excluded phosphopeptides already determined to be CDPK1-dependent. CDPK1-independent phosphopeptides were clustered into Groups B, C, and D using projection-based clustering (Thrun and Ultsch, 2021).

Gene ontology enrichment

Gene ontology terms were obtained for all genes present in the enriched zaprinast phosphoproteome from [ToxoDB.org](https://toxodb.org) (Computed GO function and GO function IDs). Gene ontology IDs within each group of zaprinast-dependent genes (Groups A-D) were tested for enrichment against the entire enriched zaprinast phosphoproteome. Enrichment *p* values were generated using a hypergeometric test. Enrichment ratios were calculated by dividing the gene ratio (overlap/signatures) by the relative frequency of gene sets (gene sets/background). Only GO IDs with significant enrichment and an overlap of 2 were plotted. Thiophosphorylation enrichment was performed similarly.

Metabolic tagging, click reaction, pull down, and Western blotting

Metabolic tagging and cell lysis

Upon infection of HFF monolayers the medium was removed and replaced by fresh culture media supplemented with 25 μM YnMyr (Iris Biotech) or Myr (Tokyo Chemical Industry). The parasites were then incubated for 16 hrs, washed with PBS (2x) and lysed on ice using a lysis buffer (PBS, 0.1% SDS, 1% Triton X-100, EDTA-free complete protease inhibitor (Roche Diagnostics)). Lysates were kept on ice for 20 min and centrifuged at 17,000 × *g* for 20 min to remove insoluble material. Supernatants were collected and protein concentration was determined using a BCA protein assay kit (Pierce).

Click reaction and pull down

Lysates were thawed on ice. Proteins (100–300 μg) were taken and diluted to 1 mg/mL using the lysis buffer. A click mixture was prepared by adding reagents in the following order and by vortexing between the addition of each reagent: a capture reagent (stock solution 10 mM

in water, final concentration 0.1 mM), CuSO₄ (stock solution 50 mM in water, final concentration 1 mM), TCEP (stock solution 50 mM in water, final concentration 1 mM), TBTA (stock solution 10 mM in DMSO, final concentration 0.1 mM) (Heal et al., 2011). Capture reagent used herein was the Trypsin cleavable reagents (Broncel et al., 2020). Following the addition of the click mixture the samples were vortexed (room temperature, 1 hr), and the reaction was stopped by addition of EDTA (final concentration 10 mM). Subsequently, proteins were precipitated (chloroform/methanol, 0.25:1, relative to the sample volume), the precipitates isolated by centrifugation (17,000 x g, 10 min), washed with methanol (1 x 400 µL) and air dried (10 min). The pellets were then resuspended (final concentration 1 mg/mL, PBS, 0.4 % SDS) and the precipitation step was repeated to remove excess of the capture reagent. Next, samples were added to 15 µL of pre-washed (0.2 % SDS in PBS (3 x 500 µL)) Dynabeads® MyOne™ Streptavidin C1 (Invitrogen) and gently vortexed for 90 min. The supernatant was removed, and the beads were washed with 0.2 % SDS in PBS (3 x 500 µL).

SDS-PAGE and Western blotting Beads were supplemented with 2% SDS in PBS (20 µL) and 4x SLB (Invitrogen), boiled (95°C, 10 min), centrifuged (1,000 x g, 2 min) and loaded on 10% or 4–20% SDS-PAGE gel (Bio-Rad). Following electrophoresis (60 min, 160V), gels were briefly washed with water and proteins were transferred (25 V, 1.3 A, 7 min) onto nitrocellulose membranes (Bio-Rad) using Bio-Rad Trans Blot Turbo Transfer system. After brief wash with PBS-T (PBS, 0.1% Tween-20) membranes were blocked (5% milk, TBS-T, 1h) and incubated with primary antibodies (5% milk, TBS-T, overnight, 4°C) at the following dilutions: rat anti-HA (1:1000; Roche Diagnostics), mouse anti-Myc (1:1000; Millipore), rabbit anti-Gra29 (1:1000; Moritz Treeck Lab), rabbit anti-SFP1 (1:1000; Moritz Treeck Lab), mouse anti-*T. gondii* [TP3] (1:1000; Abcam), mouse anti-CDPK1 (1:3000; John Boothroyd Lab), rabbit anti-SAG1 (1:10,000; John Boothroyd Lab), rabbit anti-GAP45 (1:1000; Peter Bradley Lab), mouse anti-GFP (1:1000, Roche Diagnostics) and rabbit anti-mCherry (1:1000, Abcam). Following washing (TBS-T, 3x) membranes were incubated with IR dye-conjugated secondary antibodies (1:10,000, 5% milk, TBS-T, 1 hr) and after a final washing step imaged on a LiCOR Odyssey imaging system (LI-COR Biosciences).

MS detection of myristoylated CDPK1

Mass spectrometry proteomics methods and data for myristoylated CDPK1 are available from the ProteomeXchange Consortium via the PRIDE partner repository (ID PXD019677) and the associated publication (Broncel et al., 2020).

Depletion of mAID tagged CDPK1 (iKD)

Parasites were treated with 500 µM auxin or equivalent volume of vehicle (ethanol) for at least 2 hrs prior to Western blot analysis.

Subcellular fractionation

RH $\Delta ku80\Delta hxp1$ YFP expressing parasites were metabolically tagged with 25 µM Myr or YnMyr for 16 hrs. Following a PBS wash, the parasites were syringe lysed in Endo buffer (44.7 mM K₂SO₄, 10 mM MgSO₄, 106 mM sucrose, 5 mM glucose, 20 mM Tris—H₂SO₄, 3.5 mg/mL BSA, pH 8.2) and collected by centrifugation (512 x g, 10 min). The parasites were then lysed in 300 µL of cold hypotonic buffer (10 mM HEPES, pH 7.5) supplemented with protease inhibitors (Roche), passed through 25G needle (5x) and left on ice for 40 min. Next, lysates were pelleted by centrifugation (16,000 x g, 20 min, 4 °C) and the resulting supernatant was subjected to an additional high speed (100,000 x g, 1 hr, 4 °C) centrifugation step. To avoid the loss of the high-speed pellet, only half of the supernatant was removed at this point. Each fraction was then taken up in 0.4% (final) SDS HEPES, clicked to a capture

reagent and pulled down as described above. Myristoylation-dependent partitioning was revealed by SDS-PAGE and Western blotting.

Myristoylation-dependent fractionation for CDPK1 complemented WT and Mut lines: parasites were seeded 24 hrs prior experiment. Following a PBS wash, the parasites were syringe lysed in Endo buffer (44.7 mM K_2SO_4 , 10 mM $MgSO_4$, 106 mM sucrose, 5 mM glucose, 20 mM Tris— H_2SO_4 , 3.5 mg/mL BSA, pH 8.2) and collected by centrifugation (512 x g, 10 min). The parasites were then lysed in 300 μ L of cold hypotonic buffer (10 mM HEPES, pH 7.5) supplemented with protease inhibitors (Roche), passed through 25G needle (5x) and left on ice for 40 min. Next, lysates were pelleted by centrifugation (100,000 x g, 1 hr, 4 °C), the supernatant was removed, and cytosolic proteins precipitated with methanol/chloroform. Proteins from the pellet and supernatant fractions were dissolved in 2% (final) SDS PBS and myristoylation-dependent partitioning was revealed by SDS-PAGE and Western blotting.

Immunoprecipitation of cWT and cMUT CDPK1

Parasite harvest

cWT, cMUT, and TIR1 (untagged) parasites were infected onto confluent HFFs in 15 cm dishes. At 1-day post-infection (dpi), 50 μ M auxin or vehicle was added to deplete endogenous mAID-tagged CDPK1 and 1 μ M compound 1 was added to block egress until parasites were ready to harvest. At 2 dpi, infected HFFs were washed twice with PBS to wash out drugs. Parasites were mechanically released in Endo buffer with a 27G needle, passed through a 5 μ m filter, and spun at 1000 x g for 10 min. Parasite pellets were resuspended in a cold hypotonic buffer with 1X HALT protease inhibitors to parasite concentrations of 1.1×10^9 tg/mL, passed through a 27G needle five times, and incubated on ice for 1 hr to complete hypotonic lysis. The samples were spun at 1000 x g for 5 min to pellet unlysed parasites and the supernatant was saved. NaCl was added to a final concentration of 150 mM and this was used as the immunoprecipitation input.

Immunoprecipitation

25 μ L of anti-HA magnetic beads (Thermo) were used per condition. Beads were washed twice with a wash buffer (10 mM HEPES, 150 mM NaCl, pH 7.5). To begin pulldown, parasite lysate was used to resuspend washed beads and incubated for 1 hr rotating at room temperature. Beads were washed four times with a wash buffer. Proteins were eluted by resuspending beads in 20 μ L of 1X S-trap sample buffer (5% SDS, 50 mM TEAB, pH 7.5) and incubated at 70°C for 10 min. The eluate was collected for MS sample processing and analysis. Results are representative of two independent experiments.

Protein cleanup and digestion

Proteins were prepared for mass spectrometry as described above in “Sub-minute phosphoproteomics - Protein cleanup and digestion”. Eluted peptides were frozen in liquid nitrogen, lyophilized, and stored at -80°C until MS analysis.

MS data acquisition

Lyophilized peptides were resuspended in 20 μ L of 0.1% formic acid and were analyzed on an Exploris 480 Orbitrap mass spectrometer equipped with a FAIMS Pro source (Bekker-Jensen et al., 2020) connected to an EASY-nLC chromatography system using 0.1% formic acid as Buffer A and 80% acetonitrile/0.1% formic acid as Buffer B. Peptides were separated at 300 nL/min on a gradient of 1–6% B for 1 min, 6–21% B for 41 min and 30 sec, 21–36% B for 20 min and 45 sec, 36–50% B for 10 min and 15 sec, 100% B for 14 min and 30 sec, 100–2% B for 3 min, 2% B for 3 min, 2–98% B for 3 min, and 98% B for 3 min. The orbitrap and FAIMS

were operated in positive ion mode with a positive ion voltage of 1800V; with an ion transfer tube temperature of 270°C; using a standard FAIMS resolution and an inner and outer electrode temperature of 100°C with 4.5 mL/min carrier gas. Samples were analyzed twice in DIA mode with a compensation mode of -50 and -65V. Full scan spectra were acquired in profile mode at a resolution of 120,000, with a scan range of 400–1000 m/z, 300% AGC target, and auto mode for maximum injection time. MS2 spectra for the DIA scan were generated with a isolation window of 20 m/z with a 0 m/z window overlap, 30 scan events, a HCD collision energy of 30 at a resolution of 30,000, first mass at 200 m/z, precursor mass range of 400–1000 m/z, and a standard AGC target and automatically determined maximum injection time.

Immunoprecipitation data analysis

DIA-MS samples were analyzed using Scaffold DIA (2.0.0). DIA-MS data files were converted to mzML format using ProteoWizard (3.0.19254) (Chambers et al., 2012). Analytic samples were aligned based on retention times and individually searched against dku80_-FAIMS_DIA_90min_autoIT.blib with a peptide mass tolerance of 10 ppm and a fragment mass tolerance of 0.02 Da. The ToxoDB release 46 GT1 protein database was used for protein identification. The following modifications were included in the search: dynamic oxidation (+15.995 Da; M), dynamic phosphorylation (+79.966 Da; S,T,Y), and static methylthio (+45.988 Da; C). The digestion enzyme was trypsin with a maximum of 2 missed cleavage sites allowed. Only peptides with charges in the range of 2 to 3 and length in the range 6 to 30 were considered. Peptides identified in each sample were filtered by Percolator to achieve a maximum FDR of 0.01 ((Käll et al., 2007), (2008a),b). Individual search results were combined, and peptide identifications were assigned posterior error probabilities and filtered to an FDR threshold of 0.01 by Percolator. Peptide quantification was performed by Encyclopedia (0.9.2). For each peptide, the 5 highest quality fragment ions were selected for quantification. Proteins that contained similar peptides and could not be differentiated based on MS/MS analysis were grouped to satisfy the principles of parsimony. Protein groups were thresholded to achieve a protein FDR less than 1%. Significance values were derived from t-tests across two replicates and adjusted with Benjamini-Hochberg correction with an FDR of 0.05. Exported protein abundance files from Scaffold DIA were loaded into R (version 4.1.1).

Thiophosphorylation of CDPK1 substrates

Parasite harvest and treatment

T. gondii tachyzoites from the RH strain (CDPK1^G and CDPK1^M) were passaged twice across 4 days in SILAC media in T12.5 flasks. CDPK1^G parasites were grown in “heavy” SILAC media (DMEM 88364, 10% dialyzed FBS, 0.1 mg/mL ¹³C¹⁵N L-arginine, 0.1 mg/mL ¹³C¹⁵N L-lysine) and CDPK1^M parasites were grown in “light” SILAC media (DMEM 88364, 10% dialyzed FBS, 0.1 mg/mL L-Arginine, 0.1 mg/mL L-Lysine). On day 4, confluent HFFs in 15 cm dishes were infected with CDPK1^G and CDPK1^M parasites in SILAC media. On day 6, extracellular parasites were harvested by filtering through a 5 µm filter and pelleted at 1000 x g for 7 min at 4°C. Parasites were washed once in 1X intracellular buffer (ICB) (137 mM KCl, 5 mM NaCl, 20 mM HEPES, 10 mM MgCl₂, pH 7.5 KOH) and then resuspended in 400 µL of 1X ICB. Parasites were semi-permeabilized after the addition of 400 µL of 6 µg/mL aerolysin diluted in 1X ICB and incubated at 37°C for 10 min. After semi-permeabilization, 400 µL of 4X Ca²⁺ solution (16 mM CaEGTA, 100 ng/mL 1B7 nanobody in 1X ICB) followed by 400 µL of 4X ATP solution (4 mM GTP, 0.4 mM ATP, 0.2 mM KTPyS, 1X HALT protease and phosphatase inhibitor in 1X ICB). The kinase reaction was initiated by incubating parasites at 30°C for 5 min. Parasites were pelleted at 1000 x g at 4°C for 10 min. Parasite pellets were resuspended in 250 µL of 1X lysis buffer (10% TritonX-100, 1X HALT protease and phosphatase inhibitor, 10 mM K₂EGTA in 1X ICB).

Protein quantification and thiophosphorylation immunoblotting

Proteins in lysates were quantified using DC assay (BioRad) utilizing BSA as a protein standard and a diluent (150 mM NaCl, 20 mM Tris pH 7.6) to prepare standard curves and dilution series. Thiophosphorylation was verified using immunoblot by first incubating 3 μ L of sample with p-nitrobenzyl mesylate diluted in 1X ICB at a final concentration at 2 mM for 2 hrs at room temperature. 5X Laemmli sample buffer was added (see “Immunoblotting” for recipe) and samples were boiled for 10 min. Samples were resolved on a homemade polyacrylamide gel (5% stacking, 15% resolving, 15-well, 0.75 mm) and transferred overnight at 4°C. Nitrocellulose membranes were blocked with 5% milk in TBS-T for 1 hr. Primary antibody incubations were performed with an anti-thiophosphate ester antibody (rabbit 51-8; 1:5000) and anti-tubulin (mouse 12G10; 1:2000) for 1 hr at room temperature. Secondary incubations were performed with LI-COR antibodies (rabbit 680, mouse 800; 1:10,000) for 1 hr at room temperature. Imaging was performed using a LI-COR Odyssey.

Protein cleanup and digestion

Proteins were precipitated using methanol chloroform extraction. For 250 μ L of lysate, 800 μ L methanol and 200 μ L of chloroform was added, followed by vortexing. After adding 600 μ L of water, the sample was vortexed and centrifuged at max speed for 5 min at 4°C. After removing the supernatant without disrupting the precipitate, 375 μ L of methanol was added and vortexed. Samples were centrifuged at max speed for 15 min at 4°C. The protein pellet was allowed to air dry after removing the supernatant. Dried protein pellets were resuspended in 200 μ L of 8M urea. 1 mg of protein (determined from protein quantification; see above) from CDPK1G and CDPK1M parasites were pooled for a total of 2 mg of protein. To digest protein, 5X volume of 1X Trypsin Digest Buffer (100 mM ammonium acetate pH 8.9, 1mM CaCl_2 , 2 mM TCEP) was added to the sample followed by 40 μ g of sequencing grade trypsin (Promega). Proteins were digested overnight rotating at room temperature. To prepare samples for desalting, glacial acetic acid was added to 10% (v/v) and debris was briefly spun down. A C18 Sep-Pak Plus cartridge (Waters) was prepared using a syringe pump and 10 mL syringe with three 10 mL washes at a flow rate of 2 mL/min: 0.1% acetic acid, 90% acetonitrile/0.1% acetic acid, and 0.1% acetic acid. The sample was loaded in a 5 mL syringe at a flow rate of 0.5 mL/min. The syringe and cartridge were washed with 5 mL of 0.1% acetic acid at a flow rate of 0.5 mL/min. A final wash was performed using 10 mL of 0.1% acetic acid at a flow rate of 2 mL/min. Peptides were eluted with 4.5mL of 40% acetonitrile/0.1% acetic acid at a flow rate of 0.5 mL/min. Samples were spun in a speed vac for 3 hrs until samples could be pooled into a single 2 mL tube. Samples were frozen in liquid nitrogen and lyophilized overnight. Lyophilized peptides were stored at -80°C.

Thiophosphate enrichment

To enrich for thiophosphorylated peptides, 400 μ L of SulfoLink Coupling Resin slurry was used (Thermo). Incubations were performed in the dark using aluminum foil due to the light sensitivity of the resin. The resin was washed twice with 1 mL of binding buffer (25 mM HEPES, 50% acetonitrile, pH 7.0 NaOH + HCl) rotating for 5 min followed by a 1000 rpm spin for 10 sec. The supernatant was removed without disturbing the pelleted resin. The beads were blocked with 1mL of blocking buffer (binding buffer with 25 μ g/mL β -casein and 2 mM TCEP) and rotated for 5 min at room temperature. After pelleting the resin and removing the supernatant, the resin was resuspended with lyophilized peptides dissolved in 500 μ L of the blocking buffer. Samples were incubated overnight at room temperature. Samples were spun at 1000 rpm for 10 sec and the supernatant was spun again, lyophilized, and stored at -80°C prior to MS analysis. The beads received the following series of 1 mL washes for 5 min rotating and spun at 1000 rpm for 10 sec: twice with binding buffer with 2 mM TCEP, once with quenching buffer (25 mM HEPES, 50% acetonitrile, 5 mM DTT, pH 8.5 NaOH), once with binding buffer with 2 mM TCEP, once with 5% formic acid (no rotation), once with binding

buffer with 2 mM TCEP, and three times with 0.1% acetic acid. The resin was no longer light sensitive after incubation with the quenching buffer. To elute captured peptides, resin was resuspended in 500 μ L OXONE (2 mg/mL potassium monopersulfate) and rotated for 5 min at room temperature. The supernatant containing eluted peptides was collected after spinning at 1000 rpm for 10 sec. OXONE was removed from the sample using C18 spin columns (Pierce) according to manufacturer instructions. A total of 4 washes with the equilibrium/wash buffer was performed. Peptides were spun in a speed vac until dry and stored at -80°C until MS analysis.

MS data acquisition

The samples were resuspended in 10–20 μ L of 0.1% formic acid for MS analysis and were analyzed on a Q-Exactive HF-X Orbitrap mass spectrometer connected to an EASY-nLC 1200 chromatography system using 0.1% formic acid as Buffer A and 80% acetonitrile/0.1% formic acid as Buffer B. Peptides were loaded onto a analytical column (column: PF360-75-15-N-5, New Objective, 360 μ m OD, 75 μ m ID, 15 μ m Tip PicoFrit Emitter; resin: 04A-4506, Phenomenex Aeris Peptide, C18 1.7 μ m) via trapping column (column: 360 μ m OD, 100 μ m ID; resin: AA12S11, YMC Gel ODS-A, C18 10 μ m). Peptides were separated at 300 nL/min on a gradient of 2% B for 5 min, 2–25% B for 100 min, 25–40% B for 20 min, 40–100% B for 1 min, and 100% B for 12 min. The orbitrap was operated in positive ion mode with a positive ion voltage of 2700V with an ion transfer tube temperature of 300°C . Full scan spectra were acquired in profile mode at a resolution of 60,000, with a scan range of 375 to 1600 m/z, 1×10^6 AGC target, maximum injection time of 50 msec, intensity threshold of 4×10^5 , dynamic exclusion of 13 sec, and 20 data dependent scans (DDA Top 20). MS2 spectra were generated with a HCD collision energy of 27 at a resolution of 15,000, first mass at 100 m/z, isolation window of 1.5 m/z, an AGC target of 1×10^5 with a maximum injection time of 20 msec, and scan range of 200 to 2000 m/z.

Thiophosphorylation analysis

Raw files were analyzed in Proteome Discoverer 2.2 (Thermo Fisher Scientific) to generate peak lists and protein and peptides identifications using Sequest HT (Thermo Fisher Scientific) and the ToxoDB release 34 GT1 protein database. The maximum missed cleavage sites for trypsin was limited to 2. The following modifications were included in the search: dynamic oxidation (+15.995 Da; M), dynamic phosphorylation (+79.966 Da; S,T,Y), dynamic 13C615N4 (+10.008 Da; R), dynamic 13C615N2 (+8.014 Da; K), and dynamic acetylation (+42.011 Da; N-terminus). Site localization scores were generated using ptmRS, with phosphoRS and use of diagnostic ions set to true. SILAC 2plex (Arg10, Lys8) method was used for relative quantification of protein and unique peptide abundances. For peptide level analysis, ratios of unique peptides comparing CDPK1^G and CDPK1^M were generated and low abundance resampling (5%) was used to impute missing values. For protein level analysis, ratios of proteins were determined from the summed abundance of unique peptides comparing CDPK1G and CDPK1M strains.

Peptide and protein level data were exported from Proteome Discoverer for analysis in R. For enriched peptides, abundance ratios were calculated within each replicate for high confidence peptides (CDPK1^G/CDPK1^M) and normalized to the median abundance ratio of the whole proteome peptides derived from the flow through samples. Normalized abundance ratios in the flow through proteome samples were calculated by dividing abundance ratios by the median abundance ratios within each replicate. For enriched peptides, an average \log_2 normalized abundance ratio was calculated from three replicates. Significantly enriched peptides were calculated using a one-tailed *t*-test using the normalized abundance ratios for three replicates. A non-linear significance threshold was calculated using the function ($y = |4/x|$), where significantly enriched peptides had product value of $-\log_{10}(p) * (\text{mean } \log_2 \text{ abundance ratio})$ greater than 4.

Immunoblotting

Samples were combined with 5X Laemmli sample buffer (10% SDS, 50% glycerol, 300 mM Tris HCl pH 6.8, 0.05% bromophenol blue, 5% beta-mercaptoethanol) and were incubated at 95°C for 10 min. The samples were run on precast 4–15% or 7.5% SDS gels (Bio-Rad) and were transferred overnight onto a nitrocellulose membrane in transfer buffer (25 mM TrisHCl, 192 mM glycine, 0.1% SDS, 20% methanol) at 4°C. Blocking was performed with 5% milk in PBS for 1 hr rocking at room temperature. Antibody incubations were performed with 5% milk in TBS-T for 1 hr rocking at room temperature. Three 5 min TBS-T washes were performed before and after secondary antibody incubations rocking at room temperature. After a final PBS wash, imaging was performed using a LI-COR Odyssey.

For immunoblot detection of the HA tag in AID-HOOK and FTS-AID after auxin-mediated depletion, secondary antibody incubations were performed with antirabbit HRP antibodies (Jackson ImmunoResearch) and detected with chemiluminescence (Azure) for increased sensitivity. Imaging was performed using a Bio-Rad Gel Doc XR.

Immunofluorescence analysis

HFFs were seeded onto coverslips and grown until confluence. Confluent HFFs were infected with parasites. Approximately 2 hrs later, media was exchanged with media containing either 50 μ M auxin or vehicle solution of PBS. At 24 hrs post-infection, the media was aspirated, and the coverslips were washed with PBS three times before fixation with 4% formaldehyde in PBS for 20 min. Following three washes in PBS, the fixed cells were permeabilized with 0.25% Triton X-100 for 15 min. After three washes in PBS, the coverslips were incubated in a blocking solution (5% IFS/ 5% NGS in PBS) for 10 min at room temperature. Coverslips were incubated for 1–2 hrs with primary antibody diluted in blocking solution. Anti-GAP45 or anti-MIC2 was used as a parasite counterstain. After three washes in PBS, the coverslips were incubated in blocking solution for 5 min, followed by secondary antibody diluted in blocking solution containing Hoechst 33342 for 1 hr. The coverslips were washed three times in PBS, once in water, and finally mounted with Prolong Diamond overnight at room temperature. Microscope images were acquired with the Nikon Ti Eclipse and NIS Elements software package.

Immunofluorescence analysis - Figure 2

Parasite-infected HFF monolayers grown on glass coverslips were fixed with 3% formaldehyde for 15 min prior to washing with PBS. Fixed cells were then permeabilized (PBS, 0.1% Triton X-100, 10 min), blocked (3% BSA in PBS, 1 hr), and labeled with anti-HA (1:1000, 1 hr; Roche). HA-tagged CDPK1 in the cWT and cMut lines was visualized with secondary goat antibodies (1:2000, 1 hr; Life Technologies) conjugated to Alexa Fluor 594 and 488, respectively. Cytosolic GFP (cWT) and mCherry (cMut) were used as parasite counterstains. Nuclei were visualized with the DNA stain (DAPI; Sigma) added at 5 μ g/mL with the secondary antibody. Stained coverslips were mounted on glass slides with Slowfade (Life Technologies) and imaged on a Nikon Eclipse Ti-U inverted fluorescent microscope. Images were analyzed using Nikon NIS Elements imaging software.

Plaque Assays

600 and 1200 parasites were used to infect 6-well plates of HFFs in 10% IFS media. At 1 dpi, media was exchanged with 10% IFS media containing either 50 μ M auxin or vehicle solution of PBS. Parasites were allowed to grow undisturbed for 8 days total. Plates were washed with PBS and fixed for 10 min with 100% ethanol at room temperature. After removing ethanol,

plates were allowed to dry prior to staining with crystal violet solution for 30 min to 1 hr. Plates were washed 3 times with PBS, once with water, and allowed to dry before scanning.

Plaque assays - Figure 2

Parasites were harvested by syringe lysis, counted, and 200 parasites were seeded on confluent HFF monolayers grown in 24-well plates (Falcon). Wells were treated with 500 μ M auxin or vehicle (ethanol) and plaques were allowed to form for 5 days. Plaque formation was assessed by inspecting the methanol fixed and 0.1% crystal violet stained HFF monolayers.

Invasion assays

Confluent HFFs seeded in T12.5 flasks were infected with parasites. Approximately 2 hrs later, the media was exchanged for 10% IFS media containing either 50 μ M auxin or vehicle solution of PBS. Parasites were harvested at 2 dpi and the media was exchanged for 1% IFS in invasion media (DMEM Sigma D2902, 20 mM HEPES, pH 7.4) with auxin or vehicle PBS added. Confluent HFFs seeded in clear-bottomed 96-well plates were infected with 2×10^5 extracellular parasites. After centrifuging the plate at $290 \times g$ for 5 min to synchronize invasion, the infected 96-well plate was incubated by floating on a water bath at 37°C/5% CO₂ for 90 min. Wells were washed once with PBS before fixing infected HFFs with 4% formaldehyde in PBS for 20 min at room temperature. Wells were washed three times with a wash buffer (1% NGS in PBS) and then incubated in a blocking buffer (5% IFS and 1% NGS in PBS) overnight at 4°C. To stain extracellular parasites, wells were incubated with anti-SAG1 antibody for 30 min at room temperature. After washing wells three times with a wash buffer, fixed HFFs were permeabilized in 0.25% TritonX-100 in blocking buffer for 8 min room temperature. After washing the wells three times with a wash buffer, the wells were incubated in a blocking buffer for 10 min at room temperature, followed by anti-GAP45 antibody for 30 min at room temperature to label all parasites. After three washes in a wash buffer, wells were incubated with a secondary antibody solution containing Hoechst for 30 min. After three washes in PBS, wells were imaged using a Biotek Cytation 3.

Egress assays

Confluent HFFs seeded in glass bottomed 35 mm dishes (Ibidi or Mattek) were infected with approximately 2×10^5 parasites. Approximately 2 hrs later, the media was exchanged for 10% IFS media containing either 50 μ M auxin or vehicle solution of PBS. At 24 hrs post-infection, the media was replaced with 1% IFS in Ringer's (155 mM NaCl, 2 mM CaCl₂, 3 mM KCl, 1 mM MgCl₂, 3 mM NaH₂PO₄, 10 mM HEPES, 10 mM glucose, pH 7.4). Zaprinast (final concentration 500 μ M) was added into the dishes after 15 sec of imaging and imaging of infected HFFs continued for a total of 10 min. Images were acquired using a Nikon Ti Eclipse with an enclosure maintained at 37°C. The number of intracellular vacuoles was quantified at 0 min and 10 min. Results are the sum of four fields of view per condition and are representative of three independent experiments.

Egress assays - Figure 2

Parasites were added to HFF monolayer and grown for 24 hrs in a 96 well plate. The wells were then treated with 500 μ M auxin or an equivalent volume of vehicle (ethanol) for 2 hrs and then washed with PBS (2x). The media was exchanged for 100 μ l Ringer's solution (155 mM NaCl, 3 mM KCl, 2 mM CaCl₂, 1 mM MgCl₂, 3 mM NaH₂PO₄, 10 mM HEPES, 10 mM glucose) and the plate was placed on a heating block to maintain the temperature at 37°C. To artificially induce egress, 50 μ L of Ringer's solution containing 24 μ M ionophore (8 μ M final, Thermo) was added to each well. At specified time points the cells were fixed by adding 33

μL 16% formaldehyde (3% final) for 15 min. Cells were washed in PBS (3x) and stained with rabbit anti-TgCAP 1:2000 (Hunt et al., 2019) followed by goat anti-rabbit Alexa Fluor 488 (1:2000) and DAPI (5 μg/mL). Automated image acquisition of 25 fields per well was performed on a Cellomics Array Scan VTI HCS reader (Thermo Scientific) using a 20x objective. Image analysis was performed using the Compartmental Analysis BioApplication on HCS Studio (Thermo Scientific). Egress levels were determined in triplicate for three independent assays. Vacuole counts were normalized to $t = 0$ to determine how many intact vacuoles had remained after egress. The results were statistically tested using oneway ANOVA with Tukey's multiple comparison test in GraphPad Prism 7. The data are presented as mean \pm s.d.

Replication assays

Confluent HFFs seeded on coverslips were infected with parasites. Parasites were centrifuged at 290 x g for 5 min to synchronize invasion of host cells. Approximately 2 hrs later, the media was exchanged for 10% IFS media containing either 50 μM auxin or vehicle solution of PBS. At 24 hrs post-infection, the media was aspirated and fixed as described in "Immunofluorescence Analysis". Coverslips were incubated in primary and secondary antibodies for 30 min. Anti-GAP45 antibody was used to visualize parasites. Microscope images were acquired with the Nikon Ti Eclipse and NIS Elements software package. Tiled images were acquired in a four-by-four manner using a 40x objective. Parasites per vacuole were quantified for at least 100 vacuoles for three biological replicates.

Immunoprecipitation of HOOK and FTS complex

Parasite harvest

HOOK-3xHA, CDPK1-AID (parental), FTS-3xHA and TIR1 (parental) parasites were infected onto confluent HFFs in 15 cm dishes. After the parasites lysed the HFF monolayer (approximately 40 hrs post-infection), extracellular parasites were passed through 5 μm filters and washed twice with DMEM by pelleting at 1000 x g for 10 min. Parasite pellets were resuspended in 1X Dynein Lysis Buffer (DLB) (30 mM HEPES, 50 mM KOAc1, 2 mM MgOAc, 10% glycerol, 1 mM EGTA pH 8.0, 1 mM DTT, 0.5 mM ATP, 125 units/mL benzonase, 1X HALT protease and phosphatase inhibitor, and 1% NP-40 IGEPAL CA 630) to achieve a concentration of 6.67×10^8 parasites/mL (Redwine et al., 2017). Parasites were lysed on ice for 10 min and vortexed periodically to facilitate lysis. Lysates were centrifuged at 1000 x g for 5 min at room temperature to pellet unlysed parasites and the lysate supernatant was collected and used as the immunoprecipitation input.

Immunoprecipitation

25 μL of anti-HA magnetic beads (Thermo Scientific 88836) was used for 200 μL of parasite lysate. Beads were aliquoted and washed three times with a wash buffer (30 mM HEPES, 50 mM KOAc1, 2 mM MgOAc, 10% glycerol, 1 mM EGTA pH 8.0, 1 mM DTT, 0.5 mM ATP, and 0.01% NP-40 IGEPAL CA 630) using a magnetic rack. To begin the pulldown, 200 μL of parasite lysate was used to resuspend washed beads. Tubes were rotated at 4°C for 1 hr (FTS-AID and TIR1) and 3 hrs (HOOK-3xHA and CDPK1-AID). Beads were resuspended in 250 μL of wash buffer, transferred to a new tube, and received two additional washes with the same volume. Proteins were eluted by resuspending beads in 22 μL of 1X S-trap sample buffer (5% SDS, 50 mM TEAB, pH 7.5) and incubated at 70°C for 10 min. The eluate was collected for MS sample processing and analysis. Results are representative of three independent experiments.

Protein cleanup and digestion

Proteins were prepared for mass spectrometry as described above in “Sub-minute phosphoproteomics - Protein cleanup and digestion”. Eluted peptides were frozen in liquid nitrogen, lyophilized, and stored at -80°C until MS analysis.

MS data acquisition

Lyophilized peptides were resuspended in 25 μL of 0.1% formic acid and were analyzed on an Exploris 480 Orbitrap mass spectrometer equipped with a FAIMS Pro source (Bekker-Jensen et al., 2020) connected to an EASY-nLC chromatography system using 0.1% formic acid as Buffer A and 80% acetonitrile/0.1% formic acid as Buffer B. Peptides were separated at 300 nL/min on a gradient of 1–6% B for 1 min, 6–21% B for 41 min and 30 sec, 21–36% B for 20 min and 45 sec, 36–50% B for 10 min and 15 sec, 100% B for 14 min and 30 sec, 100–2% B for 3 min, 2% B for 3 min, 2–98% B for 3 min, and 98% B for 3 min. The orbitrap and FAIMS were operated in positive ion mode with a positive ion voltage of 1800V; with an ion transfer tube temperature of 270°C ; using a standard FAIMS resolution and compensation voltage of -50 and -65V , an inner and outer electrode temperature of 100°C with 4.5 mL/min carrier gas. Full scan spectra were acquired in profile mode at a resolution of 60,000, with a scan range of 350–1400 m/z, 300% AGC target, 25 msec maximum injection time, intensity threshold of 5×10^3 , 2–6 charge state, dynamic exclusion of 20 sec, 15 data dependent scans (DDA Top 15), and mass tolerance of 10 ppm. MS2 spectra were generated an HCD collision energy of 30 at a resolution of 15,000, first mass at 110 m/z, with an isolation window of 1.3 m/z, and an automatically determined AGC target and maximum injection time in standard and auto mode.

Immunoprecipitation MS analysis

Raw files were analyzed in Proteome Discoverer 2.4 (Thermo Fisher Scientific) to generate peak lists and protein and peptides identifications using Sequest HT (Thermo Fisher Scientific) and the ToxoDB release 49 GT1 protein database. The maximum missed cleavage sites for trypsin was limited to 2. The following modifications were included in the search: dynamic oxidation (+15.995 Da; M), dynamic phosphorylation (+79.966 Da; S,T,Y), dynamic acetylation (+42.011 Da; N-terminus), and static methylthio (+45.988 Da; C). Label free quantification of proteins was performed using summed abundances from unique peptides. Abundances were normalized on the total peptide amount. Pairwise ratios were calculated for protein abundances comparing strains and conditions. Significance values were derived from t-tests across three replicates and adjusted with Benjamini-Hochberg correction. Exported protein abundance files from Proteome Discoverer 2.4 were loaded into R (version 4.1.1).

Proximity labeling FTS-TurboID

Parasite harvest and treatment

FTS-TurboID and mNG-TurboID (cytosolic control) parasites were infected onto confluent HFFs in 15 cm dishes. After the parasites lysed the HFF monolayer (approximately 40 hrs post-infection), extracellular parasites were passed through 5 μm filters and washed twice with DMEM by pelleting at $1000 \times g$ for 10 min. At least 1×10^8 Parasites were resuspended in 200 μL of DMEM. 200 μL of biotin (final concentration 500 μM) or vehicle DMSO in DMEM was mixed with parasites. Tubes were incubated in a water bath at 37°C for 5 min. Parasites were pelleted at $12,000 \times g$ for 1 min at 4°C for a total of three 1 mL PBS washes. Parasites were resuspended in a RIPA NP-40 lysis buffer (10 mM Tris-HCl pH 7.5, 140 mM NaCl, 1% NP-

lysed at room temperature for 15 min and stored at -20°C . Results are representative of three independent experiments.

Biotinylated protein enrichment

Streptavidin magnetic beads were washed three times with a RIPA NP-40 lysis buffer. Thawed lysates were spun at $16,000 \times g$ for 5 min at 4°C and the supernatant was used as the pulldown input. 20 μL of streptavidin magnetic beads was used for 200 μL of lysates (1×10^8 parasites). Beads were incubated with lysate rotating for 1 hr. Beads received a series of 1 mL washes: twice with the RIPA NP-40 lysis buffer, once with 1 M KCl, once with 0.1M Na_2CO_3 (pH 11), once with 2 M urea in 10 mM Tris pH 8.0), and twice with RIPA NP-40 lysis buffer. Proteins were eluted by incubating beads with 2.5 mM biotin in S-trap sample buffer (5% SDS, 50 mM TEAB, pH 7.5) for 10 min at 95°C .

Protein cleanup and digestion

Proteins were prepared for mass spectrometry as described above in “Sub-minute phosphoproteomics - Protein cleanup and digestion”. Eluted peptides were frozen in liquid nitrogen, lyophilized, and stored at -80°C until MS analysis.

MS data acquisition

Lyophilized peptides were resuspended in 25 μL of 0.1% formic acid and were analyzed on an Exploris 480 Orbitrap mass spectrometer equipped with a FAIMS Pro source (Bekker-Jensen et al., 2020) connected to an EASY-nLC chromatography system using 0.1% formic acid as Buffer A and 80% acetonitrile/0.1% formic acid as Buffer B. Peptides were separated at 300 nL/min on a gradient of 2% B for 1 min, 2—25% B for 41 min, 25—40% B for 6 min, 40—100% B for 12 min, 100—2% B for 3 min, 2% B for 3 min, 2—98% B for 3 min, and 98% B for 3 min. The orbitrap and FAIMS were operated in positive ion mode with a positive ion voltage of 1800V; with an ion transfer tube temperature of 270°C ; using a standard FAIMS resolution and compensation voltage of -50 and -65V , an inner and outer electrode temperature of 100°C with 4.5 mL/min carrier gas. Full scan spectra were acquired in profile mode at a resolution of 60,000, with a scan range of 350—1400 m/z, 300% AGC target, 25 msec maximum injection time, intensity threshold of 5×10^3 , 2—6 charge state, dynamic exclusion of 20 sec, 15 data dependent scans (DDA Top 15), and mass tolerance of 10 ppm. MS2 spectra were generated with a HCD collision energy of 30 at a resolution of 15,000, first mass at 110 m/z, with an isolation window of 1.3 m/z, and a normalized AGC target of 200% with an automatically determined maximum injection time.

Proximity labeling MS analysis

Raw files were analyzed in Proteome Discoverer 2.4 (Thermo Fisher Scientific) to generate peak lists and protein and peptides identifications using Sequest HT (Thermo Fisher Scientific) and the ToxoDB release 49 GT1 protein database. The maximum missed cleavage sites for trypsin was limited to 2. The following modifications were included in the search: dynamic oxidation (+15.995 Da; M), dynamic phosphorylation (+79.966 Da; S,T,Y), dynamic biotinylation (+226.078 Da; K, N-terminus), dynamic acetylation (+42.011 Da; N-terminus), and static methylthio (+45.988 Da; C). Label free quantification of proteins was performed using summed abundances from unique peptides. Abundances were normalized on the total peptide amount. Pairwise ratios were calculated for protein abundances comparing strains and conditions. Significance values were derived from t-tests across three replicates and adjusted with Benjamini-Hochberg correction. Exported protein abundance files from Proteome Discoverer 2.4 were loaded into R (version 4.1.1).

MIC2 secretion assays

Parasite harvest and treatment

Extracellular parasites were harvested in chilled DMEM and washed twice in DMEM after centrifugation at 1000 x *g* for 10 min at 4°C. Parasites were resuspended at a concentration of 6×10^8 parasites/mL in cold DMEM. 3×10^7 parasites were aliquoted into round-bottom 96-well plates. An additional aliquot of parasites was lysed in 5X Laemmli sample buffer (see “Immunoblotting” for recipe) to obtain the total parasite lysate used to determine total MIC2 levels. Secretion was stimulated in plates with IFS and ethanol in DMEM (final concentration 3% IFS and 1% ethanol) or a vehicle solution of DMEM. Plates were incubated by floating on a water bath at 37°C/5% CO₂ for 90 min. Plates were spun at 1000 x *g* for 5 min at 4°C to separate parasites from secreted proteins. Supernatants were transferred to a new well and spun again. The final supernatant was mixed with a 5X Laemmli sample buffer, boiled at 95°C for 10 min, and stored at –20°C along with total lysates until immunoblot analysis.

Immunoblot analysis and quantification

To quantify MIC2 protein levels, a standard curve derived from the total parasite lysate was generated alongside supernatants containing secreted microneme proteins. The standard curve was derived from 3-fold serial dilutions of the total parasite lysate (undiluted, 1:3, 1:9, and 1:27) in a 1X Laemmli sample buffer. The serial dilutions and supernatants of auxin- and vehicle-treated parasites of a single strain were loaded onto the same precast 4–15% gel (Bio-Rad). Subsequent immunoblotting steps were performed as described in “Immunoblotting”. Anti-MIC2 was used to detect total and secreted MIC2 proteins. Secreted MIC2 proteins have a lower molecular weight due to parasite-mediated proteolytic cleavage. Anti-CDPK1 was used as a loading control for total parasite lysate and to reveal any parasite lysis or carry over in the supernatant. Immunoblots confirming the depletion of tagged proteins were also collected. Imaging was performed on a LI-COR Odyssey at high resolution for quantification.

Immunoblot quantification was performed in Fiji on unadjusted inverted images. For a single immunoblot, lane profiles of uniform dimensions were generated for MIC2 signal. Background-subtracted signal intensity was measured as an area using the line and wand tool. A standard curve was derived from the quantified MIC2 signal of the dilution series. Standard curves across all conditions and replicates had R^2 values greater than 0.90. Secreted MIC2 signals were within the linear range of the standard curve and were used to calculate the percent of total MIC2 secreted. Results are representative of three independent experiments for each parasite strain.

Microneme relocation

Parasites expressing the CLAMP-mNG reporter were grown in HFFs in glass-bottomed 35 mm dishes (Ibidi and Mattek) for approximately 20 hrs. For 3-MB-PP1 treatment, media was exchanged 30 min prior to live microscopy for 3% IFS in Ringer’s buffer (155 mM NaCl, 2mM CaCl₂, 3mM KCl, 1mM MgCl₂, 3mM NaH₂PO₄, 10mM HEPES, 10 mM glucose, pH 7.4) containing either 3 μM 3-MB-PP1 or vehicle solution of DMSO. At approximately 1 min after beginning live microscopy, parasites were stimulated with zaprinast (500 μM final concentration) or a vehicle solution of DMSO in corresponding Ringer’s buffer. For TIR1/CLAMP-mNG and AID-HOOK/CLAMP-mNG parasite, media was exchanged 2 hrs after infection for 10% IFS media containing either 50 μM auxin or vehicle solution of PBS. Media was exchanged for 3% IFS in Ringer’s buffer just prior to live microscopy. At approximately 30 sec after beginning live microscopy, parasites were stimulated with zaprinast (500 μM final concentration) or a vehicle solution of DMSO in corresponding Ringer’s buffer. Images

were recorded every 5–7 sec until egress or approximately 5 min using a Nikon Ti Eclipse with an enclosure maintained at 37°C.

Microneme relocation was quantified using built-in commands from ImageJ (v. 1.53e). To determine the distribution of fluorescent micronemes at a specific time frame, a line was drawn from the parasite's apical end to its basal end. The “plot profile” command was applied to this line to calculate fluorescence intensity at regularly spaced intervals (0.13 microns) across the parasite on unadjusted images. This process was repeated for each time frame of interest and for each parasite in the analyzed vacuole. Regression analysis was performed on relocation data from each time frame, resulting in logarithmic regression plots that display how fluorescence intensity correlates with distance from the parasite's apical end. Microneme relocation is shown as SuperPlots to simultaneously visualize the median relocation of an entire vacuole and the relocation of individual parasites within each vacuole (Lord et al., 2020).

Microneme localization in extracellular parasites

Microneme localization in extracellular parasites was quantified using a custom-built, image analysis pipeline. ImageJ's built-in commands were used to measure the length of the parasite's major axis. Based on the patterns of vehicle-treated TIR1/CLAMP-mNG data, 1/8th of the parasite closest to the apical end was deemed the apical region. The remaining region was deemed the body. Using the Interactive Learning and Segmentation Toolkit (ilastik v. 1.3.3) (Berg et al., 2019), the apical region and body of parasites were isolated from each other and from the surrounding media. Ilastik's pixel and object quantification tools were then used to determine the total intensity of fluorescence in each of these regions. Comparing these values to each other yielded the percentage of fluorescent micronemes present in each of these sections in relation to the total fluorescence present in the parasite. This process was repeated for several extracellular parasites in each of the conditions tested.

Supporting information

supplements/523553_file02.avi Video 1
 supplements/523553_file03.avi Video 2
 supplements/523553_file04.avi Video 3
 supplements/523553_file05.avi Video 4
 supplements/523553_file06.avi Video 5
 supplements/523553_file07.avi Video 6
 supplements/523553_file08.avi Video 7
 supplements/523553_file09.avi Video 8
 supplements/523553_file10.avi Video 9

Acknowledgements

We thank all the members of the Lourido laboratory for helpful discussions and support, especially Tyler Smith for aiding with the tagging vector design and Christopher Giuliano for insights during data analysis. We thank Forest M. White for generous support in developing the mass spectrometry methodologies used in this study and for helpful discussions. For data in [Figure 2](#), we thank Matthew Child and Matt Bogyo for the CDPK1 antibody, Peter Bradley for the GAP45 antibody, John Boothroyd for the SAG1 antibody. We thank Marc-Jan Gubbels for the alpha-tubulin antibody, L. David Sibley for the MIC2, SAG1, and ALD antibody, Peter Bradley for the ROP1 antibody, Drew Etheridge for the GAP45 antibody, and Dominique Soldati-Favre for the GAP45 antibody. This work relied on [VEu-PathDB.org](https://www.ebi.ac.uk/PathDB/) and we thank all contributors to this resource. This research was supported by funds from National Institutes of Health grants to SL (R01AI144369) and MB and MT (R01AI123457), a National Science Foundation Graduate Research Fellowship to AWC and ALH (174530). MT received funding

from the Francis Crick Institute which receives its core funding from Cancer Research UK (CC2132), the UK Medical Research Council (CC2132), and the Wellcome Trust (CC2132). The Science Technology Proteomics Platform at the Francis Crick Institute received funding from Cancer Research UK (CC0199), the UK Medical Research Council (CC0199), and the Wellcome Trust (CC0199). For the purpose of Open Access, the authors have applied a CC BY public copyright license to any Author Accepted Manuscript version arising from this submission.

Competing Interests

The authors declare no competing interests.

Data availability

Proteomics data will be deposited in ProteomeXchange Consortium via the PRIDE partner repository. Accession numbers will be listed in the appropriate Methods section. The sequences of cloning vectors generated for this study have been or will be deposited in GenBank, as listed in Supplementary File 10. Custom analysis scripts in the R computing language are available upon request. Strains generated for this study are available upon request.

Supplemental Figures

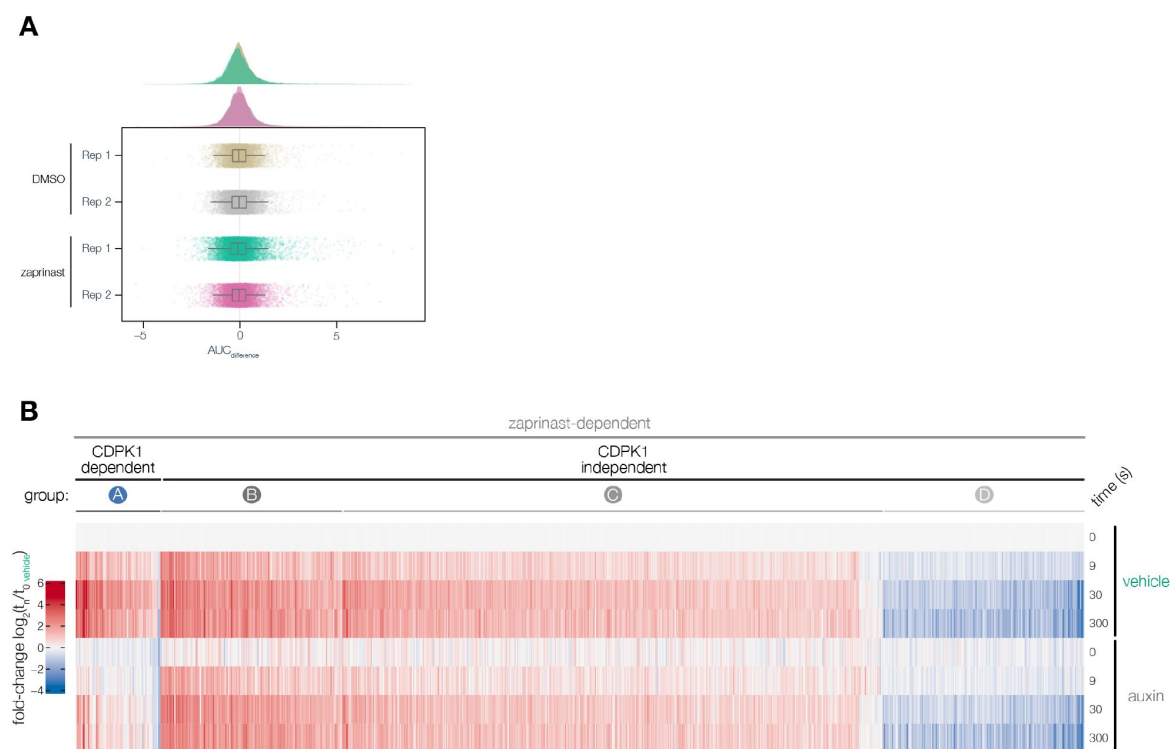


Figure S1.

Zaprinst-dependent phosphoproteome.

(A) Distribution of $AUC_{\text{difference}}$ values for individual peptides in the enriched DMSO phosphoproteome and enriched zaprinst phosphoproteome across two biological replicates. **(B)** Heatmap of zaprinst-dependent phosphopeptide abundance ratios across time relative to the vehicle t0 interval during auxin or vehicle treatment. Peptides are organized by CDPK1-dependent phosphopeptides (Group A) and CDPK1-independent phosphopeptides (Group B, C, D).

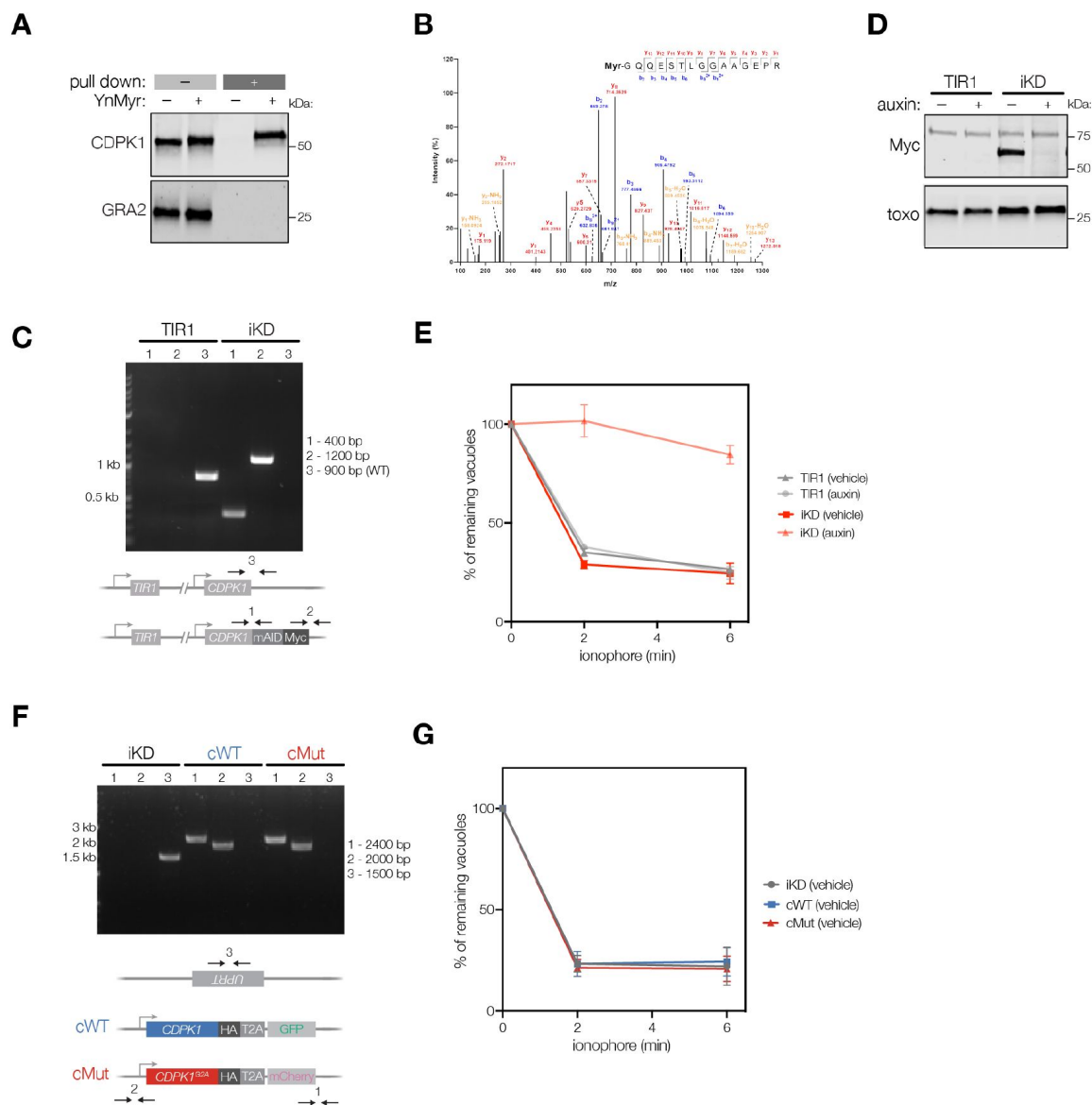


Figure S2.

CDPK1 myristoylation, inducible knockdown, and complementation.

(A) YnMyr-dependent pull down confirming myristoylation of CDPK1. GRA2 antibody was used as a loading control. **(B)** MS2 fragmentation spectra indicating myristoylation of Gly2 of CDPK1 after YnMyr-dependent pull down. **(C)** PCR analysis confirming correct integration of the *maID* cassette at the C terminus of endogenous *CDPK1* in the TIR1 line. **(D)** Immunoblot validation of auxin-dependent depletion of CDPK1 in the iKD line using the anti-Myc antibody and the anti-toxo antibody as a loading control. The band at 75 kDa represents anti-Myc-related background. **(E)** Conditional depletion of CDPK1 abolishes ionophore-induced egress from host cells. Intracellular parasites were treated with auxin or vehicle (EtOH) for 2 hrs and egress was initiated by addition of 8 μ M A23187. The number of intact vacuoles was monitored over the course of 6 min. Each data point is an average of two biological replicates, each in technical triplicate, error bars represent standard deviation. **(F)** PCR analysis confirming correct integration of the complementation constructs encoding the WT (cWT) and myristoylation mutant (cMut) copies of CDPK1 at the *UPRT* locus of the iKD line. Primers are indicated by arrows. Base pairs (bp). **(G)** In the absence of auxin, both cWT and cMut parasites egress from host cells within 2 min post-ionophore treatment.

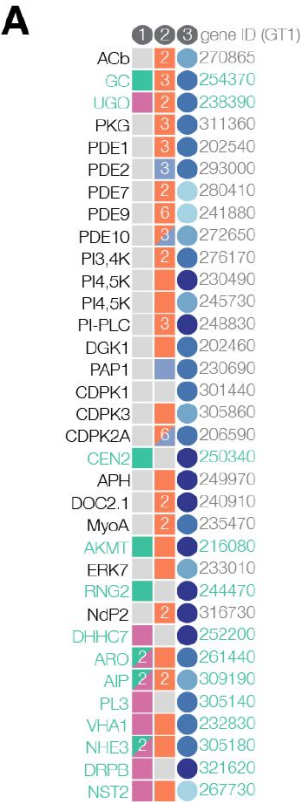


Figure S3.
Factors controlling parasite motility.
(A) Expanded list of factors involved in parasite motile stages from [Figure. 3H](#)

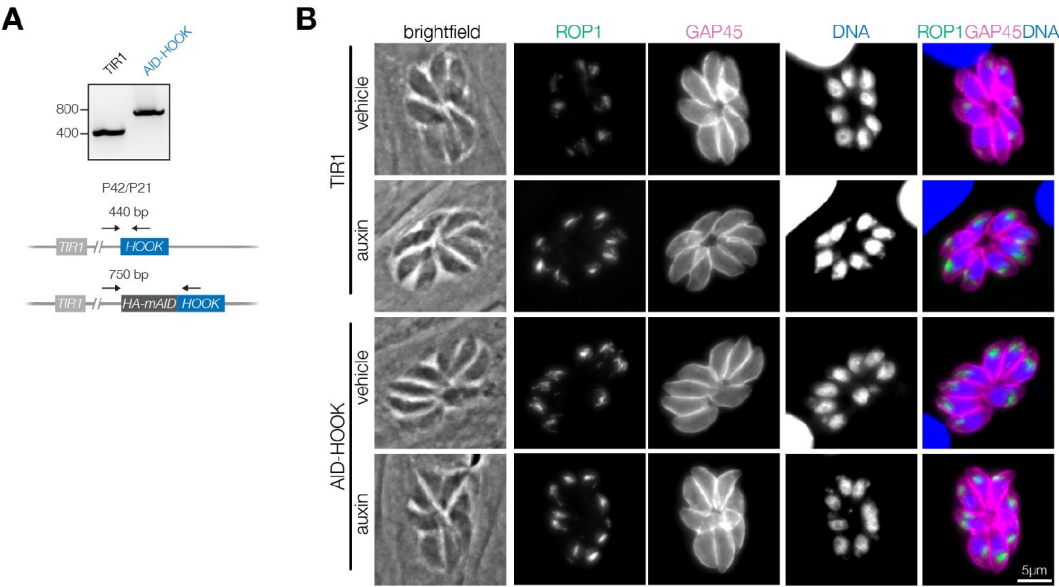


Figure S4.
Extended analysis of HOOK knockdown.
(A) PCR analysis confirming correct integration of the *HA-mAID* cassette at the N terminus of endogenous *HOOK* (*TGGT1*-289100) in the *TIR1* line. **(B)** Rhoptries (ROP1) are visualized in fixed intracellular parasites by immunofluorescence after treatment with auxin for 24 hrs. Hoechst and GAP45 are used as counterstains.

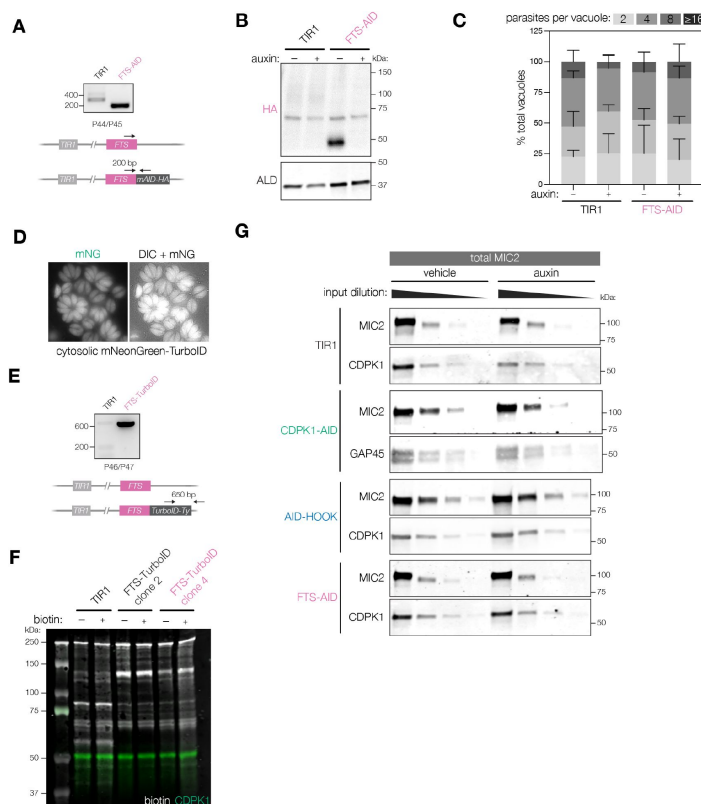


Figure S5.

Extended analysis of FTS knockdown, proximity labeling, and microneme protein secretion.

(A) PCR analysis confirming correct integration of the *mAID-HA* cassette at the C terminus of endogenous FTS (*TGGT1_264050*) in the TIR1 line. **(B)** Uncropped immunoblot shown in Figure 5D confirming C-terminal tagging of FTS. The band at 70 kDa represents anti-HA/anti-ALD-related background present in all conditions. **(C)** Replication assays of host cells infected with TIR1 or FTS-AID parasites in auxin for 24 hrs. Parasites per vacuole were quantified from immunofluorescence on fixed intracellular parasites. $p > 0.9$. Two-way ANOVA. **(D)** Live microscopy of HFFs infected with parasites expressing cytosolic mNeonGreen-TurboID as the cytosolic control for proximity labeling. **(E)** PCR analysis confirming presence of *TurboID-Ty* cassette in the TIR1 line. **(F)** Immunoblot detection of biotinylated proteins in FTS-TurboID and cytosolic mNG-TurboID parasites treated with 500 μ M of biotin or a vehicle of DMSO. Biotinylated proteins detected with a labeled streptavidin. anti-CDPK1 antibody was used as a loading control. **(G)** Serial dilution of total parasite lysate for cKD strains for TIR1, CDPK1, HOOK, and FTS used in microneme protein secretion assays in Figure 5J to generate standard curves.

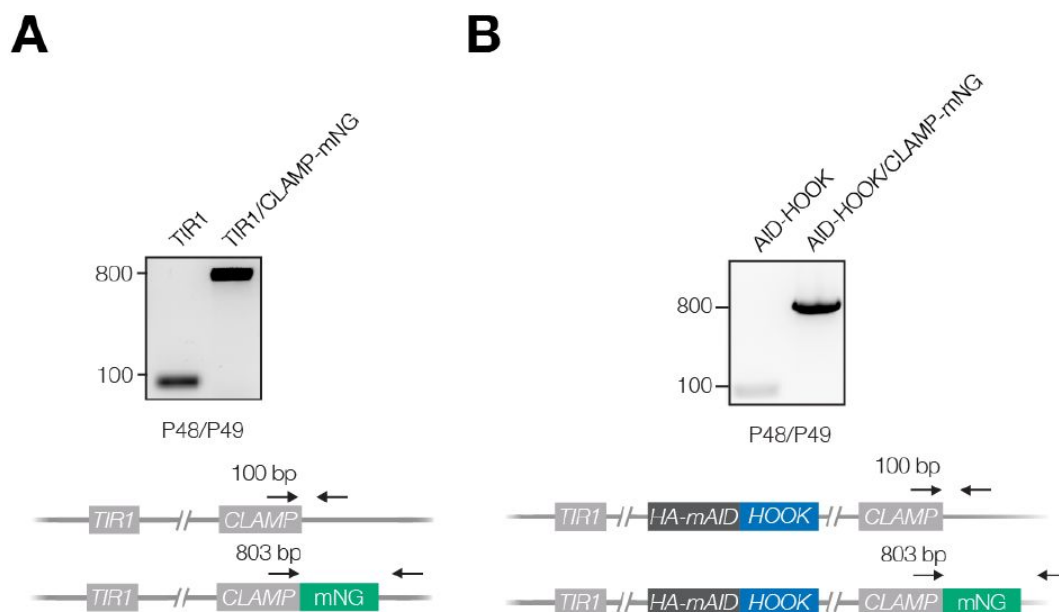


Figure S6.

Extended analysis of FTS knockdown, proximity labeling, and microneme protein secretion.

(A) PCR analysis confirming correct integration of the *mNeonGreen* reporter at the C terminus of endogenous *CLAMP* (*TGGT1*_-265790) in the TIR1 line. **(B)** PCR analysis confirming correct integration of the mNeonGreen reporter at the C terminus of endogenous *CLAMP* in the AID-HOOK line.

Supplemental Files

Video 1. Representative image series of parasites expressing endogenously tagged CLAMP-mNG following pre-treatment with DMSO and stimulation with DMSO.

Video 2. Representative image series of parasites expressing endogenously tagged CLAMP-mNG following pre-treatment with DMSO and stimulation with 500 μ M zaprinast.

Video 3. Representative image series of parasites expressing endogenously tagged CLAMP-mNG following pre-treatment with 3 μ M 3-MB-PP1 and stimulation with 500 μ M zaprinast.

Video 4. Representative image series of parasites expressing endogenously tagged TIR1/CLAMP-mNG following pre-treatment with vehicle and stimulation with DMSO.

Video 5. Representative image series of parasites expressing endogenously tagged TIR1/CLAMP-mNG following pretreatment with vehicle and stimulation with 500 μ M zaprinast.

Video 6. Representative image series of parasites expressing endogenously tagged TIR1/CLAMP-mNG following pre-treatment with auxin and stimulation with 500 μ M zaprinast.

Video 7. Representative image series of parasites expressing endogenously tagged AID-HOOK/CLAMP-mNG following pre-treatment with vehicle and stimulation with DMSO.

Video 8. Representative image series of parasites expressing endogenously tagged AID-HOOK/CLAMP-mNG following pretreatment with vehicle and stimulation with 500 μ M zaprinast.

Video 9. Representative image series of parasites expressing endogenously tagged AID-HOOK/CLAMP-mNG following pre-treatment with auxin and stimulation with 500 μ M zaprinast.

Supplementary file 1. Sub-minute phosphoproteomics time course peptide and abundance assignments from Proteome Discoverer 2.4 and analysis for the zaprinast enriched samples.

Supplementary file 1.1. RAW peptide and abundance assignments.

Supplementary file 1.2. Replicate 1 analysis with AUCdifference and p values.

Supplementary file 1.3. Replicate 2 analysis with AUCdifference and p values.

Supplementary file 1.4. Replicate 1 and 2 analysis with $AUC_{vehicle}$ values for CDPK1-independent phosphorylation.

Supplementary file 1.5. Group assignments for zaprinast-dependent phosphopeptides.

Supplementary file 2. Sub-minute phosphoproteomics time course protein and abundance assignments from Proteome Discoverer 2.4 for the zaprinast proteome.

Supplementary file 3. Sub-minute phosphoproteomics time course peptide and abundance assignments from Proteome Discoverer 2.4 and analysis for the DMSO enriched samples.

Supplementary file 3.1. RAW peptide and abundance assignments.

Supplementary file 3.2. Replicate 1 analysis with AUCdifference values.

Supplementary file 3.3. Replicate 2 analysis with AUCdifference values.

Supplementary file 3.4. Replicate 1 and 2 analysis with $AUC_{vehicle}$ values for CDPK1-independent phosphorylation.

Supplementary file 4. Sub-minute phosphoproteomics time course protein and abundance assignments from Proteome Discoverer 2.4 for the DMSO proteome.

Supplementary file 5. CDPK1 immunoprecipitation protein and abundance assignments from Scaffold DIA.

Supplementary file 6. Thiophosphorylation of CDPK1 substrates. Peptide and abundance assignments from Proteome Discoverer 2.4 and analysis.

Supplementary file 6.1. RAW peptide and abundance assignments.

Supplementary file 6.2. Analyzed peptides with enrichment significance values.

Supplementary file 6.3. Analyzed flowthrough peptides used for normalization.

Supplementary file 7. Thiophosphorylation of CDPK1 substrates. Protein and abundance assignments from Proteome Discoverer 2.4 and analysis.

Supplementary file 8. HOOK and FTS immunoprecipitation protein and abundance assignments from Proteome Discoverer 2.4.

Supplementary file 9. FTS proximity labeling protein and abundance assignments from Proteome Discoverer 2.4.

Supplementary file 10. Sequences and accessions of oligonucleotides and plasmids used in this study.

References

Alam M. M. , Solyakov L. , Bottrill A. R. , Flueck C. , Siddiqui F. A. , Singh S. , Mistry S. , Viskaduraki M. , Lee K. , Hopp C. S. , Chitnis C. E. , Doerig C. , Moon R. W. , Green J. L. , Holder A. A. , Baker D. A. , Tobin A. B. (2015) **Phosphoproteomics reveals malaria parasite protein kinase G as a signalling hub regulating egress and invasion** *Nat. Commun* **6**:7285

Aquilini E. , Cova M. M. , Mageswaran S. K. , Dos Santos Pacheco N. , Sparvoli D. , Penarete-Vargas D. M. , Najm R. , Graindorge A. , Suarez C. , Maynadier M. , Berry-Sterkers L. , Urbach S. , Fahy P. R. , Guérin A. N. , Striepen B. , Dubremetz J.-F. , Chang Y.-W. , Turkewitz A. P. , Lebrun M. (2021) **An alveolata secretory machinery adapted to parasite host cell invasion** **6**:425–434

Bandini G. , Leon D. R. , Hoppe C. M. , Zhang Y. , Agop-Nersesian C. , Shears M. J. , Mahal L. K. , Routier F. H. , Costello C. E. , Samuelson J. (2019) **O-Fucosylation of thrombospondin-like repeats is required for processing of microneme protein 2 and for efficient host cell invasion by toxoplasma gondii tachyzoites** **294**:1967–1983

Barylyuk K. , Koreny L. , Ke H. , Butterworth S. , Crook O. M. , Lassadi I. , Gupta V. , Tromer E. , Mourier T. , Stevens T. J. , Breckels L. M. , Pain A. , Lilley K. S. , Waller R.F. (2020) **A comprehensive subcellular atlas of the toxoplasma proteome via hyperLOPIT provides spatial context for protein functions** **28**:752–766

Beck J. R. , Fung C. , Straub K. W. , Coppens I. , Vashisht A. A. , Wohlschlegel J. A. , Bradley P. J. (2013) **A toxoplasma palmitoyl acyl transferase and the palmitoylated armadillo repeat protein TgARO govern apical rhoptry tethering and reveal a critical role for the rhoptries in host cell invasion but not egress** **9**:

Bekker-Jensen D. B. , Martínez-Val A. , Steigerwald S. , Rüther P. , Fort K. L. , Arrey T. N. , Harder A. , Makarov A. , Olsen J. V. (2020) **A compact Quadrupole-Orbitrap mass spectrometer with FAIMS interface improves proteome coverage in short LC gradients** **19**:716–729

Ben Chaabene R. , Lentini G. , Soldati-Favre D. (2021) **Biogenesis and discharge of the rhoptries: Key organelles for entry and hijack of host cells by the apicomplexa** **115**:453–465

Berg S. , Kutra D. , Kroeger T. , Straehle C. N. , Kausler B. X. , Haubold C. , Schiegg M. , Ales J. , Beier T. , Rudy M. , Eren K. , Cervantes J. I. , Xu B. , Beuttenmueller F. , Wolny A. , Zhang C. , Koethe U. , Hamprecht F. A. , Kreshuk A. (2019) **ilastik: interactive machine learning for (bio)image analysis** **16**:1226–1232

Bielska E. , Schuster M. , Roger Y. , Berepiki A. , Soanes D. M. , Talbot N. J. , Steinberg G. (2014) **Hook is an adapter that coordinates kinesin-3 and dynein cargo attachment on early endosomes** **204**:989–1007

- Billker O. , Lourido S. , Sibley L. D. (2009) **Calcium-dependent signaling and kinases in apicom-plexan parasites** *5*:612–622
- Bisio H. , Soldati-Favre D. (2019) **Signaling cascades governing entry into and exit from host cells by toxoplasma gondii** *Annu. Rev. Microbiol* **73**:579–599
- Bisio H. , Lunghi M. , Brochet M. , Soldati-Favre D. (2019) **Phosphatidic acid governs natural egress in toxoplasma gondii via a guanylate cyclase receptor platform** *4*:420–428
- Blader I. J. , Coleman B. I. , Chen C.-T. , Gubbels M.-J. (2015) **Lytic cycle of toxoplasma gondii: 15 years later** *Annu. Rev. Microbiol* **69**:463–485
- Blader I. , Coleman B. , Chen C. , Gubbels M. , Hill C. (2016) **Blader, I., Coleman, B., Chen, C., Gubbels, M., and Hill, C. The lytic cycle of toxoplasma gondii: 15 years later, 463–485, 2016.** 463–485
- Blethrow J. D. , Glavy J. S. , Morgan D. O. , Shokat K. M. (2008) **Covalent capture of kinasespecific phosphopeptides reveals cdk1-cyclin B substrates** *105*:1442–1447
- Blomqvist K. , Helmelt M. , Wang C. , Absalon S. , Labunska T. , Rudlaff R. M. , Adapa S. , Jiang R. , Steen H. , Dvorin J. D. (2020) **Blomqvist, K., Helmelt, M., Wang, C., Absalon, S., Labunska, T., Rudlaff, R. M., Adapa, S., Jiang, R., Steen, H., and Dvorin, J. D. Influence of plasmodium falciparum Calcium-Dependent protein kinase 5 (PfCDPK5) on the late schizont stage phosphoproteome, 2020.**
- Bradley P. J. , Sibley L. D. (2007) **Rhoptries: an arsenal of secreted virulence factors** *10*:582–587
- Branon T. C. , Bosch J. A. , Sanchez A. D. , Udeshi N. D. , Svinkina T. , Carr S. A. , Feldman J. L. , Perrimon N. , Ting A.Y. (2018) **Efficient proximity labeling in living cells and organisms with TurboID** *36*:880–887
- Breinich M. S. , Ferguson D. J. P. , Foth B. J. , van Dooren G. G. , Lebrun M. , Quon D. V. , Striepen B. , Bradley P. J. , Frischknecht F. , Carruthers V. B. , Meissner M. (2009) **A dynamin is required for the biogenesis of secretory organelles in toxoplasma gondii** *19*:277–286
- Brenes A. , Hukelmann J. , Bensaddek D. , Lamond A. I. (2019) **Multibatch TMT reveals false positives, batch effects and missing values** *18*:1967–1980
- Brochet M. , Collins M. O. , Smith T. K. , Thompson E. , Sebastian S. , Volkmann K. , Schwach F. , Chappell L. , Gomes A. R. , Berriman M. , Rayner J. C. , Baker D. A. , Choudhary J. , Billker O. (2014) **Phosphoinositide metabolism links cGMP-Dependent protein kinase G to essential ca2+ signals at key decision points in the life cycle of malaria parasites** *12*:
- Broncel M. , Dominicus C. , Vigetti L. , Nofal S. D. , Bartlett E. J. , Touquet B. , Hunt A. , Wallbank B. A. , Federico S. , Matthews S. , Young J. C. , Tate E. W. , Tardieux I. , Treeck M. (2020) **Profiling of myristoylation in toxoplasma gondii reveals an n-myristoylated protein important for host cell penetration** *Elife* **9**:

Brown K. M. , Sibley L. D. (2018) **Essential cGMP signaling in toxoplasma is initiated by a hybrid P-Type ATPase-Guanylate cyclase** *24*:804–816

Brown K. M. , Long S. , Sibley L. D. (2017) **Plasma membrane association by N-Acylation governs PKG function in toxoplasma gondii** *8*:

Brown K. M. , Long S. , Sibley L. D. (2018) **Conditional knockdown of proteins using auxininducible degron (AID) fusions in toxoplasma gondii** *8*:

Buguliskis J. S. , Brossier F. , Shuman J. , Sibley L. D. (2010) **Rhomboid 4 (ROM4) affects the processing of surface adhesins and facilitates host cell invasion by toxoplasma gondii** *6*:

Butler C. L. , Lucas O. , Wuchty S. , Xue B. , Uversky V. N. , White M. (2014) **Identifying novel cell cycle proteins in apicomplexa parasites through co-expression decision analysis** *9*:

Carruthers V. B. , Sibley L. D. (1997) **Sequential protein secretion from three distinct organelles of toxoplasma gondii accompanies invasion of human fibroblasts** *73*:114–123

Carruthers V. B. , Tomley F. M. (2008) **Microneme proteins in apicomplexans** *Subcell. Biochem* **47**:33–45

Carruthers V. B. , Giddings O. K. , Sibley L. D. (1999) **Secretion of micronemal proteins is associated with toxoplasma invasion of host cells** *1*:225–235

Carruthers V. B. , Moreno S. N. , Sibley L. D. (1999) **Ethanol and acetaldehyde elevate intracellular [ca²⁺] and stimulate microneme discharge in toxoplasma gondii** *342*:379–386

Carruthers V. B. , Sherman G. D. , Sibley L. D. (2000) **The toxoplasma adhesive protein MIC2 is proteolytically processed at multiple sites by two parasite-derived proteases** *275*:14346–14353

Chambers M. C. , Maclean B. , Burke R. , Amodei D. , Ruderman D. L. , Neumann S. , Gatto L. , Fischer B. , Pratt B. , Egertson J. , Hoff K. , Kessner D. , Tasman N. , Shulman N. , Frewen B. , Baker T. A. , Brusniak M.-Y. , Paulse C. , Creasy D. , Flashner L. , Kani K. , Moulding C. , Seymour S. L. , Nuwaysir L. M. , Lefebvre B. , Kuhlmann F. , Roark J. , Rainer P. , Detlev S. , Hemenway T. , Huhmer A. , Langridge J. , Connolly B. , Chadick T. , Holly K. , Eckels J. , Deutsch E. W. , Moritz R. L. , Katz J. E. , Agus D. B. , MacCoss M. , Tabb D. L. , Mallick P. (2012) **A cross-platform toolkit for mass spectrometry and proteomics** *30*:918–920

Chen C.-T. , Kelly M. , Leon J. d. , Nwagbara B. , Ebbert P. , Ferguson D. J. P. , Lowery L. A. , Morrisette N. , Gubbels M.-J. (2015) **Compartmentalized toxoplasma EB1 bundles spindle microtubules to secure accurate chromosome segregation** *26*:4562–4576

Christensen J. R. , Kendrick A. A. , Truong J. B. , Aguilar-Maldonado A. , Adani V. , Dzieciatkowska M. , Reck-Peterson S. L. (2021) **Cytoplasmic dynein-1 cargo diversity is mediated by the combinatorial assembly of FTS-Hook-FHIP complexes** *Elife* **10**:

- Coleman B. I. , Saha S. , Sato S. , Engelberg K. , Ferguson D. J. P. , Coppens I. , Lodoen M. B. , Gubbels M.-J. (2018) **A member of the ferlin calcium sensor family is essential for toxoplasma gondii rhoptry secretion 9:**
- Courjol F. , Mouveau T. , Lesage K. , Saliou J.-M. , Werkmeister E. , Bonabaud M. , Rohmer M. , Slomianny C. , Lafont F. , Gissot M. (2017) **Characterization of a nuclear pore protein sheds light on the roles and composition of the toxoplasma gondii nuclear pore complex 74:2107–2125**
- Doggett J. S. , Ojo K. K. , Fan E. , Maly D. J. , Van Voorhis W. C. (2014) **Bumped kinase inhibitor 1294 treats established toxoplasma gondii infection 58:3547–3549**
- Donald R. G. K. , Zhong T. , Wiersma H. , Nare B. , Yao D. , Lee A. , Allocco J. , Liberator P. A. (2006) **Anticoccidial kinase inhibitors: identification of protein kinase targets secondary to cGMP-dependent protein kinase 149:86–98**
- Endo T. , Sethi K. K. , Piekarski G. (1982) **Toxoplasma gondii: Calcium ionophore a23187-mediated exit of trophozoites from infected murine macrophages 53:179–188**
- Fang H. , Klages N. , Baechler B. , Hillner E. , Yu L. , Pardo M. , Choudhary J. , Brochet M. (2017) **Multiple short windows of calcium-dependent protein kinase 4 activity coordinate distinct cell cycle events during plasmodium gametogenesis Elife 6:**
- Farrell A. , Thirugnanam S. , Lorestani A. , Dvorin J. D. , Eidell K. P. , Ferguson D. J. P. , Anderson-White B. R. , Duraisingh M. T. , Marth G. T. , Gubbels M.-J. (2012) **A DOC2 protein identified by mutational profiling is essential for apicomplexan parasite exocytosis 335:218–221**
- Francia M. E. , Wicher S. , Pace D. A. , Sullivan J. , Moreno S. N. J. , Arrizabalaga G. (2011) **A toxoplasma gondii protein with homology to intracellular type Na/H exchangers is important for osmoregulation and invasion 317:1382–1396**
- Gaji R. Y. , Johnson D. E. , Treeck M. , Wang M. , Hudmon A. , Arrizabalaga G. (2015) **Phosphorylation of a myosin motor by TgCDPK3 facilitates rapid initiation of motility during toxoplasma gondii egress 11:**
- Garrison E. , Treeck M. , Ehret E. , Butz H. , Garbuz T. , Oswald B. P. , Settles M. , Boothroyd J. , Arrizabalaga G. (2012) **A forward genetic screen reveals that calcium-dependent protein kinase 3 regulates egress in toxoplasma 8:**
- Gillingham A. K. , Sinka R. , Torres I. L. , Lilley K. S. , Munro S. (2014) **Toward a comprehensive map of the effectors of rab GTPases 31:358–373**
- Guo X. , Farías G. G. , Mattera R. , Bonifacino J. S. (2016) **Rab5 and its effector FHF contribute to neuronal polarity through dynein-dependent retrieval of somatodendritic proteins from the axon 113:–27**
- Havelaar A. H. , Kirk M. D. , Torgerson P. R. , Gibb H. J. , Hald T. , Lake R. J. , Praet N. , Bellinger D. C. , de Silva N. R. , Gargouri N. , Speybroeck N. , Cawthorne A. , Mathers C. , Stein C. , Angulo F. J. , Devleeschauwer B. , undefined undefined (2015) **World health organization global estimates and regional comparisons of the burden of foodborne disease in 2010 12:**

- Heal W. P. , Wright M. H. , Thinon E. , Tate E. W. (2011) **Multifunctional protein labeling via enzymatic n-terminal tagging and elaboration by click chemistry** 7:105–117
- Heaslip A. T. , Nishi M. , Stein B. , Hu K. (2011) **The motility of a human parasite, toxoplasma gondii, is regulated by a novel lysine methyltransferase** 7:
- Herneisen A. L. , Li Z.-H. , Chan A. W. , Moreno S. N. J. , Lourido S. (2022) **Temporal and thermal profiling of the toxoplasma proteome implicates parasite protein phosphatase 1 in the regulation of ca²⁺-responsive pathways** *Elife* 11:
- Hopp C. S. , Bowyer P. W. , Baker D. A. (2012) **The role of cGMP signalling in regulating life cycle progression of plasmodium** 14:831–837
- Huynh M.-H. , Carruthers V. B. (2009) **Tagging of endogenous genes in a toxoplasma gondii strain lacking ku80** 8:530–539
- Iacovache I. , Paumard P. , Scheib H. , Lesieur C. , Sakai N. , Matile S. , Parker M. W. , van der Goot F. G. (2006) **A rivet model for channel formation by aerolysin-like pore-forming toxins** 25:457–466
- Ingram J. R. , Knockenhauer K. E. , Markus B. M. , Mandelbaum J. , Ramek A. , Shan Y. , Shaw D. E. , Schwartz T. U. , Ploegh H. L. , Lourido S. (2015) **Allosteric activation of apicomplexan calcium-dependent protein kinases** 112:–84
- Invergo B. M. , Brochet M. , Yu L. , Choudhary J. , Beltrao P. , Billker O. (2017) **Sub-minute phosphoregulation of cell cycle systems during plasmodium gamete formation** 21:2017–2029
- Johnson S. M. , Murphy R. C. , Geiger J. A. , DeRocher A. E. , Zhang Z. , Ojo K. K. , Larson E. T. , Perera B. G. K. , Dale E. J. , He P. , Reid M. C. , Fox A. M. W. , Mueller N. R. , Merritt E. A. , Fan E. , Parsons M. , Van Voorhis W. C. , Maly D. J. (2012) **Development of toxoplasma gondii calcium-dependent protein kinase 1 (TgCDPK1) inhibitors with potent anti-toxoplasma activity** 55:2416–2426
- Kafsack B. F. C. , Pena J. D. O. , Coppens I. , Ravindran S. , Boothroyd J. C. , Carruthers V. B. (2009) **Rapid membrane disruption by a perforin-like protein facilitates parasite exit from host cells** 323:530–533
- Käll L. , Canterbury J. D. , Weston J. , Noble W. S. , MacCoss M. J. (2007) **Semi-supervised learning for peptide identification from shotgun proteomics datasets** 4:923–925
- Käll L. , Storey J. D. , Noble W. S. (2008) **Non-parametric estimation of posterior error probabilities associated with peptides identified by tandem mass spectrometry** 24:–8
- Käll L. , Storey J. D. , MacCoss M. J. , Noble W. S. (2008) **Assigning significance to peptides identified by tandem mass spectrometry using decoy databases** 7:29–34

- Katris N. J. , van Dooren G. G. , McMillan P. J. , Hanssen E. , Tilley L. , Waller R. F. (2014) **The apical complex provides a regulated gateway for secretion of invasion factors in toxoplasma 10:**
- Kessler H. , Herm-Götz A. , Hegge S. , Rauch M. , Soldati-Favre D. , Frischknecht F. , Meissner M. (2008) **Microneme protein 8—a new essential invasion factor in toxoplasma gondii** *J. Cell Sci* **121**:947–956
- Krämer H. , Phistry M. (1996) **Mutations in the drosophila hook gene inhibit endocytosis of the boss transmembrane ligand into multivesicular bodies 133:1205–1215**
- Kremer K. , Kamin D. , Rittweger E. , Wilkes J. , Flammer H. , Mahler S. , Heng J. , Tonkin C. J. , Langsley G. , Hell S. W. , Carruthers V. B. , Ferguson D. J. P. , Meissner M. (2013) **An overexpression screen of toxoplasma gondii Rab-GTPases reveals distinct transport routes to the micronemes 9:**
- Kumar S. , Kumar M. , Ekka R. , Dvorin J. D. , Paul A. S. , Madugundu A. K. , Gilberger T. , Gowda H. , Duraisingh M. T. , Keshava Prasad T. S. , Sharma P. (2017) **PfCDPK1 mediated signaling in erythrocytic stages of plasmodium falciparum 8:63**
- Lamarque M. , Besteiro S. , Papoin J. , Roques M. , Vulliez-Le Normand B. , Morlon-Guyot J. , Dubremetz J.-F. , Fauquenoy S. , Tomavo S. , Faber B. W. , Kocken C. H. , Thomas A. W. , Boulanger M. J. , Bentley G. A. , Lebrun M. (2011) **The RON2-AMA1 interaction is a critical step in moving junction-dependent invasion by apicomplexan parasites 7:**
- Lamarque M. H. , Roques M. , Kong-Hap M. , Tonkin M. L. , Rugarabamu G. , Marq J.-B. , Penarete-Vargas D. M. , Boulanger M. J. , Soldati-Favre D. , Lebrun M. (2014) **Plasticity and redundancy among AMA-RON pairs ensure host cell entry of toxoplasma parasites** *Nat. Commun* **5**:4098
- Lasonder E. , Green J. L. , Camarda G. , Talabani H. , Holder A. A. , Langsley G. , Alano P. (2012) **The plasmodium falciparum schizont phosphoproteome reveals extensive phosphatidylinositol and cAMP-protein kinase a signaling 11:5323–5337**
- Lee I.-G. , Olenick M. A. , Boczkowska M. , Franzini-Armstrong C. , Holzbaur E. L. F. , Dominguez R. (2018) **A conserved interaction of the dynein light intermediate chain with dynein-dynactin effectors necessary for processivity 9:986**
- Lentini G. , Dubois D. J. , Maco B. , Soldati-Favre D. , Fréna K. (2019) **The roles of centrin 2 and dynein light chain 8a in apical secretory organelles discharge of toxoplasma gondii 20:583–600**
- Leung J. M. , He Y. , Zhang F. , Hwang Y.-C. , Nagayasu E. , Liu J. , Murray J. M. , Hu K. (2017) **Stability and function of a putative microtubule-organizing center in the human parasite toxoplasma gondii 28:1361–1378**
- Leung J. M. , Liu J. , Wetzel L. A. , Hu K. (2019) **Centrin2 from the human parasite toxoplasma gondii is required for its invasion and intracellular replication 132:**

- Li J. , Van Vranken J. G. , Pontano Vaite L. , Schweppe D. K. , Huttlin E. L. , Etienne C. , Nandhikonda P. , Viner R. , Robitaille A. M. , Thompson A. H. , Kuhn K. , Pike I. , Bomgarden R. D. , Rogers J. C. , Gygi S. P. , Paulo J. A. (2020) **TMTpro reagents: a set of isobaric labeling mass tags enables simultaneous proteome-wide measurements across 16 samples** 17:399–404
- Long S. , Anthony B. , Drewry L. L. , David Sibley L. (2017) **Long, S., Anthony, B., Drewry, L. L., and David Sibley, L.A conserved ankyrin repeatcontaining protein regulates conoid stability, motility and cell invasion in toxoplasma gondii, 2017.**
- Lord S. J. , Velle K. B. , Mullins R. D. , Fritz-Laylin L. K. (2020) **SuperPlots: Communicating reproducibility and variability in cell biology** 219:
- Lourido S. , Moreno S. N. J. (2015) **The calcium signaling toolkit of the apicomplexan parasites toxoplasma gondii and plasmodium spp** 57:186–193
- Lourido S. , Shuman J. , Zhang C. , Shokat K. M. , Hui R. , Sibley L. D. (2010) **Calciumdependent protein kinase 1 is an essential regulator of exocytosis in toxoplasma** 465:359–362
- Lourido S. , Tang K. , Sibley L. D. (2012) **Distinct signalling pathways control toxoplasma egress and host-cell invasion** 31:4524–4534
- Lourido S. , Zhang C. , Lopez M. S. , Tang K. , Barks J. , Wang Q. , Wildman S. A. , Shokat K. M. , Sibley L. D. (2013) **Optimizing small molecule inhibitors of calcium-dependent protein kinase 1 to prevent infection by toxoplasma gondii** 56:3068–3077
- Lourido S. , Jeschke G. R. , Turk B. E. , David Sibley L. (2013) **Lourido, S., Jeschke, G. R., Turk, B. E., and David Sibley, L.Exploiting the unique ATP-Binding pocket of Toxoplasma Calcium-Dependent protein kinase 1 to identify its substrates, 2013.**
- Luo S. , Ruiz F. A. , Moreno S. N. J. (2005) **The acidocalcisome Ca²⁺-ATPase (TgA1) of toxoplasma gondii is required for polyphosphate storage, intracellular calcium homeostasis and virulence** 55:1034–1045
- Mageswaran S. K. , Guérin A. , Theveny L. M. , Chen W. D. , Martinez M. , Lebrun M. , Striepen B. , Chang Y.-W. (2021) **In situ ultrastructures of two evolutionarily distant apicomplexan rhoptry secretion systems** 12:4983
- Markus B. M. , Bell G. W. , Lorenzi H. A. , Lourido S. (2019) **Optimizing systems for cas9 expression in toxoplasma gondii** 4:
- Márquez-Nogueras K. M. , Hortua Triana M. A. , Chasen N. M. , Kuo I. Y. , Moreno S. N. (2021) **Calcium signaling through a transient receptor channel is important for toxoplasma gondii growth** *Elife* 10:
- Martin D. D. O. , Beauchamp E. , Berthiaume L. G. (2011) **Post-translational myristoylation: Fat matters in cellular life and death** 93:18–31

McCoy J. M. , Whitehead L. , van Dooren G. G. , Tonkin C. J. (2012) **TgCDPK3 regulates calcium-dependent egress of toxoplasma gondii from host cells** 8:

McCoy J. M. , Stewart R. J. , Ubaldi A. D. , Li D. , Schröder J. , Scott N. E. , Papenfuss A. T. , Lehane A. M. , Foster L. J. , Tonkin C. J. (2017) **A forward genetic screen identifies a negative regulator of rapid Ca^{2+} -dependent cell egress (MS1) in the intracellular parasite toxoplasma gondii** 292:7662–7674

Mueller C. , Klages N. , Jacot D. , Santos J. M. , Cabrera A. , Gilberger T. W. , Dubremetz J.-F. , Soldati-Favre D. (2013) **The toxoplasma protein ARO mediates the apical positioning of rhoptry organelles, a prerequisite for host cell invasion** 13:289–301

Mueller C. , Samoo A. , Hammoudi P.-M. , Klages N. , Kallio J. P. , Kursula I. , Soldati-Favre D. (2016) **Structural and functional dissection of toxoplasma gondii armadillo repeats only protein 129** 1031–1045

Nofal S. D. , Dominicus C. , Broncel M. , Katris N. J. , Flynn H. R. , Arrizabalaga G. , Botté C. Y. , Invergo B. M. , Treeck M. (2022) **A positive feedback loop mediates crosstalk between calcium, cyclic nucleotide and lipid signalling in calcium-induced toxoplasma gondii egress** 18:

Ojo K. K. , Larson E. T. , Keyloun K. R. , Castaneda L. J. , Derocher A. E. , Inampudi K. K. , Kim J. E. , Arakaki T. L. , Murphy R. C. , Zhang L. , Napuli A. J. , Maly D. J. , Verlinde C. L. M. J. , Buckner F. S. , Parsons M. , Hol W. G. J. , Merritt E. A. , Van Voorhis W. C. (2010) **Toxoplasma gondii calcium-dependent protein kinase 1 is a target for selective kinase inhibitors** 17:602–607

Ong Y.-C. , Reese M. L. , Boothroyd J. C. (2010) **Toxoplasma rhoptry protein 16 (ROP16) subverts host function by direct tyrosine phosphorylation of STAT6*** 285:28731–28740

Pang Z. P. , Südhof T. C. (2010) **Cell biology of Ca^{2+} -triggered exocytosis** 22:496–505

Pease B. N. , Huttlin E. L. , Jedrychowski M. P. , Talevich E. , Harmon J. , Dillman T. , Kannan N. , Doerig C. , Chakrabarti R. , Gygi S. P. , Chakrabarti D. (2013) **Pease, B. N., Huttlin, E. L., Jedrychowski, M. P., Talevich, E., Harmon, J., Dillman, T., Kannan, N., Doerig, C., Chakrabarti, R., Gygi, S. P., and Chakrabarti, D. Global analysis of protein expression and phosphorylation of three stages of Plasmodium falciparum in-traerythrocytic development, 2013.**

Pease B. N. , Huttlin E. L. , Jedrychowski M. P. , Dorin-Semlat D. , Sebastiani D. , Segarra D. T. , Roberts B. F. , Chakrabarti R. , Doerig C. , Gygi S. P. , Chakrabarti D. (2018) **Characterization of plasmodium falciparum atypical kinase PfPK7-dependent phosphoproteome** 17:2112–2123

Pomel S. , Luk F. C. Y. , Beckers C. J. M. (2008) **Host cell egress and invasion induce marked relocations of glycolytic enzymes in toxoplasma gondii tachyzoites** 4:

Redwine W. B. , DeSantis M. E. , Hollyer I. , Htet Z. M. , Tran P. T. , Swanson S. K. , Florens L. , Washburn M. P. , Reck-Peterson S. L. (2017) **The human cytoplasmic dynein interactome reveals novel activators of motility** *Elife* 6:

- Reese M. L. , Zeiner G. M. , Saeij J. P. J. , Boothroyd J. C. , Boyle J. P. (2011) **Polymorphic family of injected pseudokinases is paramount in toxoplasma virulence** 108:9625–9630
- Rothenberg D. A. , Gordon E. A. , White F. M. , Lourido S. (2016) **Identification of direct kinase substrates using Analogue-Sensitive alleles** *Methods Mol. Biol* 1355:71–84
- Sebastian S. , Brochet M. , Collins M. O. , Schwach F. , Jones M. L. , Goulding D. , Rayner J. C. , Choudhary J. S. , Billker O. (2012) **A plasmodium calcium-dependent protein kinase controls zygote development and transmission by translationally activating repressed mRNAs** 12:9–19
- Segev-Zarko L.-A. , Dahlberg P. D. , Sun S. Y. , Pelt D. M. , Kim C. Y. , Egan E. S. , Sethian J. A. , Chiu W. , Boothroyd J. C. (2022) **Cryo-electron tomography with mixed-scale dense neural networks reveals key steps in deployment of toxoplasma invasion machinery** 1:
- Shen B. , Brown K. M. , Lee T. D. , David Sibley L. (2014) **Shen, B., Brown, K. M., Lee, T. D., and David Sibley, L. Efficient gene disruption in diverse strains of toxoplasma gondii using CRISPR/CAS9, 2014.**
- Shortt E. , Hackett C. G. , Stadler R. V. , Ward G. E. , Lourido S. (2022) **Shortt, E., Hackett, C. G., Stadler, R. V., Ward, G. E., and Lourido, S. CDPK2A and CDPK1 form a signaling module upstream of toxoplasma motility. July 2022.**
- Sidik S. M. , Valteau D. , Acevedo-Sánchez Y. , Godoy L. C. , Pasaje C. F. A. , Huynh M.-H. , Carruthers V. B. , Niles J. C. , Lourido S. (1970) **Sidik, S. M., Valteau, D., Acevedo-Sánchez, Y., Godoy, L. C., Pasaje, C. F. A., Huynh, M.-H., Carruthers, V. B., Niles, J. C., and Lourido, S. A conserved complex of microneme proteins mediates rhoptry discharge in Toxoplasma.**
- Sidik S. M. , Huet D. , Ganesan S. M. , Huynh M.-H. , Wang T. , Nasamu A. S. , Thiru P. , Saeij J. P. J. , Carruthers V. B. , Niles J. C. , Lourido S. (2016) **A genome-wide CRISPR screen in toxoplasma identifies essential apicomplexan genes** 166:1423–1435
- Sidik S. M. , Hortua Triana M. A. , Paul A. S. , El Bakkouri M. , Hackett C. G. , Tran F. , Westwood N. J. , Hui R. , Zuercher W. J. , Duraisingh M. T. , Moreno S. N. J. , Lourido S. (2016) **Using a genetically encoded sensor to identify inhibitors of toxoplasma gondii ca²⁺ signaling** 291:9566–9580
- Simm D. , Hatje K. , Kollmar M. (2015) **Waggawagga: comparative visualization of coiled-coil predictions and detection of stable single α -helices (SAH domains)** 31:767–769
- Singer M. , Simon K. , Forné I. , Meissner M. (2022) **Singer, M., Simon, K., Forné, I., and Meissner, M. A central protein complex essential for invasion in toxoplasma gondii. Feb. 2022.**
- Smith T. A. , Lopez-Perez G. S. , Herneisen A. L. , Shortt E. , Lourido S. (2022) **Screening the toxoplasma kinome with high-throughput tagging identifies a regulator of invasion and egress** 7:868–881
- Söding J. , Biegert A. , Lupas A. N. (2005) **The HHpred interactive server for protein homology detection and structure prediction** *Nucleic Acids Res* 33:–8

Solyakov L. , Halbert J. , Alam M. M. , Semblat J.-P. , Dorin-Semblat D. , Reininger L. , Bottrill A. R. , Mistry S. , Abdi A. , Fennell C. , Holland Z. , Demarta C. , Bouza Y. , Sicard A. , Nivez M.-P. , Eschenlauer S. , Lama T. , Thomas D. C. , Sharma P. , Agarwal S. , Kern S. , Pradel G. , Graciotti M. , Tobin A. B. , Doerig C. (2011) **Solyakov, L., Halbert, J., Alam, M. M., Semblat, J.-P., Dorin-Semblat, D., Reininger, L., Bottrill, A. R., Mistry, S., Abdi, A., Fennell, C., Holland, Z., Demarta, C., Bouza, Y., Sicard, A., Nivez, M.-P., Eschenlauer, S., Lama, T., Thomas, D. C., Sharma, P., Agarwal, S., Kern, S., Pradel, G., Graciotti, M., Tobin, A. B., and Doerig, C. Global kinomic and phospho-proteomic analyses of the human malaria parasite plasmodium falciparum, 2011.**

Sparvoli D. , Delabre J. , Penarete-Vargas D. M. , Kumar Mageswaran S. , Tsylin L. M. , Heckendorn J. , Theveny L. , Maynadier M. , Mendonça Cova M. , Berry-Sterkers L. , Guérin A. , Dubremetz J.-F. , Urbach S. , Striepen B. , Turkewitz A. P. , Chang Y.-W. , Lebrun M. (2022) **An apical membrane complex for triggering rhoptry exocytosis and invasion in toxoplasma 41:**

Stasic A. J. , Chasen N. M. , Dykes E. J. , Vella S. A. , Asady B. , Starai V. J. , Moreno S. N. J. (2019) **The toxoplasma vacuolar H⁺-ATPase regulates intracellular pH and impacts the maturation of essential secretory proteins 27:2132–2146**

Sun S. Y. , Segev-Zarko L. , Chen M. , Pintilie G. D. , Schmid M. F. , Ludtke S. J. , Boothroyd J. C. , Chiu W. (2022) **Cryo-ET of Toxoplasma parasites gives subnanometer insight into tubulin-based structures 119:**

Tang Q. , Andenmatten N. , Hortua Triana M. A. , Deng B. , Meissner M. , Moreno S. N. J. , Ballif B. A. , Ward G. E. (2014) **Calcium-dependent phosphorylation alters class XIVa myosin function in the protozoan parasite toxoplasma gondii 25:2579–2591**

Taus T. , Köcher T. , Pichler P. , Paschke C. , Schmidt A. , Henrich C. , Mechtler K. (2011) **Universal and confident phosphorylation site localization using phosphoRS 10:5354–5362**

Taylor H. M. , McRobert L. , Grainger M. , Sicard A. , Dluzewski A. R. , Hopp C. S. , Holder A. A. , Baker D. A. (2010) **The malaria parasite cyclic GMP-dependent protein kinase plays a central role in blood-stage schizogony 9:37–45**

Thrun M. C. , Ultsch A. (2021) **Using Projection-Based clustering to find distance- and Density-Based clusters in High-Dimensional data 38:280–312**

Tosetti N. , Dos Santos Pacheco N. , Soldati-Favre D. , Jacot D. (2019) **Three f-actin assembly centers regulate organelle inheritance, cell-cell communication and motility in toxoplasma gondii Elife 8:**

Treeck M. , Sanders J. L. , Elias J. E. , Boothroyd J. C. (2011) **The phosphoproteomes of plasmodium falciparum and toxoplasma gondii reveal unusual adaptations within and beyond the parasites' boundaries 10:410–419**

Treeck M. , Sanders J. L. , Gaji R. Y. , LaFavers K. A. , Child M. A. , Arrizabalaga G. , Elias J. E. , Boothroyd J. C. (2014) **The calcium-dependent protein kinase 3 of toxoplasma influences basal calcium levels and functions beyond egress as revealed by quantitative phosphoproteome analysis 10:**

Tsai C.-F. , Hsu C.-C. , Hung J.-N. , Wang Y.-T. , Choong W.-K. , Zeng M.-Y. , Lin P.-Y. , Hong R.-W. , Sung T.-Y. , Chen Y.-J. (2014) **Sequential phosphoproteomic enrichment through complementary metal-directed immobilized metal ion affinity chromatography** 86:685–693

Tyler J. S. , Boothroyd J. C. (2011) **The c-terminus of toxoplasma RON2 provides the crucial link between AMA1 and the host-associated invasion complex** 7:

Van Vranken Pontano Vaiteas , Schweppe undefined (1970) **TMTpro reagents: a set of isobaric labeling mass tags enables simultaneous proteome-wide measurements across 16 samples**

Wang X. , Fu Y. , Beatty W. L. , Ma M. , Brown A. , Sibley L. D. , Zhang R. (2021) **Cryo-EM structure of cortical microtubules from human parasite toxoplasma gondii identifies their microtubule inner proteins** 12:3065

Wernimont A. K. , Artz J. D. , Finerty P. , Lin Y.-H. , Amani M. , Allali-Hassani A. , Senis-terra G. , Vedadi M. , Tempel W. , Mackenzie F. , Chau I. , Lourido S. , Sibley L. D. , Hui R. (2010) **Structures of apicomplexan calcium-dependent protein kinases reveal mechanism of activation by calcium** 17:596–601

Wichroski M. J. , Melton J. A. , Donahue C. G. , Tweten R. K. , Ward G. E. (2002) **Clostridium septicum alpha-toxin is active against the parasitic protozoan toxoplasma gondii and targets members of the SAG family of glycosylphosphatidylinositol-anchored surface proteins** 70:4353–4361

Wilson S. K. , Heckendorn J. , Martorelli Di Genova B. , Koch L. L. , Rooney P. J. , Morrisette N. , Lebrun M. , Knoll L. J. (2020) **A toxoplasma gondii patatin-like phospholipase contributes to host cell invasion** 16:

Winzer P. , Müller J. , Aguado-Martínez A. , Rahman M. , Balmer V. , Manser V. , Ortega-Mora L. M. , Ojo K. K. , Fan E. , Maly D. J. , Van Voorhis W. C. , Hemphill A. (2015) **In vitro and in vivo effects of the bumped kinase inhibitor 1294 in the related Cyst-Forming apicomplexans toxoplasma gondii and neospora caninum** 59:6361–6374

Wright M. H. , Clough B. , Rackham M. D. , Rangachari K. , Brannigan J. A. , Grainger M. , Moss D. K. , Bottrill A. R. , Heal W. P. , Broncel M. , Serwa R. A. , Brady D. , Mann D. J. , Leatherbarrow R. J. , Tewari R. , Wilkinson A. J. , Holder A. A. , Tate E. W. (2014) **Wright, M. H., Clough, B., Rackham, M. D., Rangachari, K., Brannigan, J. A., Grainger, M., Moss, D. K., Bottrill, A. R., Heal, W. P., Broncel, M., Serwa, R. A., Brady, D., Mann, D. J., Leatherbarrow, R. J., Tewari, R., Wilkinson, A. J., Holder, A. A., and Tate, E. W. Validation of n-myristoyltransferase as an antimalarial drug target using an integrated chemical biology approach, 2014.**

Xu L. , Sowa M. E. , Chen J. , Li X. , Gygi S. P. , Harper J. W. (2008) **An FTS/Hook/p107FHIP complex interacts with and promotes endosomal clustering by the homotypic vacuolar protein sorting complex** 19:5059–5071

Yang L. , Uboldi A. D. , Seizova S. , Wilde M.-L. , Coffey M. J. , Katris N. J. , Yamaryo-Botté Y. , Kocan M. , Bathgate R. A. D. , Stewart R. J. , McConville M. J. , Thompson P. E. , Botté C. Y. , Tonkin C. J. (2019) **An apically located hybrid guanylate cyclase—ATPase is critical for the initiation of ca2+ signaling and motility in toxoplasma gondii** 294:8959–8972

Yao X. , Wang X. , Xiang X. (2014) **FHIP and FTS proteins are critical for dynein-mediated transport of early endosomes in aspergillus** *25*:2181–2189

Yuasa K. , Mi-Ichi F. , Kobayashi T. , Yamanouchi M. , Kotera J. , Kita K. , Omori K. (2005) **PfPDE1, a novel cGMP-specific phosphodiesterase from the human malaria parasite plasmodium falciparum** *Biochem. J* **392**:221–229

Zecha J. , Satpathy S. , Kanashova T. , Avanesian S. C. , Kane M. H. , Clauser K. R. , Mertins P. , Carr S. A. , Kuster B. (2019) **TMT labeling for the masses: A robust and costefficient, in-solution labeling approach** *18*:1468–1478

Zhang J. , Qiu R. , Arst H. N. , Peñalva M. A. , Xiang X. (2014) **HookA is a novel dynein—early endosome linker critical for cargo movement in vivo** *204*:1009–1026

Author information

1. Alex W Chan

Whitehead Institute for Biomedical Research, Cambridge, MA, USA, Biology Department, Massachusetts Institute of Technology, Cambridge, MA, USA
ORCID iD: [0000-0002-5444-5756](https://orcid.org/0000-0002-5444-5756)

2. Malgorzata Broncel

Signaling in Apicomplexan Parasites Laboratory, The Francis Crick Institute, London, UK
ORCID iD: [0000-0003-2991-3500](https://orcid.org/0000-0003-2991-3500)

3. Nicole Haseley

Whitehead Institute for Biomedical Research, Cambridge, MA, USA
ORCID iD: [0000-0002-9346-2161](https://orcid.org/0000-0002-9346-2161)

4. Sundeep Chakladar

Whitehead Institute for Biomedical Research, Cambridge, MA, USA

5. Elena Andree

Whitehead Institute for Biomedical Research, Cambridge, MA, USA

6. Alice L Herneisen

Whitehead Institute for Biomedical Research, Cambridge, MA, USA, Biology Department, Massachusetts Institute of Technology, Cambridge, MA, USA
ORCID iD: [0000-0003-3368-0893](https://orcid.org/0000-0003-3368-0893)

7. Emily Shortt

Whitehead Institute for Biomedical Research, Cambridge, MA, USA

8. Moritz Treeck

Signaling in Apicomplexan Parasites Laboratory, The Francis Crick Institute, London, UK
ORCID iD: [0000-0002-9727-6657](https://orcid.org/0000-0002-9727-6657)

9. Sebastian Lourido

Whitehead Institute for Biomedical Research, Cambridge, MA, USA, Biology Department, Massachusetts Institute of Technology, Cambridge, MA, USA

For correspondence:

lourido@wi.mit.edu

ORCID iD: [0000-0002-5237-1095](https://orcid.org/0000-0002-5237-1095)

Editors

Reviewing Editor

Arturo Casadevall

Johns Hopkins Bloomberg School of Public Health, United States of America

Senior Editor

Arturo Casadevall

Johns Hopkins Bloomberg School of Public Health, United States of America

Reviewer #1 (Public Review):

This carefully done research paper presents a fundamental model of techniques that are useful for the elucidation of kinase substrates. The paper utilizes state-of-the-art approaches to define a kinetic phosphoproteome and how to integrate that data with complementary approaches using a chemical probe (in this case KTPyS, a triphosphate) to find these substrates. Using these approaches TgCDPK1 was demonstrated to affect microneme secretion via a direct interaction with a HOOK complex (defined as a HOOK protein TGG1_289100, an FTS TGGT1_264050 and 2 other proteins TGGT1_316650 and 306920).

This work is carefully controlled and the analysis pathways are logical and provide paradigms for how to approach the question of identifying substrates of kinases using proteomic approaches employing genetic and chemical strategies.

The authors succeeded in the identification of candidate substrates for TgCDPK1. Validation of the results was provided by previous studies in the literature that characterized some of these substrates as well as the experiments in this manuscript on the characterization of the HOOK complex that is phosphorylated by CDPK1.

The HOOK complex (defined as a HOOK protein TGG1_289100, an FTS TGGT1_264050, and 2 other proteins TGGT1_316650 and 306920) was clearly demonstrated to be involved in invasion via its role in microneme trafficking.

Reviewer #2 (Public Review):

In this study, the authors take a multipronged approach to identify the substrate repertoire of calcium-dependent protein kinase, CDPK1 in *Toxoplasma* that includes quantitative phosphoproteomics, myristoylation, thiophosphorylation, immunoprecipitation as well as proximity-based labeling. Their finding also reveals that CDPK1 functions in parasite invasion and egress by phosphorylating different protein candidates. More importantly, the authors successfully determine one branch of the CDPK1 signaling pathway that regulates invasion through the phosphorylation of the HOOK protein involved in the translocation and secretion of micronemal proteins.

Reviewer #3 (Public Review):

In this manuscript, Chan and collaborators investigate the role of CDPK1 in regulating microneme trafficking and exocytosis in *Toxoplasma gondii*. Micronemes are apicomplexan-specific organelles localized at the apical end of the parasite and depending on cortical microtubules. Micronemes contain proteins that are exocytosed in a Ca^{2+} -dependent manner and are required for *T. gondii* egress, motility, and host-cell invasion. In Apicomplexa, Ca^{2+} signaling is dependent on Ca^{2+} -dependent protein kinases (CDPKs). CDPK1 has been demonstrated to be essential for Ca^{2+} -stimulated micronemes exocytosis allowing parasite egress, gliding motility, and invasion. It is also known that intracellular calcium storages are mobilized following a cyclic nucleotide-mediated activation of protein kinase G. This step, occurs upstream of CDPK1 functions. However, the exact signaling pathway regulated by CDPK1 remains unknown. In this paper, the authors used phosphoproteomic analysis to identify new proteins phosphorylated by CDPK1. They demonstrated that CDPK1 activity is required for calcium-stimulated trafficking of micronemes to the apical end, depending on a complex of proteins that include HOOK and FTS, which are known to link cargo to the dynein machinery for trafficking along microtubules. Overall, the authors identified evidence for a new protein complex involved in microneme trafficking through the exocytosis process for which circumstantial evidence of its functionality is demonstrated here.